IN VITRO AND IN VIVO IDENTIFICATION AND QUANTIFICATION OF CARMOFUR AND 5-FLUOROURACIL USING TANDEM MASS SPECTROMETRY

by

Mohammad Mohiminul Islam

A Dissertation Submitted in

Partial Fulfillment of the

Requirements for the Degree of

Doctor of Philosophy

in Chemistry

at

University of Wisconsin-Milwaukee

May 2022

ABSTRACT

IN VITRO AND IN VIVO IDENTIFICATION AND QUANTIFICATION OF CARMOFUR AND 5-FLUOROURACIL USING TANDEM MASS SPECTROMETRY

by

Mohammad Mohiminul Islam

The University of Wisconsin-Milwaukee, 2022
Under the Supervision of Professor Shama P. Mirza

Glioblastoma is the most aggressive solid tumor of the brain. Prior studies from our lab found that carmofur, also known as 1-hexylcarbanoyl 5-fluorouracil (HCFU) is a promising candidate in suppressing and killing tumor cell lines compared to the FDA-approved drug temozolomide. Originally developed as pro-drug of 5-fluorouracil (5-FU), carmofur has been in use in clinic for the treatment of colorectal cancer for over four decades in Japan. Having it used in clinics, it has a high probability of repurposing for diseases with no cure such as glioblastoma. Carmofur has also been found effective against other cancers such as head and neck, breast, cervical, pancreatic, gastrointestinal, ovarian, bladder, gastric, and solid tumors of the brain. Several recent studies also found carmofur efficacious against Krabbe disease, lipopolysaccharide-induced acute lung injury and as a potential lead inhibitor of the main protease (M^{PRO}) of SARS-CoV-2 etc. However, there is no efficient analytical method for the qualitative and quantitative bioanalysis of carmofur to support further pre-clinical and clinical studies.

First, we have described the development of a liquid-liquid extraction technique to extract carmofur from mouse plasma. We have also developed a sensitive and accurate LC-MS/MS method to quantify carmofur in mouse plasma with an application to a pharmacokinetic study. The C_{max}, T_{max}, and $T_{1/2}$ was found 10.28±1.53 $\mu g.mL^{-1}$, 5 min, and 9.6 min respectively.

Second, we performed a LC-MS/MS based parallel artificial membrane permeability assay (PAMPA) to understand the membrane and blood-brain-barrier (BBB) permeability of two compounds, carmofur and ARN14988-M, a potential metabolite of ARN14988, another promising acid ceramidase inhibitor. Our study indicates that both analytes are likely to cross BBB through passive diffusion which is an important consideration to drugs targeting glioblastoma.

Third, we have developed an analyte extraction technique to simultaneously extract carmofur and 5-FU. We also validated a LC-MS/MS method to quantify carmofur and 5-FU in mouse brain, liver, and kidney tissues after intraperitoneal injection of carmofur solution. Carmofur was found to cross the BBB which confirms our observations from in vitro study described in chapter 3.

Carmofur also immediately distributes among the tissues with a T_{max} of 5 min. T_{max} for 5-FU was found 20 min in mouse plasma, brain, kidney, and 40 min for liver.

Lastly, we used imaging mass spectrometry (MALDI-TOF-MS) to understand the spatial distribution of carmofur/5-FU in mouse brain. We found that carmofur distributes itself throughout the brain tissue which is important for glioblastoma drug development given that the tumor can grow any location of the brain.

To

My parents for their endless contributions to my life

&

My wife for being the positive reinforcement in my life.

TABLE OF CONTENTS

LIST OF FIGURES

LIST OF TABLES

LIST OF ABBREVIATIONS

%CV	percent coefficient of variance
2-PA	2-picolinic acid
3-HC	3-hydroxycoumarin
5-CU	5-chlorouracil
5-FU	5-fluorouracil
5'-FUMP	5-fluorouridine-5'-monophosphate
9-AA	9-aminoacridine
ACN	acetonitrile
APCI	atmospheric pressure chemical ionization
ARC	Lapham animal resource center
ASAH1	acid ceramidase
AUC	area-under-the concentration-time curve
BBB	blood-brain barrier
BCS	biopharmaceutical classification system
C18	octadecyl silyl
C8	octyl
CE	collision energy
CHCA	α-cyano-4-hydroxycinnamic acid
CID	collusion-induced dissociation
CL	clearance
C_{max}	the maximum drug concentration

CMEFU	1-(carboxymethylcarbamoyl)-5-fluorouracil
CNS	central nervous system
COVID-19	novel coronavirus disease-2019
CPEFU	1-(carboxypentylcarbamoyl)-5-fluorouracil
CPRFU	1-(carboxypropylcarbamoyl)-5-fluorouracil
DC	direct current
DESI	desorption electrospray ionization
DHAP	2’,6’-dihydroxyacetophenone
DHB	2,5-dihydroxybenzoic acid
DHFU	5,6-dihydro-5-fluorouracil
DL	desolvation line
DMSO	dimethyl sulfoxide
DUIS	dual source ionization
EGFR	epidermal growth factor receptor
ESI	electrospray ionization
f	bioavilability/fraction of the drug administered available systemically
FAAH	fatty acid amide hydrolase
FBAL	α-fluoro-β-alanine
FDA	Food and Drug Administration
F-dUMP	5-fluoro-2'-deoxyuridine-5'-monophosphate
FGPA	α-fluoro-β-guanidopropionic acid
FUDR	5-fluoro-2'-deoxyuridine

FUPA	α-fluoro-β-ureidopropionic acid
FUrd	5-fluorouridine
GALC	galactosylceramidase
GLD	globoid cell leukodystrophy
HCFU	1-hexylcarbamoyl-5-fluorouracil
HHCFU	1-(5'-hydroxyhexylcarbamoyl)-5-fluorouracil
HQC	high quality control
IACUC	institutional animal care and use committee
IDH	Isocitrate dehydrogenase
IS	internal standard
LAESI	laser ablation electrospray ionization
LC-MS	liquid chromatography-mass spectrometry
LC-MS/MS	liquid chromatography-tandem mass spectrometry
LD_{50}	median lethal dose
LDI	laser desorption ionization
LLE	liquid-liquid extraction
LOD	limit of detection
LOQ	limit of quantification
LQC	low quality control
MALDI	matrix-assisted laser desorption/ionization
MARG	microautoradiography
MGMT	methylguanine-DNA methyl-transferase

M^{pro}	main protease
MQC	medium quality control
MRM	multiple reaction monitoring
MSI	mass spectrometry imaging
NAAA	N-acylethanolamine
NIMS	nanostructure initiator mass spectrometry
NOS	not otherwise specified
OHCFU	1-(5'-oxohexylcarbamoyl)-5-fluorouracil
OS	overall survival
PAMPA	parallel artificial membrane permeability assay
Papp	apparent permeability
PBS	phosphate buffered saline
PDGF	platelet-derived growth factor
PET	positron emission tomography
PFS	progression-free survival
PTEN	phosphate and tensin homolog
QC	quality control
QqQ	triple quadrupole
R^2	correlation coefficient
Rf	radio frequency
S/N	signal-to-noise
S1P	sphingosin-1-phosphate

SA	sinapinic acid
SHH	sonic hedgehog
SIMS	secondary ion mass spectrometry
SLN-carmofur	solid lipid nanoparticle loaded with carmofur
SRM	selected reaction monitoring
$T_{1/2}$	elimination half life
TFM	tissue freezing medium
THAP	2,4,6- trihydroxyacetophenone
TLC	thin layer chromatography
T_{max}	time to reach maximum drug concentration after administration
TOF	time of flight
TS	thymidylate synthase
UPLC	ultra-performance liquid chromatography
UV	ultraviolet
UWM	University of Wisconsin-Milwaukee
V_d	volume of distribution
VEGF	vascular endothelial growth factor
WBA	whole-body autoradiography
WHO	World Health Organization

ACKNOWLEDGEMENTS

Becoming a researcher was a childhood dream of mine. I always wanted to become a scientist. I am thankful that I had the opportunity to pursue Ph.D. at the University of Wisconsin-Milwaukee (UWM). The challenges that came along with my Ph.D. project has shaped my understanding of research and helped me to grow as a researcher. The memories from the lab will accompany me in days to come.

The over 5-years journey would been impossible without the support and assistance of my supervisor Professor Shama P. Mirza. I express my sincere gratitude for giving me the opportunity to work in her lab and for the guidance over time. Working with Professor Mirza was an intellectually benefiting experience for me.

My thesis committee members were a great resource for me in the path of completion of this thesis. I would like to thank Professor Alexander Arnold, Professor Ava Udvadia, Professor Nicholas Silvaggi, and Professor Xiaohua Peng for their help and suggestions. I would also like to thank Dr. Anna Benko for teaching me various instruments in the Shimadzu mass spectrometry facility. I would like to acknowledge the contribution of all faculties with whom I have taken a course especially Professor Joseph Aldstadt, Professor Shama Mirza, Professor Alexander Arnold, Professor Nicholas Silvaggi, Professor Xiaohua Peng, Professor James Cook, and Professor Alan Schwabacher at UWM that shaped my knowledge of chemistry.

I would like to thank all my co-workers, the present and past members of the Mirza group, members of the Udvadia group, members of the Arnold group, the chemistry department support staff, and the welcoming Bangladeshi community in Milwaukee for their consistent

cooperation over time, especially I would like to thank M S Rashid Roni, Vilashini Rajaratnam, and Ethan Frank Kub.

I would also like to extend the gratitude to Prof. Md. Aslam Hossain and Prof. Mohammad Rashedul Haque from the University of Dhaka who encouraged and supported me to pursue a Ph.D.

I would not have become what I am today without the lifelong dedication and support from my parents, maternal grandparents, and my maternal uncle who was there whenever I needed anything towards the path of educating myself.

Finally, I would like to thank my wife Sadia Noosrat Boshra for her unconditional support and positive reinforcement in my life.

Chapter 1-Introduction and Background

1.1. Introduction to Glioblastoma

Glioblastoma is the most aggressive and the most common malignant primary tumor of the brain[1]. According to 2016 CNS WHO, there are three general forms of the disease, and they are i) glioblastoma, IDH (isocitrate dehydrogenase-wildtype) ii) glioblastoma, IDH mutant and iii) glioblastoma, not otherwise specified (NOS). IDH-wildtype glioblastoma involve majority (almost 90%) of the cases and are considered as primary glioblastoma, affecting preferentially the older population. The IDH-mutant form of the disease is known as secondary glioblastoma and entails about 10% of the cases. Unlike primary glioblastoma, the secondary glioblastoma are tumors that develop from a lower-grade glioma and affects predominantly younger population. The World Health Organization (WHO) also categorized all forms of glioblastoma as grade IV glioma which designates it as the most advanced and most deleterious form of all the solid brain tumors originating from the glial or astrocytic cell lineage[2].

Every year over 10,000 new cases are reported in the United States, accounting for about 54% of all malignant central nervous system (CNS) tumors in adults[3-4]. The incidence of glioblastoma can occur at any age. However, it is observed at a higher rate in elderly, males, and non-Hispanic white population[4]. Despite being the deadliest CNS tumor, the treatment options are limited, and the disease remains incurable even with multidisciplinary therapy. Patients diagnosed with glioblastoma are treated with a combination of surgery, radiotherapy, chemotherapy and in some cases with tumor treating field. Yet, the median survival is just about 14.6 months, and 5-

year survival are observed in only about 5 percent of the patients. Almost all patients develop recurrence of the tumor[3, 5-6].

Currently, three chemotherapeutic agents (temozolomide, bevacizumab, and carmustine) are available to patients with glioblastoma[7-8]. Results from randomized clinical study in 573 patients demonstrate that addition of temozolomide to radiotherapy significantly increases overall survival (OS) (27.2% vs 10.9% in radiotherapy alone at 2 years). The same study found that O6-methylguanine-DNA methyl-transferase (MGMT) gene methylation is a positive prognostic indicator for temozolomide chemotherapy for newly diagnosed patients[9]. On the other hand, bevacizumab is an anti-VEGF (anti-vascular endothelial growth factor) monoclonal antibody that has been approved by the FDA for the treatment of recurrent glioblastoma. It has been clinically observed that bevacizumab has anti-glioma activity with improvement in progression-free survival (PFS); however, it has no significant activity in terms of OS[10]. A clinical trial on newly diagnosed glioblastoma patients with bevacizumab has shown no significant improvement in terms of OS but has shown longer PFS compared to placebo group (10.7 months vs 7.3 months)[11]. Previously, carmustine, a nitrosourea compound, which is used in the treatment of the disease, is now avoided for clear demonstration of severe bone marrow, liver and kidney toxicity[5]. However, local delivery of carmustine in the form of implant in the resection cavity followed by surgery can reduce systemic adverse events and can improve median survival of the patients both in recurrent and newly diagnosed glioblastoma[12].

Currently, significant effort is ongoing to introduce better therapeutic drug against glioblastoma. Between January 2017 and December 2019, the data of 62 clinical trials of major drugs and biologicals were published, revealing both somewhat encouraging and not-so-encouraging

outcomes. In March 2020, we listed a total of 286 ongoing clinical trials as registered on www.clinicaltrials.gov[3]. Among the drug targets IDH mutation, Notch pathway, VEGF signaling pathway, Platelet-derived Growth Factor (PDGF) signaling, Epidermal Growth Factor Receptor (EGFR) Pathway, PI3K/AKT/mTOR Pathway, Phosphate and Tensin Homolog (PTEN) Signaling, Sonic Hedgehog (SHH) signaling are some of the extensively studied[3]. Given the extremely heterogeneous nature of the tumor, it is imperative to search for new therapeutic targets and their inhibitors.

1.2. Introduction to Acid Ceramidase

One key concept in cancer research is molecular target-based development of chemotherapeutic agents. Targeting a specific component of molecular signaling pathways can lead to effective drug discovery. The Mirza lab has previously performed comprehensive characterization of glioblastoma tumor tissues for biomarker identification using mass spectrometry based quantitative proteomics[13-14]. Studies found that patient derived glioblastoma tumors and irradiated cell cultures express significantly higher level of acid ceramidase (ASAH1) and lower level of its substrate, ceramides[15-16]. Comprehensive proteomic analysis has also revealed that expression of ASAH1 is associated with poor patient survival. Additionally, acid ceramidase inhibitors were able to kill the tumor cell lines in vitro more efficiently than the currently available standard drug, temozolomide[15, 17].

ASAH1 is a lysosomal hydrolase enzyme that regulates the sphingolipid pathway in the cells. It metabolizes ceramides and breaks them down into sphingosine which further phosphorylates into sphingosine-1-phosphate (S1P) by sphingosine kinase 1 or 2. The relative level of ceramides

and S1P determines the fate of the cell, whether it will undergo apoptotic cell death or survival and proliferation. Accumulation of ceramides leads to cell death while accumulation of S1P leads to survival and proliferation of the cancer cells[15]. Higher expression of acid ceramidase has been observed in a number of cancer diseases such as prostate, head and neck, breast, ovarian, colon, liver, melanoma, acute myeloid leukemia and solid brain tumors[18-19]. Nevertheless, acid ceramidase is also accountable to other diseases such as Niemann-Pick disease, Farber disease, Alzheimer's disease and insulin resistance[19].

1.3. Previous studies with carmofur

1.3.1. Acid ceramidase inhibition in brain diseases

Our group became interested in carmofur (figure 1-1) because of its acid ceramidase inhibition activity. Systemic administration of carmofur in mice produced ASAH1 inhibition in a dose-dependent manner[20]. Thus, it became a drug of choice in brain tumor study. Carmofur was found effective with low IC_{50} (13-104 μM) at targeting brain tumor cell lines[15, 17]. Additionally, it was also found to be more sensitive in killing the tumor cells compared to the food and drug administration (FDA) approved drug temozolomide which is the standard chemotherapeutic agent for the treatment of glioblastoma. Annexin-V-Alexa-488 staining and mass spectrometric analysis suggested that tumor cell undergo apoptosis and higher intracellular accumulation of ceramides upon carmofur treatment[15]. Carmofur in combination with humanized monoclonal antibody was also found effective in suppressing glioblastoma cell growth both in newly diagnosed and recurrent diseases[16]. The cell lines that were tested with carmofur include glioblastoma cells (SJGBM2, SJGBM2-10gy, CHLA200, U87, U87-10gy, GSC 22, GSC 33, GSC 44),

medulloblastoma cells (CHLA259), and atypical teratoid rhabdoid tumor cells (CHLA266)[21]. Another acid ceramidase inhibitor, ARN14988 (figure 1-2) was also found effective for inhibiting the glioblastoma tumor cell lines[17].

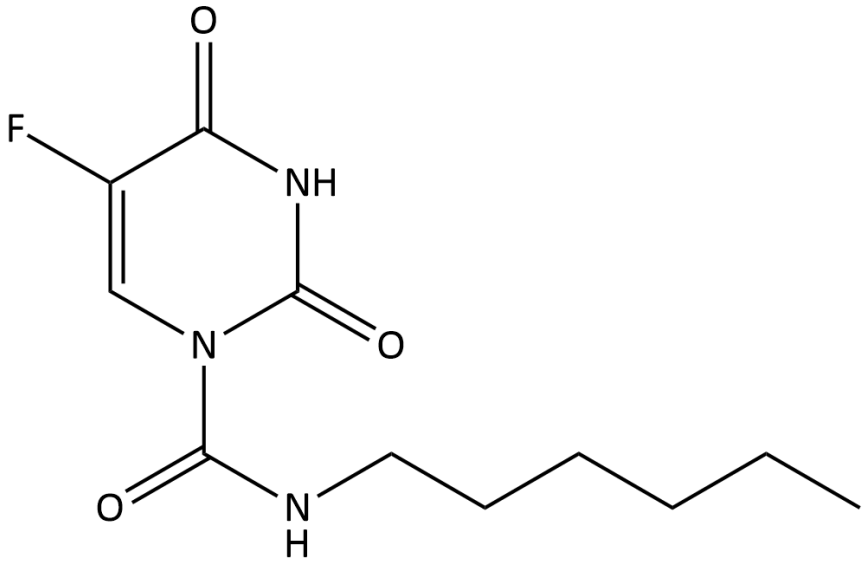

Figure 1-1. Structure of carmofur.

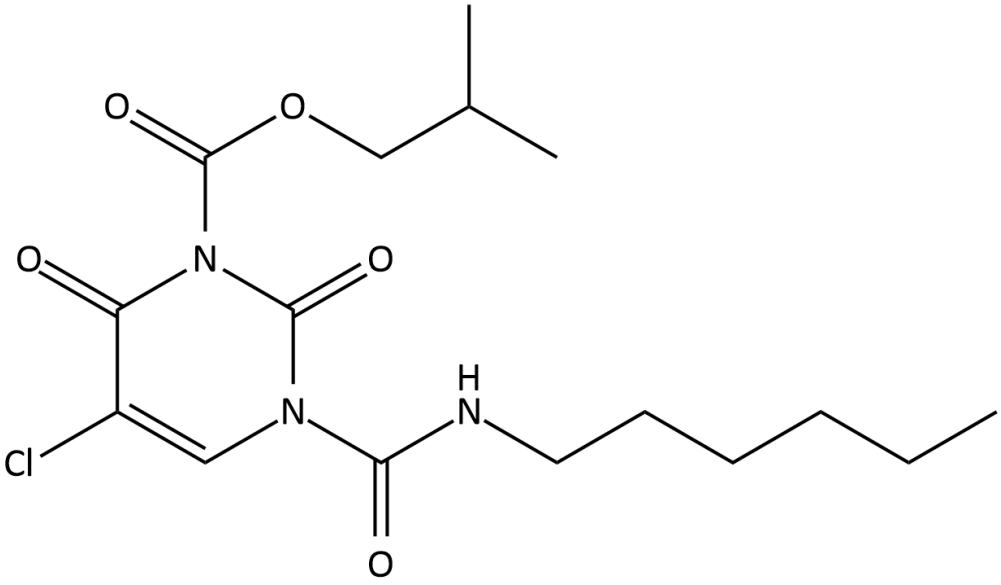

Figure 1-2. Structure of ARN14988.

More studies found that elevation of ceramide level by carmofur therapy could be a potential therapy in Parkinson's disease and dementia with lewy bodies where synucleinopathies linked to GBA1 (acid beta-glucosidase) mutations is a drug target[22]. Since acid ceramidase is overexpressed in a number of cancers, it is likely that carmofur would be beneficial in treating those cancers as well.

Dementiev et al. studied the molecular mechanism of inhibition of acid ceramidase by carmofur[23]. Initially it was perceived that the active metabolite of carmofur which is 5-FU is responsible for the anticancer properties of the molecule. They solved the crystal structure of the active human acid ceramidase in complex with carmofur. The detailed mechanism of acid ceramidase inhibition by carmofur resolved the unexplained 5-FU-independent antitumor activity. They found that the catalytic cysteine 143 (Cys143) of ASAH1 attacks the carbonyl group of carmofur and therefore, releases 5-fluorouracil forming a covalent interaction between the Cys143 residue and the hexylcarbamate group of carmofur. The fatty acid tail of carmofur occupies a hydrophobic cavity close to the enzyme active site after catalytic cleavage of the compound. The other electrostatic interactions observed were hydrogen bonds between Asp162, Glu225 and Asn320 with the carbonyl and amide groups of the free fatty acid tail. An extended conformation also found the fatty acid moiety sandwiched between the side chains of Phe136, Phe163, Met161, Leu211, and Leu223[23].

1.3.2. Breast cancer

Earlier results of objective response in breast cancer inspired Morimoto et al. to study the postoperative adjuvant use of carmofur in early breast cancer patients[24-25]. They observed an

overall survival rate of 90% among the patients (N=100) receiving carmofur compared to 88% in the patients (N=50) receiving standard carboquone. Although a slightly higher degree of second malignancy observed, no neurotoxicity, liver dysfunction or change in transaminase level were observed; making carmofur an apparent beneficial treatment in adjuvant therapy[24]. Another study from 2004 investigated the efficiacy of carmofur + cyclophosphamide + tamoxifen (HCT group) vs. CMF + tamoxifen (CMFT group) as adjuvant therapy in early breast cancer cases with 3 or lower metastatic lymph nodes. They found no significant differences in the 5-year overall survival and the 5-year disease-free survival between the two groups. Although the total number of adverse events in two groups were not significantly different, the 3-months quality of life declined significantly in the CMFT group suggesting HCT therapy as a possible replacement to CMFT therapy in early breast cancer[26].

1.3.3. Cervical cancer

Carmofur was studied for its recurrence prevention efficacy in cervical adenocarcinoma patients in a multicenter control study where patients received 300 mg/day of the drug postoperatively for a period of two years. Patients who received carmofur showed a better cumulative survival rate and disease-free survival rate compared to control group that received no adjuvant chemotherapy[27]. Later on, Liu et al. studied the efficacy of carmofur against immortalized (HeLa and Caski) and patient-derived cervical cancer cell lines. They noticed anti-growth and anti-metastasis potential of carmofur both in time (0-48 hours) and dose-dependent (0-1 μg/mL) manner. Carmofur treatment of the cell lines also demonstrated a down-regulation of intranuclear β-catenin, c-Myc, and TCF-1, but no impact on intracytophasmic β-catenin

expression which explains that carmofur perhaps blocks the Wnt/β-catenin pathway in order to suppress the cervical cancer in vitro[28].

1.3.4. Covid-19

Very recently carmofur has come into attention as a lead compound for the novel coronavirus disease 2019 (COVID-19) because of its inhibitory activity against the novel coronavirus SARS-CoV-2 through in silico and in vitro studies[29-32]. Anti-viral and cytotoxicity assay revealed that carmofur shows inhibitory effect against SARS-CoV-2 infection on Vero E6 cells with a selectivity index of 5.36. However, it also implies the need for a safer and more effective analog. X-ray crystallographic structure revealed that carmofur binds to the main protease (M^{PRO}) of SARS-CoV-2 where the carbonyl group is covalently bound to catalytic Cys145 and the fatty acid tail occupies the hydrophobic S2 subsite of the virus. Further studies indicated that carmofur is a non-specific inhibitor of SARS-CoV-2 M^{PRO}[33]. Given that, main protease is a common structural characteristic of all coronaviruses, it is likely that carmofur and/or it's analogs would divulge effective against other coronaviruses as well[31].

1.3.5. Colorectal cancer

The majority of carmofur studies both in vitro and in vivo were carried out on colorectal cancer. Carmofur is in use for the treatment of colorectal cancer in Japan since 1981[15]. Randomized trial in Dukes' B and C colon cancer with adjuvant carmofur therapy showed significant disease-free survival compared to the control group that received no adjuvant chemotherapy[34]. Retrospective meta-analysis also showed that carmofur adjuvant therapy significantly improved both overall and disease-free survival in patients with curatively resected color cancers[35-36]. A 10-year follow-

up study evaluated the carmofur and mitomycin C combination adjuvant therapy against mitomycin C alone. The results indicated that the combination therapy had statistically significant increase in survival compared to the mitomycin C treatment alone with no severe side effects[37]. Moreover, the 5-year disease free survival was also significantly higher with carmofur adjuvant therapy compared to the control group[38]. Another follow-up study reported that carmofur is effective in preventing the distant metastasis of colorectal cancer, explaining the increase in overall survival and disease free survival with carmofur therapy[39]. The utility of carmofur in early stage, advanced, and metastatic colorectal cancer is also confirmed by other studies[40-43].

Acid ceramidase inhibition property of carmofur is also useful in colon cancer chemotherapy. Investigations found that carmofur sensitizes human colon cancer cells to oxaliplatin and therefore, is a promising option for combination chemotherapy[44].

1.3.6. Lung diseases

A case study published in 1990 showed that chemoimmunotherapy including carmofur regressed lung adenocarcinoma and significantly prolonged the survival of the patient[45]. Very recently, Çömlekçi et al. studied solid lipid nanoparticles loaded with carmofur (SLN-carmofur) against human lung adenocarcinoma cell lines A549 and fond that carmofur induces apoptosis and kills the cancer lines in a dose-dependent manner[46]. Taken together, the clinical and in vitro studies into consideration, carmofur could be further studied for the treatment of lung cancer.

Based on the hypothesis that carmofur contains a urea group and it's inhibitor acid ceramidase shares a significant fraction of amino acid similarity with N-acylethanolamine acid amidase (NAAA), Wu et al. studied carmofur against chemically induced acute lung injury in a mouse

model. It is important to mention that NAAA and fatty acid amide hydrolase (FAAH) are two possible therapeutical targets for diseases that exhibit with inflammatory response such as acute lung injury. Their study found that carmofur is a dual inhibitor of NAAA and FAAH[47].

1.3.7. Krabbe disease

Krabbe disease, also known as globoid cell leukodystrophy (GLD) is a neurological disorder in infants. It is characterized by demyelination of nerves cells in the central and peripheral nervous system as a result of =deficiency in the lysosomal enzyme, galactosylceramidase (GALC)[48-49]. Treatment of the disease has traditionally been palliative with no cure[50]. Studies by Li Y et al. recognized that acid ceramidase is a therapeutic target for Krabbe disease. They have shown that genetic loss of acid ceramidase activity in the GALC-deficient mouse cures the disease. Further studies investigated the use of carmofur and observed that it decreases the cytotoxic glycolipid psychosine accumulation in the cells and prolongs the life span of a mouse model of the disease[49].

1.3.8. Other diseases

Kajanti MJ and Pyrhonen SO studied the efficacy of carmofur in pancreatic carcinoma. They carried out phase II clinical trial with 31 patients. The drug was given orally in 6-weeks cycle with an interval of 2-weeks between the cycles. No patients refused to continue the chemotherapy and reports of toxicity were moderate. The authors discussed another ongoing clinical trial to understand the effect of carmofur on survival but the results were not published[51].

A prospective phase II clinical trial evaluated the efficacy and tolerability of carmofur as part of a combination chemotherapy in therapy-resistant epithelial ovarian cancer. It has been observed that the overall survival has improved in about half of the patients (N=27) under study[52].

Adjuvant chemotherapy with carmofur increases cumulative survival and recurrence-free survival in patients with hepatocellular carcinoma[53-54], although the trial suspended for 12 of 67 patients because of side-effects. Therefore, the efficacy of carmofur therapy should be assessed based on its benefits on tumor recurrence, especially in patients with mild liver dysfunction[53]. Another group studied the correlation of carmofur metabolism to liver dysfunction in patients with hepatocellular carcinoma. Based on the blood level of carmofur and its major metabolites, they observed an accumulation of carmofur in cirrhotic patients which is related to the side-affects observed. Therefore, a low dose carmofur is recommended for cirrhotic patients with hepatocellular carcinoma[54].

In a study on gastric cancer, a clinical trial with carmofur monotherapy observed 19.4% response rate[55]. It is no surprise that acid ceramidase inhibitor activity of carmofur is found useful for the treatment of melanoma[56], and rectal cancer[57]. Carmofur was tried in combination with hyperthermia on Ehrlich Ascites tumor in vivo and Nakahara-Fukuoka sarcoma cells in vitro. Carmofur showed greater cytotoxicity compared to the control that did not receive hyperthermia in both in vitro and in vivo studies, and showed higher 5-FU concentrations when combined with hyperthermia[58].

It is also important to mention that carmofur has also been found effective against a lot of different ailments (figure 1-3) in recent years such as childhood ependymoma[59], anti-metastatic activity from gastric cancer xenograft[60], antifungal activity[61], therapeutic agent in photo-chemo therapy[62], and antimicrobial activity against *Staphylococcus aureus*[63] etc.

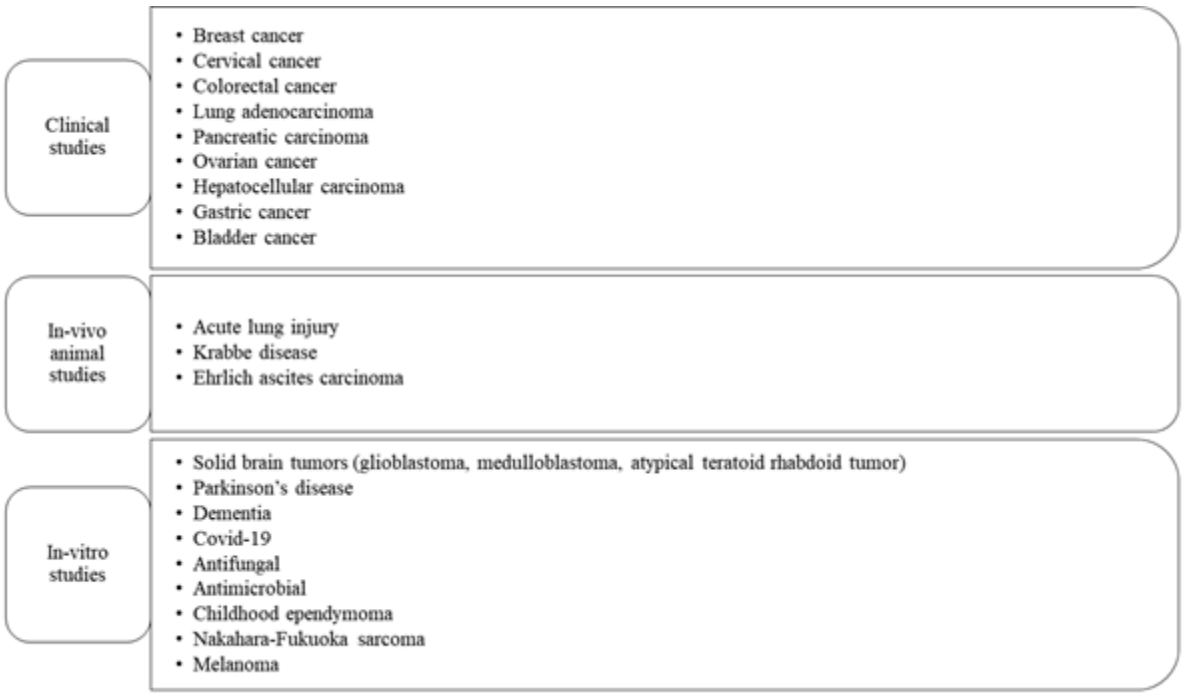

Figure 1-3. Diseases studied that are found effective upon treatment with carmofur.

1.4. Introduction to chemistry and biotransformation of carmofur

Carmofur is freely soluble in numerous organic solvents such as chloroform, acetone, dimethyl sulfoxide (DMSO) but practically insoluble in water[64]. The melting point of carmofur is 283°C[65] and the pK_a (strongest acidic) is 7.88 and the pK_a (strongest basic) is -8.30[66]. Carmofur is stable at acidic pH; however, it decomposes into 5-FU (figure 1-4) in neutral and alkaline pH (>pH 5). In phosphate buffered saline (PBS) solution, it has a half-life of just 13.1 min following first order kinetics. Domracheva et al. studied the stability of carmofur in PBS and found that the addition of 1,2-dimyristoyl-sn-glycero-3-phosphocholine (DMPC) increases its stability and thereby becomes less affected by pH[67]. Kikuchi et al. worked on improving the aqueous solubility of carmofur and thereby improving the oral and rectal bioavailability by methylated β-cyclodextrin complexation[68]. However, degradation of solid state carmofur increased due to the hygroscopic

nature of β-cyclodextrin. The authors improved its stability by the addition of organic acids such as citric, tartaric, and malic acids; thereby providing an acidic environment around the complex[69-70]. Although in vitro plasma stability study by Pizzirani et al. reported very limited stability of carmofur, Wu et al. studied biological stability in the lung tissue of mice[47, 71]. They found detectable concentration of carmofur in the lung even 8 hours after oral administration of the drug with a half-life of 45 min suggesting carmofur a suitable drug for systemic administration[47]. Carmofur is more lipophilic than it's active counterpart 5-FU and has a lipophilic index of 41.90 which is 92 times higher than tegafur, another commonly used 5-FU derivative[72].

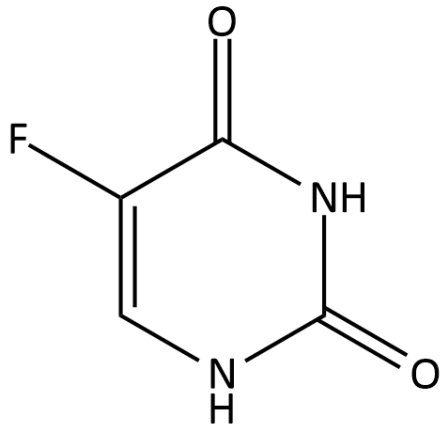

Figure 1-4. Structure of 5-FU.

1.4.1. Synthesis

Two principal routes of synthesis of carmofur are available in the literature. In both methods, 5-FU is used as the starting material. Method 1 was developed by Ozaki et al. who is also the inventor of the drug. In this method, hexyl isocyanate and 5-FU (0.15 mol to 0.10 mol ratio) is heated in 40 mL of pyridine at 90°C for an hour, followed by cooling down to room temperature. After evaporation of 30 mL of pyridine (50°C and reduced pressure), 50 mL of ethanol is added

to the resulting residue at 55°C which is kept at 0-5°C overnight and crystalline carmofur is obtained[73-74]. Method 2 involves N-formylation of 5-FU in presence of aqueous formaldehyde, which follows oxidation by potassium bromate and condensation with hexyl-amine to form carmofur[75-76]. The details of two routes are shown in figure 1-5.

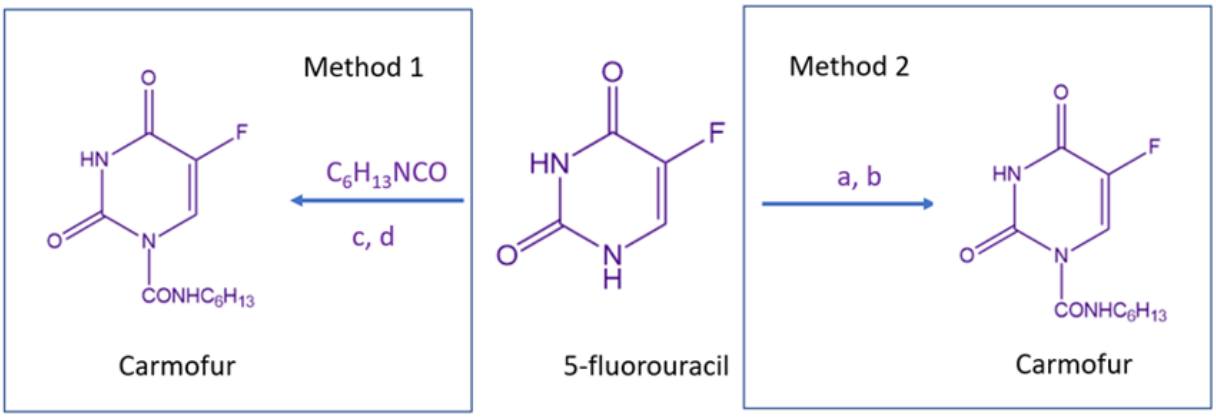

(a) HCHO, 55°C, 6 hr (b) $KBrO_3$, 80°C, then $H_2N(CH_2)_5CH_3$, DCC, MeCN, 0°C to RT, 6 hr
(c) Pyridine, 90°C, 1 hr (d) Ethanol, 0-5°C, overnight

Figure 1-5. Synthesis of carmofur[75-76].

1.4.2. Pharmacokinetics and metabolism

Pharmacokinetics of carmofur is species specific and can differ to some extent in their rate of absorption and excretion based on the model under study[77]. However, a study using ^{14}C radioactive carmofur and 5-FU demonstrated that carmofur was found rapidly absorbed and reached highest tissue concentration within 1-3 hour of oral administration, whereas it was only 0.5 hour for 5-FU in rats. Equimolar administration of the ^{14}C-carmofur and ^{14}C-5-FU indicated that the pyrimidine ring in carmofur degrades slowly and therefore, unchanged 5-FU was detected for a longer period of time (>5 hr) for carmofur than it is for ^{14}C-5-FU[78]. Ooi et al. studied

the plasma level of 5-FU after oral administration of carmofur in mice. They measured the highest plasma level of 5-FU at 30 min after treatment and then disappeared rapidly from plasma[79]. Distribution of carmofur has been observed among all the major body organs and tissues including kidney, lung, liver, intestines, pancreas, spleen, gastro-intestinal wall, urinary bladder, and bone marrow etc. Carmofur has also been observed to cross the blood-brain barrier and distribute itself in brain compartment which can be attributed to the lipophilic aliphatic tail of the compound however, to what extent is not well understood[80].

About 90% of the drug was found to be excreted through urine within 48 hours of administration, some into the air, and a very low amount in the feces[78, 81]. The peaks for carmofur were observed between 1-2 hours in human and a half-life about 2 hours. In addition, the peak concentration for the metabolite 5-FU appeared at the same time[82].

A total of 14 metabolites (table 1-1) of carmofur has been identified from human and other animals by radiolabeling the compound. The metabolic pathway involves oxidation and scission of the side chain and the consecutive degradation of the active metabolite 5-FU. The two main routes to oxidation reported are ω-oxidation and ω-1-oxidation. The details of the major metabolites are available in table 1. Among the metabolites, 5-FU is a well-known anticancer drug. Hoshi et al. observed the antitumor and inhibitory activity of CPEFU, CPRFU, HHCFU, OHCFU against L1210 leukemia in vivo and L5178Y lymphoma in vitro[83]. Although they have anticancer activity, at the same time CPEFU and CPRFU are the principal suspect for adverse events associated with carmofur therapy[84].

Entry	Metabolite Name	Abbre-viated Syno-nym	Biological specimen	Experimental model	Reference
1	5-Flurouracil	5-FU	Plasma, serum, tumor, urine, liver, kidney	Dog, mouse, Human, rat, rabbit	77-78, 81, 85-88
2	1-(5'-oxohexylcarbamoyl)-5-fluorouracil	OHCFU	Serum, plasma, urine, liver, kidney	Human, rat, rabbit, dog, mouse	77, 87, 89
3	1-(5'-hydroxyhexylcarbamoyl)-5-fluorouracil	HHCFU	Plasma, serum, urine, liver, lung, kidney	Human, rat, rabbit, dog, mouse	77, 87-89
4	1-(carboxypentylcarbamoyl)-5-fluorouracil	CPEFU	Plasma, serum, tumor, urine, liver, kidney	Human, rat, rabbit, dog, mouse	77-78, 85, 87, 90
5	1-(carboxypropylcarbamoyl)-5-fluorouracil	CPRFU	Plasma, serum, tumor, urine, liver, kidney	Human, rat, rabbit, dog, mouse	77-78, 85, 87-88, 90
6	1-(carboxymethylcarbamoyl)-5-fluorouracil	CMEFU	Plasma, urine	Human, mouse	81, 90

7	5,6-dihydro-5-fluorouracil	DHFU	Urine, plasma, liver, lung, kidney	Mouse	[81, 87-88]
8	α-fluoro-β-alanine	FBAL	Urine, plasma, liver, lung, kidney, small intestine	Mouse, rat, rabbit, dog	[77-78, 81, 87-88]
9	α-fluoro-β-ureidopropionic acid	FUPA	Liver, lung, kidney, plasma	Mouse, rat	[78, 87]
10	α-fluoro-β-guanidopropionic acid	FGPA	Plasma	Mouse, rat	[78, 87]
11	5-fluorouridine	FUrd	Small intestine	Mouse	[87]
12	5-fluoro-2'-deoxyuridine	FUDR	-	Mouse	[87]
13	5-fluorouridine-5'-monophosphate	5'-FUMP	Liver	Mouse	[87]
14	5-fluoro-2'-deoxyuridine-5'-monophosphate	F-dUMP	Liver	Mouse	[87]

Table 1-1. Metabolites of carmofur.

1.5. Introduction to analytical techniques

This thesis utilizes chromatographic and mass spectrometry-based techniques because of their high sensitivity and selectivity for identifying and quantifying analytes in complex matrices. We used hyphenated technique such as liquid chromatography and mass spectrometry (LC-MS) wherein Shimadzu Nexera X2 ultra-performance liquid chromatography (UPLC) interfaced with a Shimadzu 8040 triple quadrupole mass spectrometer for quantifying in vitro and in vivo samples. The coupling of liquid chromatography with a mass spectrometric detector has become a gold standard technique for bioanalysis. We also used a Shimadzu 7090 MALDI-TOF-TOF-MS instrument to understand the spatial distribution of carmofur.

1.5.1. Liquid chromatography-mass spectrometry

The history of chromatography goes back to early twentieth century when Russian botanist Mikhail Tswett first separated plant pigments on a calcium carbonate column by passing petroleum ether through it. He first coined the term 'chromatography' (Greek for 'color') in 1906[91-92]. Chromatography separates analytes from one another, aids to their qualification and quantification. There are two principal components in an ideal chromatographic technique: the stationary phase and the mobile phase. The stationary phase consists of static particles fixed inside a chromatography column while the mobile phase (either gas or liquid) passes through the column and separates the analytes from one another. Based on the interaction of the analyte molecules with the stationary phase, the chromatographic techniques are classified in different types such as adsorption chromatography, partition chromatography, affinity chromatography

etc[93]. Liquid chromatography is a type of adsorption chromatography named after the physical state of the mobile phase used.

A reversed phase liquid chromatography is a technique that utilizes a less polar stationary phase compared to the mobile phase. A chemically bonded phase such as octadecyl silyl (C18), octyl (C8) etc. are linked to the porous silica packing material to form the reserved-phase column. The type of bonded phase used is based on the selectivity and retention desired. In our study, we used a C18 column, because of the long hydrophobic carbon chain, with greater retention.

There are considerable number of mobile phase solvents that are available to use in liquid chromatography. However, the choice of mobile phase is limited when the liquid chromatographic system is coupled with mass spectrometry. Only mass spectrometry compatible volatile mobile phase reagents and mobile phase modifiers are used.

Typically, liquid chromatography starts with the pumps that continuously delivers the mobile phase at a fixed flow rate. Our instrument consists of a binary system and can deliver two different solvents at a time. The solvents pass through a degassing unit and then gets mixed. An autosampler injector is used to introduce the sample to the mobile phase flow without interrupting it. The analytes are then introduced to the column as a thin band. The column is kept inside an oven. Based on the interaction between the analytes and the column stationary phase, the analytes get separated. The analyte that has a greater preference for the stationary phase is retained longer and hence, elutes out slowly from the column. The eluent then goes through the detector, in our case the mass spectrometer. Herein, it is necessary to mention that our liquid

chromatographic system is equipped with Shimadzu LC-30AD pumps, Shimadzu DGU-20A 5R degassing units, Shimadzu SIL-30AC MP autosampler and Shimadzu CTO20A column oven.

Likewise, the history of mass spectrometry goes back to early twentieth century with the characterization of positive rays by J. J. Thompson. Since then, there has been a substantial advancement made both in terms of instrumentation and applications[94]. Mass spectrometers work on gaseous state and can only detect ions based on their mass over charge (m/z) ratio. The mass spectrometer has three basic components: i) ionization source ii) mass analyzer iii) detector[95].

The samples that are coming from the liquid chromatography needs to be brought into gas-phase ions first. The Shimadzu 8040 instrument has two different ionization sources, the electrospray ionization (ESI) and the atmospheric pressure chemical ionization (APCI). Both ionization techniques ionize analytes at atmospheric pressure.

ESI is a soft ionization technique. The advancement of ESI has revolutionized the world of mass spectrometry-based analysis. It uses the least amount of energy needed to ionize the analyte and is applicable toward a wide range of polar molecules such as small drug molecules to big biomolecules. The liquid sample is passed through a charged capillary and is sprayed into a charged aerosol. A nebulizing gas, N_2 is used to assist the process. The capillary is charged in either positive or negative mode based on the type of ions desired and to exclude the opposite charged ions. The charged droplets become desolvated with the help of a drying gas (usually heated nitrogen) and eventually get disintegrated into charged analytes in their gas phase which finds its way towards the mass analyzer[95].

Comparably, atmospheric pressure chemical ionization (APCI) is also a soft ionization technique but slightly stronger than ESI and occurs at atmospheric pressure outside the vacuum. Similar to ESI, the eluent from LC is passed through a capillary, although, it is not charged. The sample is vaporized using a N_2 nebulizing gas and by applying heat. A corona discharge needle is used to aid the ionization. Voltage is applied to the needle to produce corona discharge. Electrons coming out of the discharge ionizes the reagent gases such as N_2 or solvent molecules. Ionization of the reagent gases generates a series of reactions and eventually ionizes the analyte molecules. The ions produced are usually protonated ($[M + H]^+$) or deprotonated ($[M - H]^-$) ions in positive and negative mode, respectively. However, other ions such as $[M]^+$ and $[M]^-$ can also form in APCI[94-95]. One advantage of using Shimadzu LCMS 8040 instrument is that it has dual ionization mode where ESI and APCI can be executed simultaneously.

Upon ionization, the ions are separated based on their m/z (mass-to-charge ratio) in a mass analyzer which is the second component of the mass spectrometer. Traditionally, mass analyzers are divided into two groups: the beam analyzer and the trapping analyzer. The choice of mass analyzer depends on the resolution, mass accuracy, sensitivity, and the desired range of scanning. Our work utilized quadrupole mass analyzer. It's small size, low cost, and the ability to use in tandem makes it very useful in laboratory setting; however, it suffers from low resolution. Quadrupole mass analyzers consist of four rods in parallel to each other. Radio frequency (Rf) and direct current (DC) voltages are applied to each rod. Ions are scanned by changing the intensity of the Rf and DC voltages so that the ions of different m/z can sequentially reach to the detector[95].

Now-a-days, multiple mass analyzers are used in tandem to have broader applications and use. The LCMS 8040 instrument is a triple quadrupole (QqQ) instrument which means there are three quadrupoles in series to scan the analytes (figure 1-6 and 1-7)). In a typical QqQ instrument, the first quadrupole acts as a precursor ion scanner while the second quadrupole acts as a collusion chamber and the third quadrupole is used to scan the product ions. A neutral gas such as argon (Ar) is used as the collusion-induced dissociation (CID) gas. The advantage of having a triple quadrupole mass spectrometer is it's ability to develop a selected reaction monitoring (SRM) or multiple reaction monitoring (MRM) method with greater selectivity when multiple compounds generate ions with similar m/z[96]. Now-a-days they hybrid hyphenated techniques such as LC-ESI-QqQ-MS has a core instrument in small molecule, peptide and proteomics research[94]

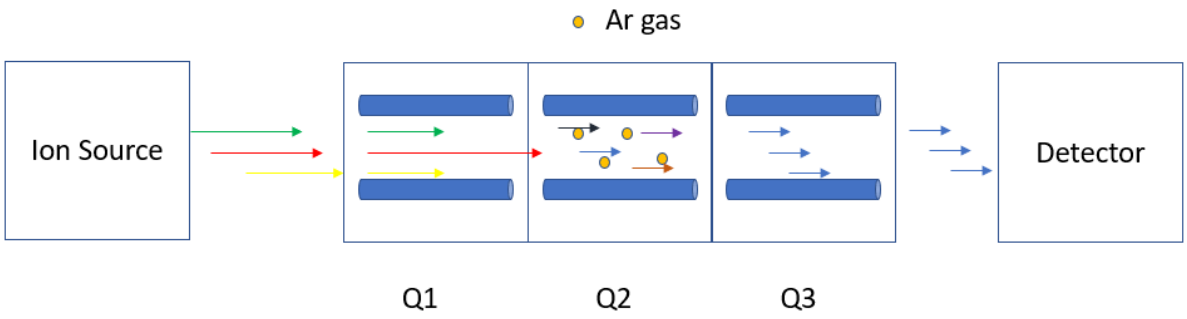

Figure 1-6. A triple quadrupole mass spectrometer in selected/multiple reaction monitoring mode.

The separated ions are detected with a photo-multiplier or electron-multiplier detector. In our case, we used an electron-multiplier detector. The detected ions generate an intensity vs. m/z spectrum with is translated in a computer system. We used LabSolutions software for operating the instrument such as data acquisition as well for post-run data analysis.

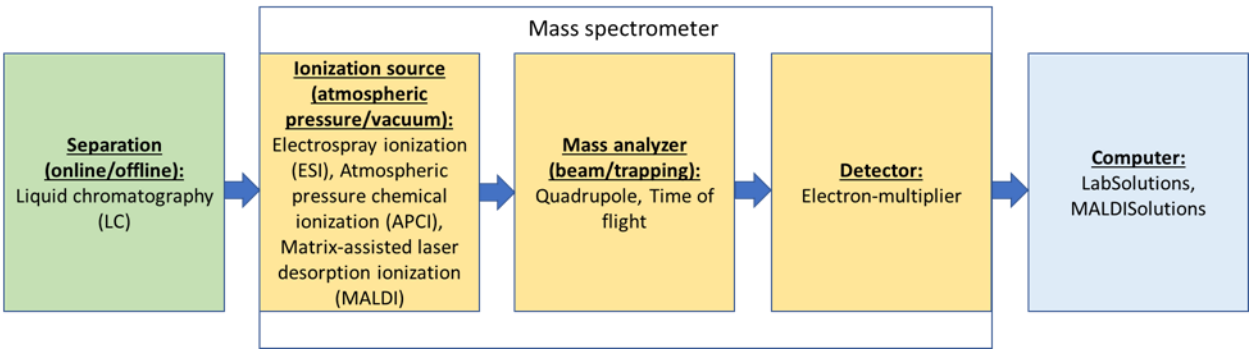

Figure 1-7. Basic components of the instruments used in this thesis.

1.5.2. Matrix-assisted laser desorption/-ionization (MALDI) mass spectrometry

The other type of mass spectrometric technique that is made use of in this thesis is matrix assisted laser desorption/-ionization (MALDI) mass spectrometry. The advantage of MALDI is that it requires minimal sample clean-up and can withstand the presence of certain buffers and salts not possible by other techniques[97]. The analyte is co-crystallized with a matrix substance in a stainless-steel plate which is inserted inside the vacuum for analysis. The matrix-substances are small organic molecules with high ultra-violet absorptivity at the wavelength of the laser. Depending on the matrix substance, MALDI can ionize small drug substances, metabolites, lipids, peptides, proteins etc[98].

The steps in ionization can be divided into three steps: i) irradiation of the analyte-matrix solid with laser ii) desorption of analyte-matrix iii) desolvation and ionization. Being a soft ionization technique, MALDI usually generates protonated or deprotonated molecular ion peaks, making their use in intact protein analysis[94, 99].

Having the pulsed nature of the MALDI, the appropriate mass analyzer is Time of Flight (TOF). Ions are accelerated by applying the same acceleration voltage and their flight time in a drift tube

is measured. The time of flight of the ions from the beginning of the mass analyzer to the detector is a function of it's m/z and therefore, the ions with low m/z travels faster and arrives the detector first. A wide range of ion masses can be scanned using TOF at a high resolution. Nevertheless, it has poor precursor ion selectivity[94-95].

There are two modes for data acquisition in MALDI-TOF 7090 instrument: i) linear and ii) reflectron. In linear mode, the ions travel a straight path towards the detector. On the contrary, ion mirrors are used in reflectron mode to increase the flight distance and therefore, to increase the resolution[94].

Besides proteomics, MALDI-TOF-MS is gaining increased popularity in drug development research for it's ability to perform mass spectrometry imaging (MSI). Conventional LC-MS/MS based techniques provides accurate quantification of drug and metabolites in plasma and tissues. However, no information on their distribution inside a tissue is obtained. On the contrary, MALDI-TOF-MS based techniques gives a clear visualization of the spatial distribution of analytes in a target organ. Therefore, MALDI MSI has earned a lot of interest in drug development research for it's label free biomarker identification and ability to demonstrate tissue localization of drugs without compromising the structure and organization of the tissue sections[100].

References

1. Tan, A. C.; Ashley, D. M.; López, G. Y.; Malinzak, M.; Friedman, H. S.; Khasraw, M., Management of glioblastoma: State of the art and future directions. *CA: A Cancer Journal for Clinicians* **2020,** *70* (4), 299-312.
2. Louis, D. N.; Perry, A.; Reifenberger, G.; von Deimling, A.; Figarella-Branger, D.; Cavenee, W. K.; Ohgaki, H.; Wiestler, O. D.; Kleihues, P.; Ellison, D. W., The 2016 World Health Organization Classification of Tumors of the Central Nervous System: a summary. *Acta Neuropathologica* **2016,** *131* (6), 803-820.
3. Rajaratnam, V.; Islam, M. M.; Yang, M.; Slaby, R.; Ramirez, H. M.; Mirza, S. P., Glioblastoma: Pathogenesis and Current Status of Chemotherapy and Other Novel Treatments. *Cancers* **2020,** *12* (4), 937-937.
4. Miller, K. D.; Ostrom, Q. T.; Kruchko, C.; Patil, N.; Tihan, T.; Cioffi, G.; Fuchs, H. E.; Waite, K. A.; Jemal, A.; Siegel, R. L.; Barnholtz-Sloan, J. S., Brain and other central nervous system tumor statistics, 2021. *CA: A Cancer Journal for Clinicians* **2021,** *71* (5), 381-406.
5. Anjum, K.; Shagufta, B. I.; Abbas, S. Q.; Patel, S.; Khan, I.; Shah, S. A. A.; Akhter, N.; Hassan, S. S. u., Current status and future therapeutic perspectives of glioblastoma multiforme (GBM) therapy: A review. *Biomedicine & Pharmacotherapy* **2017,** *92*, 681-689.
6. Delgado-López, P. D.; Corrales-García, E. M., Survival in glioblastoma: a review on the impact of treatment modalities. *Clinical and Translational Oncology* **2016,** *18* (11), 1062-1071.
7. Cohen, M. H.; Shen, Y. L.; Keegan, P.; Pazdur, R., FDA Drug Approval Summary: Bevacizumab (Avastin®) as Treatment of Recurrent Glioblastoma Multiforme. *The Oncologist* **2009,** *14* (11), 1131-1138.
8. Stupp, R.; Hegi, M. E.; Mason, W. P.; van den Bent, M. J.; Taphoorn, M. J. B.; Janzer, R. C.; Ludwin, S. K.; Allgeier, A.; Fisher, B.; Belanger, K.; Hau, P.; Brandes, A. A.; Gijtenbeek, J.; Marosi, C.; Vecht, C. J.; Mokhtari, K.; Wesseling, P.; Villa, S.; Eisenhauer, E.; Gorlia, T.; Weller, M.; Lacombe, D.; Cairncross, J. G.; Mirimanoff, R.-O., Effects of radiotherapy with concomitant and adjuvant temozolomide versus radiotherapy alone on survival in glioblastoma in a randomised phase III study: 5-year analysis of the EORTC-NCIC trial. *The Lancet Oncology* **2009,** *10* (5), 459-466.
9. Davis, M., Glioblastoma: Overview of Disease and Treatment. *Clinical Journal of Oncology Nursing* **2016,** *20* (5), S2-S8.
10. Gilbert, M. R.; Dignam, J. J.; Armstrong, T. S.; Wefel, J. S.; Blumenthal, D. T.; Vogelbaum, M. A.; Colman, H.; Chakravarti, A.; Pugh, S.; Won, M.; Jeraj, R.; Brown, P. D.; Jaeckle, K. A.; Schiff, D.; Stieber, V. W.; Brachman, D. G.; Werner-Wasik, M.; Tremont-Lukats, I. W.; Sulman, E. P.; Aldape, K. D.; Curran, W. J.; Mehta, M. P., A Randomized Trial of Bevacizumab for Newly Diagnosed Glioblastoma. *New England Journal of Medicine* **2014,** *370* (8), 699-708.
11. Chowdhary, S. A.; Ryken, T.; Newton, H. B., Survival outcomes and safety of carmustine wafers in the treatment of high-grade gliomas: a meta-analysis. *Journal of Neuro-Oncology* **2015,** *122* (2), 367-382.
12. Song, A.; Andrews, D. W.; Werner-Wasik, M.; Kim, L.; Glass, J.; Bar-Ad, V.; Evans, J. J.; Farrell, C. J.; Judy, K. D.; Daskalakis, C.; Zhan, T.; Shi, W., Phase I trial of alisertib with concurrent fractionated stereotactic re-irradiation for recurrent high grade gliomas. *Radiotherapy and Oncology* **2019,** *132*, 135-141.
13. Heroux, M. S.; Chesnik, M. A.; Halligan, B. D.; Al-Gizawiy, M.; Connelly, J. M.; Mueller, W. M.; Rand, S. D.; Cochran, E. J.; LaViolette, P. S.; Malkin, M. G.; Schmainda, K. M.; Mirza, S. P., Comprehensive characterization of glioblastoma tumor tissues for biomarker identification using mass spectrometry-based label-free quantitative proteomics. *Physiological Genomics* **2014,** *46* (13), 467-481.

14. Stetson, L. C.; Ostrom, Q. T.; Schlatzer, D.; Liao, P.; Devine, K.; Waite, K.; Couce, M. E.; Harris, P. L. R.; Kerstetter-Fogle, A.; Berens, M. E.; Sloan, A. E.; Islam, M. M.; Rajaratnam, V.; Mirza, S. P.; Chance, M. R.; Barnholtz-Sloan, J. S., Proteins inform survival-based differences in patients with glioblastoma. *Neuro-Oncology Advances* **2020,** *2* (1).
15. Doan, N. B.; Nguyen, H. S.; Montoure, A.; Al-Gizawiy, M. M.; Mueller, W. M.; Kurpad, S.; Rand, S. D.; Connelly, J. M.; Chitambar, C. R.; Schmainda, K. M.; Mirza, S. P., Acid ceramidase is a novel drug target for pediatric brain tumors. *Oncotarget* **2017,** *8* (15), 24753-24761.
16. Doan, N. B.; Nguyen, H. S.; Al-Gizawiy, M. M.; Mueller, W. M.; Sabbadini, R. A.; Rand, S. D.; Connelly, J. M.; Chitambar, C. R.; Schmainda, K. M.; Mirza, S. P., Acid ceramidase confers radioresistance to glioblastoma cells. *Oncology Reports* **2017,** *38* (4), 1932-1940.
17. Doan, N. B.; Alhajala, H.; Al-Gizawiy, M. M.; Mueller, W. M.; Rand, S. D.; Connelly, J. M.; Cochran, E. J.; Chitambar, C. R.; Clark, P.; Kuo, J.; Schmainda, K. M.; Mirza, S. P., Acid ceramidase and its inhibitors: a de novo drug target and a new class of drugs for killing glioblastoma cancer stem cells with high efficiency. *Oncotarget* **2017,** *8* (68), 112662-112674.
18. Govindarajah, N.; Clifford, R.; Bowden, D.; Sutton, P. A.; Parsons, J. L.; Vimalachandran, D., Sphingolipids and acid ceramidase as therapeutic targets in cancer therapy. *Critical Reviews in Oncology/Hematology* **2019,** *138*, 104-111.
19. Cho, S. M.; Kwon, H. J., Acid ceramidase, an emerging target for anti-cancer and anti-angiogenesis. *Archives of Pharmacal Research* **2019,** *42* (3), 232-243.
20. Realini, N.; Solorzano, C.; Pagliuca, C.; Pizzirani, D.; Armirotti, A.; Luciani, R.; Costi, M. P.; Bandiera, T.; Piomelli, D., Discovery of highly potent acid ceramidase inhibitors with in vitro tumor chemosensitizing activity. *Scientific Reports* **2013,** *3* (1), 1035-1035.
21. Nguyen, H.; Awad, A.; Shabani, S.; Doan, N., Molecular Targeting of Acid Ceramidase in Glioblastoma: A Review of Its Role, Potential Treatment, and Challenges. *Pharmaceutics* **2018,** *10* (2), 45-45.
22. Kim, M. J.; Jeon, S.; Burbulla, L. F.; Krainc, D., Acid ceramidase inhibition ameliorates α-synuclein accumulation upon loss of GBA1 function. *Human Molecular Genetics* **2018,** *27* (11), 1972-1988.
23. Dementiev, A.; Joachimiak, A.; Nguyen, H.; Gorelik, A.; Illes, K.; Shabani, S.; Gelsomino, M.; Ahn, E.-Y. E.; Nagar, B.; Doan, N., Molecular Mechanism of Inhibition of Acid Ceramidase by Carmofur. *Journal of Medicinal Chemistry* **2019,** *62* (2), 987-992.
24. Morimoto, K.; Koh, M., Postoperative adjuvant use of carmofur for early breast cancer. *Osaka city medical journal* **2003,** *49*, 77-83.
25. Kusama, M.; Tominaga, T.; Enomoto, K.; Yoshida, M.; Koyama, H.; Sonoo, H.; Takashima, S.; Abe, R.; Nishi, T.; Yamaguchi, S., [Clinical effects of carmofur (Mifurol) on advanced and recurrent breast cancer in a cooperative study. Research association for re-evaluation of direct effects of Mifurol on breast cancer]. *Gan to kagaku ryoho. Cancer & chemotherapy* **1995,** *22* (4), 467-475.
26. Tominaga, T.; Kimura, M.; Asaga, T.; Yoshida, M.; Awane, H.; Koyama, H.; Takatsuka, Y.; Mitsuyama, S.; Ikeda, T.; Ogita, M.; Aoyama, H.; Sano, M.; Abe, R.; Nishi, T.; Wada, T.; Danno, M.; Toi, M.; Takashima, S., 1-Hexylcarbamoyl-5-fluorouracil + cyclophosphamide + tamoxifen versus CMF + tamoxifen in women with lymph node-positive breast cancer after primary surgery: A randomized controlled trial. *Oncology Reports* **2004,** *12* (4), 797-803.
27. Ikeda, M.; Teshima, K.; Noda, K.; Yamagata, S.; Sugawa, T.; Okamura, S.; Kubo, H.; Sugimoto, O.; Nakajima, H.; Yamabe, T.; et al., [Long-term administration of carmofur as a post-operative adjuvant chemotherapy for cervical adenocarcinoma. Cervical Adenocarcinoma Cooperative Research Association]. *Gan to Kagaku Ryoho [Jap J Cancer Chemoth]* **1994,** *21* (12), 1967-1974.
28. Liu, P.; Ma, S.; Liu, H.; Han, H.; Wang, S., Retraction. *Journal of Cellular Biochemistry* **2019,** *120* (7), 12073-12073.

29. El Bairi, K.; Trapani, D.; Petrillo, A.; Le Page, C.; Zbakh, H.; Daniele, B.; Belbaraka, R.; Curigliano, G.; Afqir, S., Repurposing anticancer drugs for the management of COVID-19. *European Journal of Cancer* **2020,** *141*, 40-61.
30. Gao, J.; Zhang, L.; Liu, X.; Li, F.; Ma, R.; Zhu, Z.; Zhang, J.; Wu, J.; Shi, Y.; Pan, Y.; Ge, Y.; Ruan, K., Repurposing Low-Molecular-Weight Drugs against the Main Protease of Severe Acute Respiratory Syndrome Coronavirus 2. *The Journal of Physical Chemistry Letters* **2020,** *11* (17), 7267-7272.
31. Jin, Z.; Zhao, Y.; Sun, Y.; Zhang, B.; Wang, H.; Wu, Y.; Zhu, Y.; Zhu, C.; Hu, T.; Du, X.; Duan, Y.; Yu, J.; Yang, X.; Yang, X.; Yang, K.; Liu, X.; Guddat, L. W.; Xiao, G.; Zhang, L.; Yang, H.; Rao, Z., Structural basis for the inhibition of SARS-CoV-2 main protease by antineoplastic drug carmofur. *Nature Structural & Molecular Biology* **2020,** *27* (6), 529-532.
32. Jin, Z.; Du, X.; Xu, Y.; Deng, Y.; Liu, M.; Zhao, Y.; Zhang, B.; Li, X.; Zhang, L.; Peng, C.; Duan, Y.; Yu, J.; Wang, L.; Yang, K.; Liu, F.; Jiang, R.; Yang, X.; You, T.; Liu, X.; Yang, X.; Bai, F.; Liu, H.; Liu, X.; Guddat, L. W.; Xu, W.; Xiao, G.; Qin, C.; Shi, Z.; Jiang, H.; Rao, Z.; Yang, H., Structure of Mpro from SARS-CoV-2 and discovery of its inhibitors. *Nature* **2020,** *582* (7811), 289-293.
33. Ma, C.; Hu, Y.; Townsend, J. A.; Lagarias, P. I.; Marty, M. T.; Kolocouris, A.; Wang, J., Ebselen, Disulfiram, Carmofur, PX-12, Tideglusib, and Shikonin Are Nonspecific Promiscuous SARS-CoV-2 Main Protease Inhibitors. *ACS Pharmacol Transl Sci* **2020,** *3* (6), 1265-1277.
34. Watanabe, M.; Kodaira, S.; Takahashi, T.; Tominaga, T.; Hojo, K.; Kato, T.; Kunitomo, K.; Isomoto, H.; Ohashi, Y.; Yasutomi, M., Randomized trial of the efficacy of adjuvant chemotherapy for colon cancer with combination therapy incorporating the oral pyrimidine 1-hexylcarbamoyl-5-fluorouracil. *Langenbeck's Archives of Surgery* **2006,** *391* (4), 330-337.
35. Sakamoto, J.; Oba, K.; Matsui, T.; Kobayashi, M., Efficacy of Oral Anticancer Agents for Colorectal Cancer. *Diseases of the Colon & Rectum* **2006,** *49* (1), S82-S91.
36. Sakamoto, J.; Kodaira, S.; Hamada, C.; Ito, K.; Maehara, Y.; Takagi, H.; Sugimachi, K.; Nakazato, H.; Ohashi, Y., An individual patient data meta-analysis of long supported adjuvant chemotherapy with oral carmofur in patients with curatively resected colorectal cancer. *Oncology Reports* **2001,** *8* (3), 697-703.
37. Ito, K.; Yamaguchi, A.; Miura, K.; Kato, T.; Koike, A.; Takagi, H., Prospective adjuvant therapy with Mitomycin C and Carmofur (HCFU) for colorectal cancer, 10-year follow-up: Tokai HCFU Study Group, the first study for colorectal cancer. *Journal of Surgical Oncology* **1996,** *62* (1), 4-9.
38. Ito, K.; Yamaguchi, A.; Miura, K.; Kato, T.; Baba, S.; Matsumoto, S.; Ishii, M.; Takagi, H., Oral adjuvant chemotherapy with Carmofur (HCFU) for colorectal cancer: Five-year follow-up. Tokai HCFU Study Group—third study on colorectal cancer. *Journal of Surgical Oncology* **1996,** *63* (2), 107-111.
39. Ito, K.; Yamaguchi, A.; Miura, K.; Kato, T.; Baba, S.; Matsumoto, S.; Ishii, M.; Takagi, H., Effect of oral adjuvant therapy with Carmofur (HCFU) for distant metastasis of colorectal cancer. *International Journal of Clinical Oncology* **2000,** *5* (1), 29-35.
40. Österlund, P.; Elomaa, I.; Virkkunen, P.; Joensuu, H., A Phase I Study of Raltitrexed (Tomudex) Combined with Carmofur in Metastatic Colorectal Cancer. *Oncology* **2001,** *61* (2), 113-119.
41. Kotake, K.; Ohashi, Y.; Kodaira, S.; Koyama, Y., A multicenter randomized study comparing 5-fluorouracil continuous infusion (ci) plus 1-hexylcarbamoyl-5-fluorouracil and 5-FU ci alone in colorectal cancer. *Oncology Reports* **2005,** *14* (1), 129-134.
42. Nakamura, T.; Ohno, M.; Tabuchi, Y.; Kamigaki, T.; Fujii, H.; Yamagishi, H.; Kuroda, Y., Optimal duration of oral adjuvant chemotherapy with Carmofur in the colorectal cancer patients: the Kansai Carmofur Study Group trial III. *International Journal of Oncology* **2001,** *19* (2), 291-298.
43. Sakamoto, J., Efficacy of Oral Adjuvant Therapy After Resection of Colorectal Cancer: 5-Year Results From Three Randomized Trials. *Journal of Clinical Oncology* **2004,** *22* (3), 484-492.
44. Klobučar, M.; Grbčić, P.; Pavelić, S. K.; Jonjić, N.; Visentin, S.; Sedić, M., Acid ceramidase inhibition sensitizes human colon cancer cells to oxaliplatin through downregulation of transglutaminase

2 and β1 integrin/FAK−mediated signalling. *Biochemical and Biophysical Research Communications* **2018,** *503* (2), 843-848.
45. Okuyama, S.; Mishina, H.; Nunokawa, T., Medroxyprogesterone acetate for lung cancer. *The Tohoku Journal of Experimental Medicine* **1990,** *161* (2), 153-154.
46. Çömlekçi, E.; Kutlu, H. M.; Vejselova Sezer, C., Toward stimulating apoptosis in human lung adenocarcinoma cells by novel nano-carmofur compound treatment. *Anti-Cancer Drugs* **2021,** *32* (6), 657-663.
47. Wu, K.; Xiu, Y.; Zhou, P.; Qiu, Y.; Li, Y., A New Use for an Old Drug: Carmofur Attenuates Lipopolysaccharide (LPS)-Induced Acute Lung Injury via Inhibition of FAAH and NAAA Activities. *Frontiers in Pharmacology* **2019,** *10*, 818-818.
48. Beltran-Quintero, M. L.; Bascou, N. A.; Poe, M. D.; Wenger, D. A.; Saavedra-Matiz, C. A.; Nichols, M. J.; Escolar, M. L., Early progression of Krabbe disease in patients with symptom onset between 0 and 5 months. *Orphanet Journal of Rare Diseases* **2019,** *14* (1), 46-46.
49. Li, Y.; Xu, Y.; Benitez, B. A.; Nagree, M. S.; Dearborn, J. T.; Jiang, X.; Guzman, M. A.; Woloszynek, J. C.; Giaramita, A.; Yip, B. K.; Elsbernd, J.; Babcock, M. C.; Lo, M.; Fowler, S. C.; Wozniak, D. F.; Vogler, C. A.; Medin, J. A.; Crawford, B. E.; Sands, M. S., Genetic ablation of acid ceramidase in Krabbe disease confirms the psychosine hypothesis and identifies a new therapeutic target. *Proceedings of the National Academy of Sciences of the United States of America* **2019,** *116* (40), 20097-20103.
50. Guenzel, A. J.; Turgeon, C. T.; Nickander, K. K.; White, A. L.; Peck, D. S.; Pino, G. B.; Studinski, A. L.; Prasad, V. K.; Kurtzberg, J.; Escolar, M. L.; Lasio, M. L. D.; Pellegrino, J. E.; Sakonju, A.; Hickey, R. E.; Shallow, N. M.; Ream, M. A.; Orsini, J. J.; Gelb, M. H.; Raymond, K.; Gavrilov, D. K.; Oglesbee, D.; Rinaldo, P.; Tortorelli, S.; Matern, D., The critical role of psychosine in screening, diagnosis, and monitoring of Krabbe disease. *Genetics in Medicine* **2020,** *22* (6), 1108-1118.
51. Kajanti, M. J.; Pyrhonen, S. O., Short report: Phase II trial of oral carmofur in advanced pancreatic carcinoma. *Annals of Oncology* **1991,** *2* (10), 765-766.
52. Sipilä, P.; Kivinen, S.; Gröhn, P.; Vesala, J.; Heinonen, E., Phase II evaluation of peroral carmofur, cyclophosphamide, and hexamethylmelamine as a second-line therapy in advanced epithelial ovarian carcinoma. *Gynecologic Oncology* **1989,** *34* (1), 27-29.
53. Yamamoto, M.; Arii, S.; Sugahara, K.; Tobe, T., Adjuvant oral chemotherapy to prevent recurrence after curative resection for hepatocellular carcinoma. *British Journal of Surgery* **2005,** *83* (3), 336-340.
54. Takenaka, K.; Kanematsu, T.; Shimada, M.; Sugimachi, K., Low dose 1-hexylcarbamoyl-5-fluorouracil (HCFU) recommended for cirrhotic patients with hepatocellular carcinoma. *European Journal of Cancer and Clinical Oncology* **1989,** *25* (8), 1191-1195.
55. Gröhn, P.; Heinonen, E.; Kumpulainen, E.; Länsimies, H.; Lantto, A.; Salmi, R.; Pyrhönen, S.; Numminen, S., Oral Carmofur in Advanced Gastrointestinal Cancer. *American Journal of Clinical Oncology* **1990,** *13* (6), 477-479.
56. Malvi, P.; Janostiak, R.; Nagarajan, A.; Zhang, X.; Wajapeyee, N., N-acylsphingosine amidohydrolase 1 promotes melanoma growth and metastasis by suppressing peroxisome biogenesis-induced ROS production. *Mol Metab* **2021,** *48*, 101217.
57. Clifford, R. E.; Govindarajah, N.; Bowden, D.; Sutton, P.; Glenn, M.; Darvish-Damavandi, M.; Buczacki, S.; McDermott, U.; Szulc, Z.; Ogretmen, B.; Parsons, J. L.; Vimalachandran, D., Targeting Acid Ceramidase to Improve the Radiosensitivity of Rectal Cancer. *Cells* **2020,** *9* (12).
58. Tsumura, M.; Yoshiga, K.; Takada, K., Enhancement of antitumor effects of 1-hexylcarbamoyl-5-fluorouracil combined with hyperthermia on Ehrlich ascites tumor in vivo and Nakahara-Fukuoka sarcoma cell in vitro. *Cancer Res* **1988,** *48* (14), 3977-80.
59. Donson, A. M.; Amani, V.; Warner, E. A.; Griesinger, A. M.; Witt, D. A.; Levy, J. M. M.; Hoffman, L. M.; Hankinson, T. C.; Handler, M. H.; Vibhakar, R.; Dorris, K.; Foreman, N. K., Identification of FDA-

Approved Oncology Drugs with Selective Potency in High-Risk Childhood Ependymoma. *Molecular Cancer Therapeutics* **2018,** *17* (9), 1984-1994.
60. Nakanishi, H.; Abe, A.; Inada, K.-i.; Tsukamoto, T.; Yasui, K.; Tatematsu, M., Induction of apoptosis in metastatic foci from human gastric cancer xenografts in nude mice and reduction of circulating tumor cells in blood by 5-FU and 1-hexylcarbamoyl-5-fluorouracil. *Journal of Cancer Research and Clinical Oncology* **1999,** *125* (12), 660-668.
61. Zimbres, A. C. G.; Reuwsaat, J. C. V.; Barcellos, V. A.; Joffe, L. S.; Fonseca, F. L.; Staats, C. C.; Schrank, A.; Kmetzsch, L.; Vainstein, M. H.; Rodrigues, M. L., Pharmacological inhibition of pigmentation in Cryptococcus. *FEMS Yeast Research* **2019,** *19* (1).
62. Sanchez-Vazquez, B.; Amaral, A. J. R.; Yu, D.-G.; Pasparakis, G.; Williams, G. R., Electrosprayed Janus Particles for Combined Photo-Chemotherapy. *AAPS PharmSciTech* **2017,** *18* (5), 1460-1468.
63. Torres, N. S.; Abercrombie, J. J.; Srinivasan, A.; Lopez-Ribot, J. L.; Ramasubramanian, A. K.; Leung, K. P., Screening a Commercial Library of Pharmacologically Active Small Molecules against Staphylococcus aureus Biofilms. *Antimicrobial Agents and Chemotherapy* **2016,** *60* (10), 5663-5672.
64. Taguchi, T., Review of a new antimetabolic agent 1-hexylcarbamoyl-5-fluorouracil (HCFU). *Recent Results Cancer Res* **1980,** *70*, 125-32.
65. Ozaki, S.; Mori, H. 1-Carbamoyl-5-fluorouracil derivatives. US4071519A, 1978.
66. DrugBank Carmofur: Uses, Interactions, Mechanim of Action. https://go.drugbank.com/drugs/DB09010 (accessed March 29).
67. Domracheva, I.; Muhamadejev, R.; Petrova, M.; Liepinsh, E.; Gulbe, A.; Shestakova, I.; Duburs, G.; Arsenyan, P., 1,2-Dimyristoyl-sn-glycero-3-phosphocholine (DMPC) increases Carmofur stability and in vitro antiproliferative effect. *Toxicology Reports* **2015,** *2*, 377-383.
68. Kikuchi, M.; Hirayama, F.; Uekama, K., Improvement of Oral and Rectal Bioavailabilities of Carmofur by Methylated Beta-Cyclodextrin Complexations. *Int J Pharm* **1987,** *38* (1-3), 191-198.
69. Kikuchi, M.; Hirayama, F.; Uekama, K., Improvement of chemical instability of carmoful in beta-cyclodextrin solid complex by utilizing some organic acids. *Chem Pharm Bull (Tokyo)* **1987,** *35* (1), 315-9.
70. Yoshida, A.; Yamamoto, M.; Hirayama, F.; Uekama, K., Improvement of Chemical-Instability of Digitoxin in Aqueous-Solution by Complexation with Beta-Cyclodextrin Derivatives. *Chem Pharm Bull* **1988,** *36* (10), 4075-4080.
71. Pizzirani, D.; Pagliuca, C.; Realini, N.; Branduardi, D.; Bottegoni, G.; Mor, M.; Bertozzi, F.; Scarpelli, R.; Piomelli, D.; Bandiera, T., Discovery of a New Class of Highly Potent Inhibitors of Acid Ceramidase: Synthesis and Structure–Activity Relationship (SAR). *Journal of Medicinal Chemistry* **2013,** *56* (9), 3518-3530.
72. Sato, S.; Hirotani, Y.; Ogura, N.; Sasaki, E.; Kitagawa, S., Enhancing effect of N-dodecyl-2-pyrrolidone on the percutaneous absorption of 5-fluorouracil derivatives. *Chemical and Pharmaceutical Bulletin* **1998,** *46* (5), 831-836.
73. Ozaki, S.; Ike, Y.; Mizuno, H., 5-Fluorouracil derivatives. I. The synthesis of 1-carbamoyl-5-fluorouracils. *Bulletin of the Chemical Society of Japan* **1977,** *50* (9), 2406-2412.
74. Ozaki, S., Synthesis and antitumor activity of 5-fluorouracil derivatives. 1996; Vol. 16, pp 51-86.
75. Shelton, J.; Lu, X.; Hollenbaugh, J. A.; Cho, J. H.; Amblard, F.; Schinazi, R. F., Metabolism, Biochemical Actions, and Chemical Synthesis of Anticancer Nucleosides, Nucleotides, and Base Analogs. *Chemical Reviews* **2016,** *116* (23), 14379-14455.
76. Xiong, J.; Zhou, S.; Huang, Z.; Chao, G.; Wang, L.; Xu, J. 5-fluorouracil drug intermediate, preparation method and application thereof. 2011.
77. Kobari, T.; Iguro, Y.; Ujiie, A.; Namekawa, H., Metabolism of 1-hexylcarbamoyl-5-fluorouracil (HCFU), a new antitumour agent, in rats, rabbits and dogs. *Xenobiotica* **1981,** *11* (1), 57-62.

78. Kobari, T.; Tan, K.; Kumakura, M.; Watanabe, S.; Shirakawa, I.; Kobayashi, H.; Ujiie, A.; Miyama, Y.; Namekawa, H.; Yamamoto, H., Metabolic fate of 1-hexylcarbamoyl-5-fluorouracil in rats. *Xenobiotica* **1978,** *8* (9), 547-556.
79. Ooi, K.; Ohkubo, T.; Higashigawa, M.; Kawasaki, H.; Kakito, H.; Kagawa, Y.; Kojima, M.; Sakurai, M., Plasma, intestine and tumor levels of 5-fluorouracil in mice bearing L1210 ascites tumor following oral administration of 5-fluorouracil, UFT (mixed compound of tegafur and uracil), carmofur and 5'-deoxy-5-fluorouridine. *Biological and Pharmaceutical Bulletin* **2001,** *24* (11), 1329-1331.
80. Iigo, M.; Nakamura, A.; Kuretani, K.; Hoshi, A., Distribution of 1-hexylcarbamoyl-5-fluorouracil and 5-fluorouracil by oral administration in mice. *Journal of Pharmacobio-Dynamics* **1979,** *2* (1), 5-11.
81. Iigo, M.; Nakamura, A.; kuretani, K.; Hoshi, A., Excretion of 1-hexylcarbamoyl-5-fluorouracil in urine of mice. *Journal of Pharmacobio-Dynamics* **1981,** *4* (7), 490-6.
82. Ikehira, H.; Girard, F.; Obata, T.; Ito, H.; Yoshitomi, H.; Miyazaki, M.; Nakajima, N.; Kamei, H.; Kanazawa, Y.; Takano, H.; Ito, H.; Tanada, S.; Sasaki, Y., A preliminary study for clinical pharmacokinetics of oral fluorine anticancer medicines using the commercial MRI system 19F-MRS. *British Journal of Radiology* **1999**.
83. Hoshi, A.; Yoshida, M.; Inomata, M.; Ligo, M.; Ando, N.; Kuretani, K., Antitumor activity of metabolites of 1-hexylcarbamoyl-5-fluorouracil and related compounds against L1210 leukemia in vivo and L5178Y lymphoma cells in vitro. *Journal of Pharmacobio-Dynamics* **1980,** *3* (9), 478-481.
84. Kono, A.; Tanaka, M.; Eguchi, S.; Hara, Y.; Matsushima, Y., Determination of 1-hexylcarbamoyl-5-fluorouracil and its metabolites in biomedical specimens by high-performance liquid chromatography. *Journal of Chromatography B: Biomedical Sciences and Applications* **1979,** *163* (1), 109-113.
85. Kono, A.; Tanaka, M.; Eguchi, S.; Hara, Y. *Determination of I-hexylcarbamoyld-fluorouracil and its metabolites in biomedical specimens by high-performance liquid chromatography*; Biomedical Applications @ EIsevier Scientific Publishing Company: 1979; pp 109-113.
86. Isomura, H.; Higuchi, S.; Kawamura, S., GAS CIIROMATOGRAPHIC-MASS SPECTROMETRIC DETERMINATION OF PLASMA 5-FLUOROURACIL AFTER ADMINISTRATION OF l-HEXYLCARRAMOYL5-FLUOROURACIL TO DOGS AND HUMANS. *Journal of Chromatography* **1981,** *224*, 423-429.
87. Iigo, M.; Nakamura, A.; Kuretani, K.; Hoshi, A., Metabolic fate of 1-hexylcarbamoyl-5-fluorouracil after oral administration in mice. *Xenobiotica* **1980,** *10* (11), 847-854.
88. Iigo, M.; Kuretani, K.; Hoshi, A., Metabolic Fate of 1-Hexylcarbamoyl-5-fluorouracil and 5-Fluorouracil in Mice Bearing Ascites Sarcoma 180. *JNCI: Journal of the National Cancer Institute* **1981,** *66* (2), 345-349.
89. Kono, A.; Hara, Y.; Eguchi, S.; Tanaka, M.; Matsushima, Y., Determination of two new metabolites of 1-hexylcarbamoyl-5-fluorouracil in biomedical specimens by high-performance liquid chromatography. *Journal of Chromatography B: Biomedical Sciences and Applications* **1980,** *182* (1), 125-129.
90. Nakajima, O.; Yoshida, Y.; Isoda, T.; Takemasa, Y.; Imamura, Y.; Koyama, Y., Quantitative determination of 1-hexylcarbamoyl-5-fluorouracil and its metabolites in man. *Journal of Chromatography B: Biomedical Sciences and Applications* **1981,** *225* (1), 91-97.
91. Altova, E. P.; Hargittai, I., Mikhail S. Tsvet-pioneer of chromatography-150 years from his birth. *Struct Chem* **2022,** *33* (1), 1-3.
92. Livengood, J.; Edwards, A., Calibrating Chromatography: How Tswett Broke the Experimenters' Regress. *The British Journal for the Philosophy of Science* **2019**.
93. Harris, D. C., *Exploring chemical analysis*. Macmillan: 2012.
94. Greaves, J.; Roboz, J., *Mass spectrometry for the novice*. CRC Press Boca Raton, FL: 2014.
95. Glish, G. L.; Vachet, R. W., The basics of mass spectrometry in the twenty-first century. *Nature reviews drug discovery* **2003,** *2* (2), 140-150.
96. De Hoffmann, E., Tandem mass spectrometry: a primer. *J Mass Spectrom* **1996,** *31* (2), 129-137.

97. El-Aneed, A.; Cohen, A.; Banoub, J., Mass spectrometry, review of the basics: electrospray, MALDI, and commonly used mass analyzers. *Applied Spectroscopy Reviews* **2009,** *44* (3), 210-230.
98. Reyzer, M. L.; Caprioli, R. M., MALDI-MS-based imaging of small molecules and proteins in tissues. *Current opinion in chemical biology* **2007,** *11* (1), 29-35.
99. Dreisewerd, K., The desorption process in MALDI. *Chemical reviews* **2003,** *103* (2), 395-426.
100. Nishidate, M.; Hayashi, M.; Aikawa, H.; Tanaka, K.; Nakada, N.; Miura, S.; Ryu, S.; Higashi, T.; Ikarashi, Y.; Fujiwara, Y.; Hamada, A., Applications of MALDI mass spectrometry imaging for pharmacokinetic studies during drug development. *Drug Metabolism and Pharmacokinetics* **2019,** *34* (4), 209-216.

Chapter-2

The Development and validation of an LC-MS/MS method for quantitative bioanalysis of carmofur in mouse plasma and its application to pharmacokinetic study

2.1. Introduction

Pharmacokinetic evaluation of drug molecules in rodents is one of the preclinical assessments during the process of drug development. Understanding the pharmacokinetic behavior provides a good insight into how the body behaves with respect to a drug molecule which includes absorption, distribution, metabolism, and excretion in vivo[1]. Pharmacokinetics also help towards optimization of a lead and design a dosage regimen for a further clinical study.

During the process of pre-clinical pharmacokinetic study, a drug molecule is administered in a healthy rodent model (mouse, rat, dog, monkey, etc.) and the plasma/blood concentration is measured at different intervals over a period of time. The pharmacokinetic evaluation could be performed via the enteral (such as oral) or parenteral (such as intramuscular, intravenous, intraperitoneal, etc.) route of administration of the drug. The pharmacokinetic study helps to determine the minimum therapeutic concentration and the minimum toxic concentration of the drug molecule in vivo. It also helps to understand the bioavailability of the drug and its kinetics inside the body.

Furthermore, the pharmacokinetic study is also performed further than the pre-clinical evaluation and during the phase I clinical trial in human volunteers to understand the tolerance, toxicity, and bioavailability of the drug substance.

Among the in vivo pharmacokinetic characteristics that are studied are the t_{max} (time to reach maximum plasma concentration after administration), C_{max} (the maximum plasma drug concentration), V_d (the apparent volume of distribution), f (bioavailability/fraction of the drug administered available systemically), AUC (area-under-the concentration-time curve), and $t_{1/2}$ (elimination half-life), etc. The information obtained from a pharmacokinetic study helps to determine the formulation of the drug product, identify the most effective route of administration and the dosage regimen of the drug product.

Currently, liquid chromatography-tandem mass spectrometry (LC-MS/MS) based techniques are the most widely used and considered as the gold standard technique for analyzing pharmacokinetic samples[1-2]. LC-MS/MS techniques use the separation capability of chromatography and the greater specificity, sensitivity, and resolution of the mass spectrometer instrument. Coupled together, LC-MS/MS-based systems have the advantages of greater accuracy, selectivity, and reduced interferences with a proper sample preparation technique[3].

To the best of our knowledge, there is no LC-MS/MS-based method reported for analyzing carmofur (figure 2-1) in vivo. In the past, carmofur has been analyzed using a number of bioanalytical methods as described in the previous literatures[4-9]. Previous methods relied on techniques such as high-performance liquid chromatography (HPLC), thin-layer chromatography (TLC), and the measurement of total radioactivity. They either suffered from low sensitivity, high

retention time or the need for a large amount of plasma samples. Beyond that, none of the methods have been considerably validated in the present-day regulatory guidelines. Herein, we report for the first time an LC-MS/MS method for quantitative bioanalysis of carmofur in mouse plasma. We have also shown the applicability of our method in a pharmacokinetic study in mice.

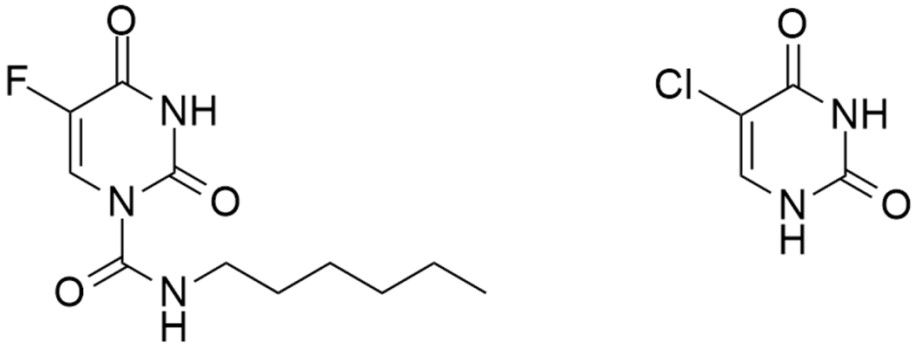

Carmofur 5-chlorouracil

Figure 2-1. Structure of carmofur and 5-chlorouracil (IS).

2.2. Materials and methods

2.2.1. Chemicals and reagents

Carmofur (CAS No. 61422-45-5) was obtained from Tokyo Chemical Co. Ltd (Portland, OR, USA). 5-chlorouracil (5-CU) (CAS No. 1820-81-1) (Figure 2-1) was obtained from Millipore-Sigma (St. Louis, MO, USA). All solvents and buffers were used in mobile phase were of analytical grade. LC-MS grade water, acetonitrile, 2-propanol, and ammonium acetate used in this work were obtained from Fisher Chemical (USA). Glacial acetic acid was purchased from Merck KGaA (Germany). Ethyl acetate was procured from BeanTown Chemical (NH, USA). Dimethyl sulfoxide (DMSO) was obtained from Honeywell International Inc. (MI, USA). PBS at pH 7.4 buffer was obtained from Corning (VA, USA). PEG E 400 was procured from Millipore-Sigma (St. Louis, Mo,

USA). Tween 80 was obtained from MP Biomedicals (Illkirch, France). 1 mL tuberculin syringe with 25 G × 5/8" needles/syringes was purchased from Covidien (Dublin, Ireland).

2.2.2. Animal handling

All animal experimentation was approved by the University of Wisconsin-Milwaukee's (UWM) Institutional Animal Care and Use Committee (IACUC) (protocol reference no. 20-21#53). Six-eight weeks old female Swiss Webster mice were supplied by Charles River Laboratories (MA, USA). The animals were housed for at least seven days in the Lapham Animal Resource Center (ARC) of UWM before performing the experiment. While housed, they were provided with free access to food and water and maintained on a 12 h light (7:00 to 19:00) and dark cycle (19:00 to 07:00) at a temperature of 22±2°C and 60±5% humidity.

2.2.3. Instruments and conditions

For the sample preparation, we used the following: Orbital Shaker M60 (Labnet, NJ, USA), Centrifuge 5430R (Eppendorf, Germany), TurboVap Evaporator (Biotage, Sweden) and Pressure + 48 Positive pressure Manifold (Biotage, Sweden). Costar® Spin-X® Centrifuge Tube Filters, 0.22 µm were purchased from Corning (Corning, NY).

Liquid chromatography was performed on a Shimadzu Nexera X2 UPLC system that consisting of binary pumps (Shimadzu LC-30AD), degasser units (Shimadzu DGU-20A 5R), autosampler (Shimadzu SIL-30AC MP) and column oven (Shimadzu CTO20A). The UPLC system was interfaced with a Shimadzu 8040 triple quadrupole mass spectrometer. The 8040 instrument is equipped with dual ionization source (Electrospray + Atmospheric Pressure Chemical Ionization). For supplying nitrogen gas to the mass spectrometer, we used an in-house nitrogen generator

(NM32LA) purchased from Peak Scientific (Glasgow, UK). The CID gas Argon (Ar) was purchased from Airgas (PA, USA).

The analytes were retained, and chromatographic separation was achieved on a XBridge BEH C18 XP column (100 mm X 3 mm, 2.5 µm, Waters Corporation, MA, USA). The data acquisition and post-run analysis were performed using LabSolutions (Shimadzu Corporation, Japan) and Microsoft Excel (Microsoft, USA) software packages.

Mass spectrometric ionization was taken place in negative electrospray ionization technique and the quantification was carried out in multiple reaction monitoring (MRM) mode. The desolvation line and ion source temperature were kept at 275°C and 420°C, respectively. The drying gas and nebulizing gas flow rate were 16 $L.min^{-1}$ and 2.5 $L.min^{-1}$, respectively. The dwell time of analysis for all analytes was 100 msec.

10 mM ammonium acetate in water at pH 6.8 was used as mobile phase A and acetonitrile was used as mobile phase B. The injection volume was 5 µL. The total runtime was 8 min with the gradient elution program as follows: 60% of B from 0-0.50 min, a linear gradient from 60% B to 95% B from 0.50 - 1.00 min, 95% of B from 1.00 - 5.00 min, a linear gradient of 95% B to 60% B from 5.00 - 5.50 min and 60% B from 5.50 to 8 min. The column oven was kept at 32°C.

2.2.4. Preparation of calibration and quality control standards

An appropriate amount of carmofur is weighed using weighing by difference technique and dissolved in dimethyl sulfoxide (DMSO) to prepare the stock solution at 5 $mg.mL^{-1}$ concentration. The stock solution was further diluted with acetonitrile to prepare the working stock solutions. Each of the working stock solutions were further diluted in blank plasma to prepare the calibration standards at concentrations 5, 25, 100, 200, 500, 1000 $ng.mL^{-1}$. Three quality control (QC) samples: low QC (LQC), medium QC (MQC) and high QC (HQC) were prepared at concentrations 5, 100, and 1000 $ng.mL^{-1}$ respectively to cover the entire range of calibration curve. The QC working stock solutions were subjected to spiking in plasma in a similar way as the standards. Thereafter, standards and QC samples underwent liquid-liquid extraction (LLE) before analyzing by mass spectrometry as described in section 2.2.5.

2.2.5. Sample preparation

On the assay day, 10 µL of 5-CU internal standard (IS) (50 $\mu g.mL^{-1}$) was added to 100 µL plasma sample. The sample is then acidified by adding 10 µL of glacial acetic acid. 1 mL of extraction solvent (ethyl acetate and 2-propanol at a ratio of 85:15) was added and vortexed for 5 min. The sample tubes were then centrifuged at 18,000 × g at 4ºC for 15 min. 800 µL of the supernatant was transferred into another tube and dried under compressed air flow at room temperature. The dried residue is then reconstituted in 100 µL of acetonitrile, filtered through 0.22 µm Spin-X filers, and 5 µL of the prepared sample was injected for LC-MS/MS analysis.

2.2.6. LC-MS/MS method validation

The developed method was validated in terms of specificity, sensitivity, accuracy, precision, recovery, matrix effect, dilution integrity and stability according to the United States Food and Drug Administration's (FDA) guideline for bioanalytical method validation[10].

2.2.6.1. Specificity and carryover

Blank plasma samples, blank plasma spiked with carmofur and IS, and plasma sample collected from the mouse after intraperitoneal injection of carmofur were treated according to extraction procedure described in section 2.2.5. before analyzing with LC-MS/MS. Specificity was evaluated by comparing the presence or absence of mass chromatograms for carmofur and IS in their respective peak regions. Carryover was evaluated by injecting a blank sample after the injection of HQC sample. Peak area below 20% of LQC for carmofur and below 5% for IS was considered acceptable in the blank sample.

2.2.6.2. Linearity and sensitivity

A series of diluted solutions of the standards were prepared to identify the lower limit of detection (LOD) and the lower limit of quantification (LOQ). A minimum signal to noise (S/N) ratio of 3 was considered for the LOD and a minimum S/N ratio of 10 was considered for LOQ. Six calibration standards (5, 25, 100, 200, 500, 1000 ng/mL) within the range of 5-1000 $ng.mL^{-1}$ including both upper and lower limit of quantification were used for generating the calibration curve. Each calibration standard was spiked with the IS at 5 $\mu g.mL^{-1}$ concentration. The calibration curves were constructed by plotting the peak area ratio (y) against the concentration ratio (x) of the analyte and IS. The curves were fitted for weighted least square linear regression analysis

with a weighing factor of $1/x^2$ and the linearity was considered acceptable with a correlation coefficient (r^2) of 0.99 or greater.

2.2.6.3. Matrix effect and recovery efficiency

The effect of the presence of endogenous compounds in the ionization of the analyte is considered matrix effect. Concurrent extraction of plasma components can either increase or decrease the ionization of the target analyte. Matrix effect was investigated for three QC samples (low, medium, and high) and calculated based on the ratio of peaks areas of the post-extracted spiked sample to the peak areas of neat standard samples[11].

$$\text{Matrix effect (\%)} = \frac{\text{Peak area of post extracted spiked sample}}{\text{Peak area of neat standard sample}} \times 100$$

A matrix effect of less than 100% indicates ion suppression and a matrix effect of greater than 100% indicates ion enhancement.

Recovery efficiency of the analyte was evaluated at the three QC (LQC, MQC, HQC) samples by comparing the peaks areas of the spiked sample in blank matrix and extracted with the extraction solvent (ethyl acetate-2-propanol) with those peak areas of the post extracted spiked sample[11].

$$\text{Recovery efficiency (\%)} = \frac{\text{Peak area of extracted spiked sample}}{\text{Peak area of post extracted spiked sample}} \times 100$$

The recovery doesn't necessarily have to be 100% but a reproducible and robust recovery is desired[12].

2.2.6.4. Accuracy and precision

Three QC samples for carmofur LQC (5 $ng.mL^{-1}$), MQC (100 $ng.mL^{-1}$) and HQC (1000 $ng.mL^{-1}$) were prepared separately in six replicates and analyzed for accuracy and precision for three consecutive days.

The data obtained from intra-day accuracy and precision were reanalyzed for inter-day accuracy and precision at all three QC sample concentration.

The precision was expressed as the percent coefficient of variance (%CV) and the accuracy was expressed as the percent mean accuracy. It was considered acceptable if the %CV is <15% and %mean accuracy is within ±15% respectively.

$$\%CV = \frac{\text{Standard deviation}}{\text{Mean measured concentration}} \times 100$$

2.2.6.5. Stability

The stability of carmofur both in mouse plasma and the final reconstituted solvent was evaluated at different stability conditions. Long term stability was assessed by the accuracy of the measured carmofur concentration at three QC (LQC, MQC, HQC) concentration after storing for 15 days at -80°C. In process stability was studied after three cycles of freeze-thaw from -80°C to room temperature. Post-operative stability was studied with the final reconstituted sample at three QC concentration by storing at room temperature for 8 hours and at the autosampler (15°C) for 24 hours. Carmofur was considered stable with an accuracy of ±15% of the desired concentration.

2.2.6.6. Dilution Integrity

Two dilution integrity QC samples (2 µg.mL^{-1} and 10 µg.mL^{-1}) were diluted 10 and 20 times in order to assess the impact of dilution on samples that are above the range of calibration curve. Dilution integrity was performed in six replicate analyses and was considered acceptable if the measured concentration is within ±20% of the target concentration.

2.2.6.7. Pharmacokinetic study in mice

Finally, we tested the applicability of our validated method in a rodent model. A total of 21 female Swiss Webster mice were selected for doing the pharmacokinetic study. Carmofur was injected at a dose of 10 mg.kg^{-1} intraperitoneally[13]. Carmofur was formulated in 2% DMSO, 5% Tween 80, 5% PEG E 400 and 88% PBS. Blood samples were collected via cardiac puncture at the following time points: immediate after administration (5 min), 20 min, 40 min, 60 min, 120 min, 180 min, and 240 min. Collected blood samples were immediately centrifuged at 18,000 × g for 10 min. Separated plasma was collected in microcentrifuge tubes and stored at -80°C until analysis. Based on the concentration of carmofur in plasma at different time points, concentration-time pharmacokinetic curve was prepared in GraphPad Prism 9 by fitting to non-linear regression. The other pharmacokinetic parameters, including C_{max}, T_{max}, $T_{1/2}$, K_e etc. were calculated by one-compartmental model.

2.3. Results and Discussion

2.3.1. Optimization of chromatographic and mass spectrometric conditions

A schematic of chromatographic and mass spectrometric method development is shown in figure 2-2.

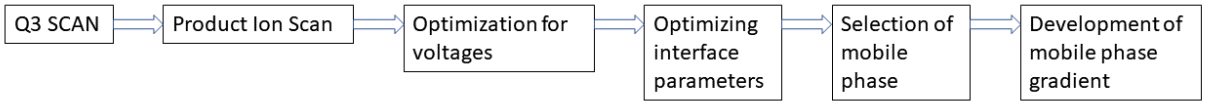

Figure 2-2. Schematic of LC-MS/MS method development.

At first, we did a Q3 scan (Figure 2-3) in dual ionization (DUIS) mode to identify the precursor ion peak of carmofur. Carmofur ionizes in negative mode as $[M-H]^-$ with a peak at m/z 256.20.

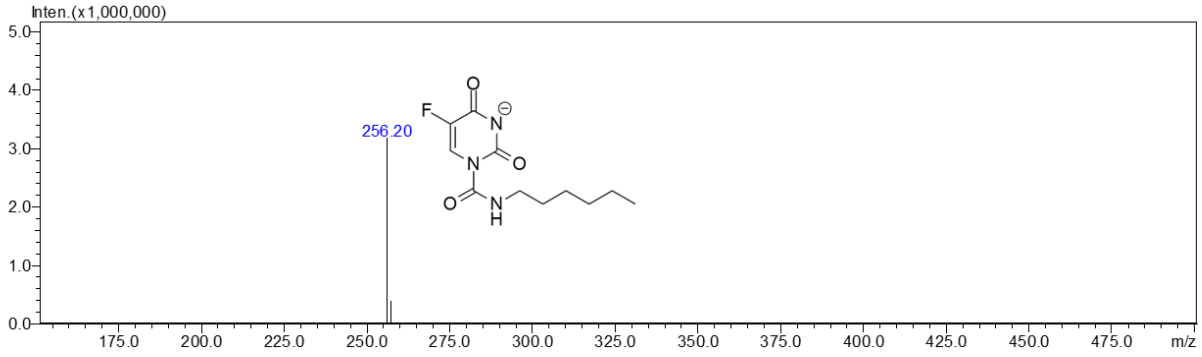

Figure 2-3. Negative mode Q3 scan of carmofur solution at a concentration of 100 µg.mL^{-1}.

Once the precursor ion is identified, we ran a product ion scan (figure 2-4) to identify the product ions of carmofur and utilized the built in 'optimization for method' tool in the LabSolutions software to optimize the voltages (table 2-1) for the MRM transitions. We identified three

predominant transitions m/z 256.25 to m/z 129.00 (used for quantification), m/z 256.25 to m/z 86.0 and m/z 256.25 to m/z 42.0.

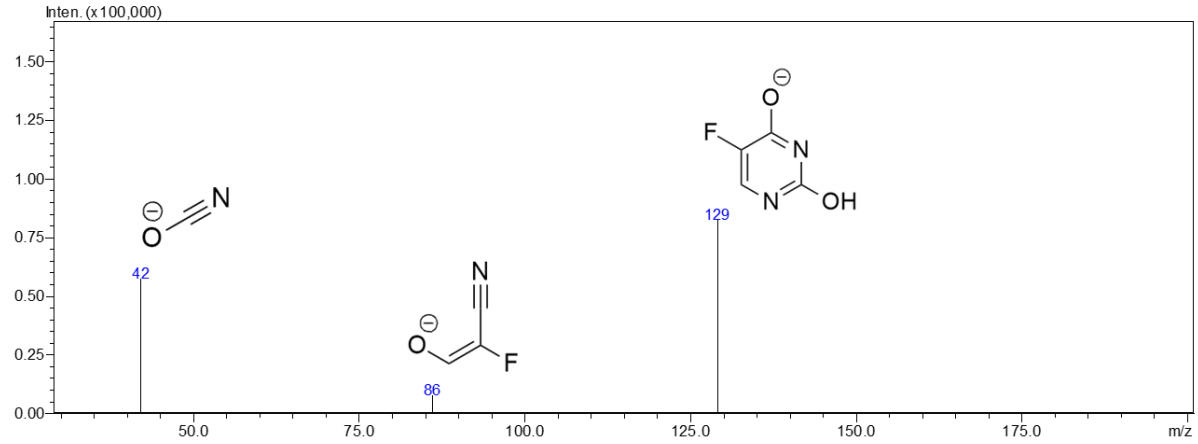

Figure 2-4. Product ion scan of carmofur.

Analyte	Precursor ion	Product ion	Q1 pre-bias (V)	CE (V)	Q3 pre-bias (V)
Carmofur	256.25	129.00	16.00	8.00	23.00
Carmofur	256.25	86.00	28.0	40.0	28.0
Carmofur	256.25	42.00	27.0	31.0	16.0
5-CU	145.10	42.00	25.00	16.00	16.00

Table 2-1. Optimized mass spectrometric parameters of carmofur and internal standard.

We also investigated the ionization efficiency in electrospray (ESI) vs. atmospheric pressure chemical ionization (APCI) (Figure 2-5) to understand the ionization efficiency in each mode and to select the right mode for analysis. We found that carmofur ionization predominantly in negative electrospray ionization technique.

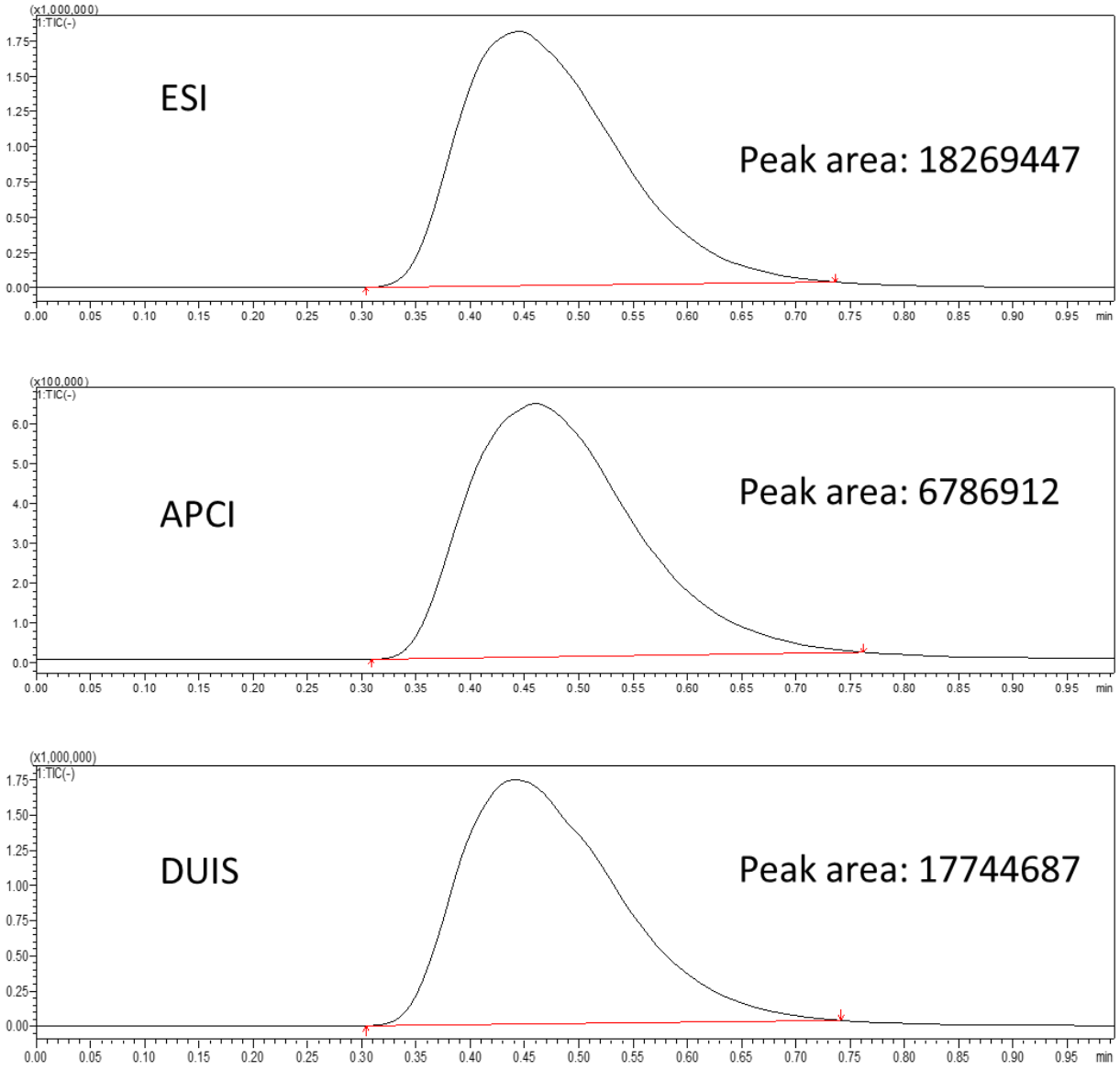

Figure 2-5. Carmofur (100 µg.mL^{-1}) ionization at different ionization techniques.

The other mass spectrometry parameters such as desolvation line (DL) temperature, ion source temperature, drying gas flow rate, nebulizing gas flow rate, dwell time for analysis, DL to ESI probe distance were optimized manually and the optimized parameters are 275°C, 420°C, 16 L.min^{-1}, 2.5 L.min^{-1}, 100 msec, and 1.5 (Appendix A1-A6).

After MS parameters are optimized, we evaluated several mass spectrometry friendly mobile phase solvents and their combinations (Appendix A7) as well as different gradients to find out the ideal mobile phases and their gradient that would improve the sensitivity, peak shape, and peak resolution for the analytes. After several trials, we selected 10 mM ammonium acetate in water at pH 6.8 as mobile phase A and acetonitrile as mobile phase B with the gradient described in section 2.2.3. With this combination, maximum sensitivity was achieved, and no carryover was observed from run to run.

The internal standard 5-chlorouracil (5-CU) had the precursor to product ion transition of m/z 145.53 to m/z 42.0 (figure 2-6 and 2-7) in compliance with what was reported in the past for this compound[14-15]. We chose 5-CU as internal standard because of its structural similarity with carmofur, similarity in ionization mode, significant and reproducible recovery with the extraction solvent. On top of that, 5-CU has also been used in the past as an internal standard for other 5-FU derivatives[14-15].

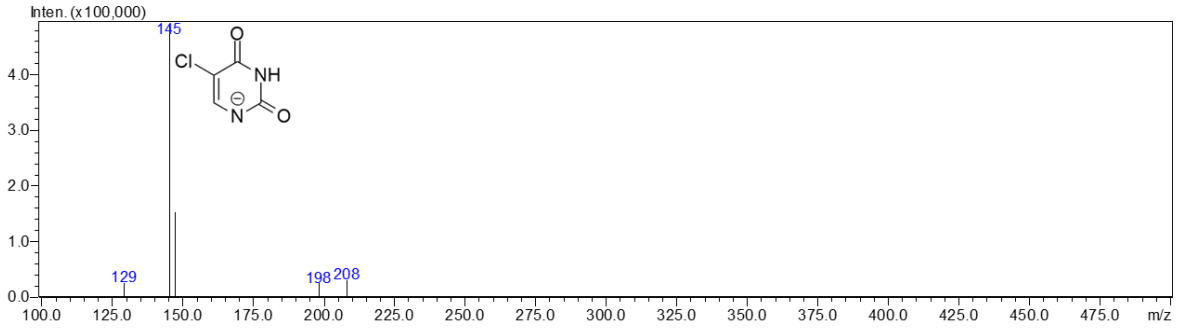

Figure 2-6. Negative mode Q3 scan of 5-CU solution at a concentration of 100 µg.mL^{-1}.

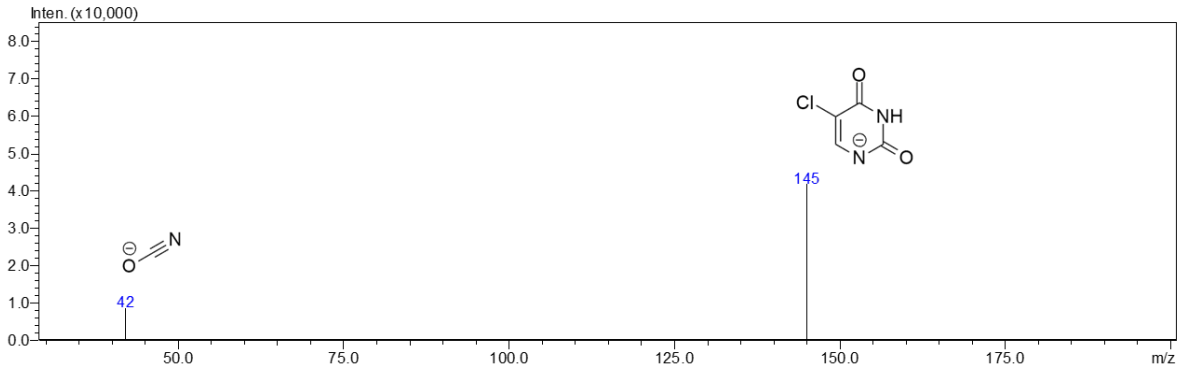

Figure 2-7. Product ion scan of 5-CU.

2.3.2. Optimization of sample preparation

We utilized different conventional sample pre-treatment techniques such as protein precipitation and liquid-liquid extraction (LLE) to find out a robust and reproducible sample preparation technique that can extract carmofur and remove the interfering endogenous substances from the mouse plasma[16-17].

Initially, we assessed protein precipitation using methanol and acetonitrile because of the simplicity of the technique. Protein precipitation using an organic solvent can remove more than 90% of the total proteins from mouse, rat, dog, and human plasma if an adequate precipitant to plasma ratio is used. A minimum organic to aqueous ratio of 1.5 for acetonitrile and 2.5 for methanol is recommended to denature the major proteins and precipitate them out of the solution[18].

During the trial in protein precipitation technique, we spiked carmofur solution in adequate into 100 µL of plasma to make a carmofur concentration of 100 $ng.mL^{-1}$ in plasma. It was followed by the acidification of the plasma by addition of 10 µL of glacial acetic acid to stabilize the carmofur

in basic plasma pH. Thereafter, we added 1000 µL of chilled organic solvent (acetonitrile or methanol) and vortexed for 1 min. The resulting sample was centrifuged at 18000 rpm for 10 min and 600 µL supernatant was transferred into another microcentrifuge tube. The supernatant was dried out under compressed air flow and reconstituted with 100 µL of acetonitrile, filtered and 5 µL of the sample was injected into LC-MS/MS for analysis. The results of protein precipitation are shown in table 2-2 and figure 2-8.

Next, we examined the feasibility of numerous organic solvents such as hexane, 2-propanol, ethyl acetate etc. as LLE solvent. The protocol for LLE was similar to protein precipitation; LLE solvent was added instead of protein precipitation solvent. The summary of extraction efficiency and matrix effect are summarized in table 2-2 and figure 2-8.

Based on the initial results, we decided to choose ethyl acetate/2-propanol (85/15) as our extraction solvent because of optimal recovery and least matrix interferences. In the final sample preparation procedure, 800 µL of supernatant was subjected to drying and reconstitution to achieve greater sensitivity. The optimized sample preparation technique is described in section 2.2.5.

Extraction solvent	Matrix effect	Recovery efficiency
Acetonitrile	72.76%	71.36%
Methanol	50.69%	75.45%
Hexane*	-	0%
2-Propanol	105.56%	74.16%
Ethyl acetate	191.69%	106.30%
Ethyl acetate/2-propanol (85/15)	102.40%	92.19%

Table 2-2. matrix effect and recovery efficiency with different extraction solvent at 100 ng.mL^{-1}. Results are expressed as average of triplicate analysis. *Extraction of pre-extracted sample with hexane resulted in no extraction of carmofur.

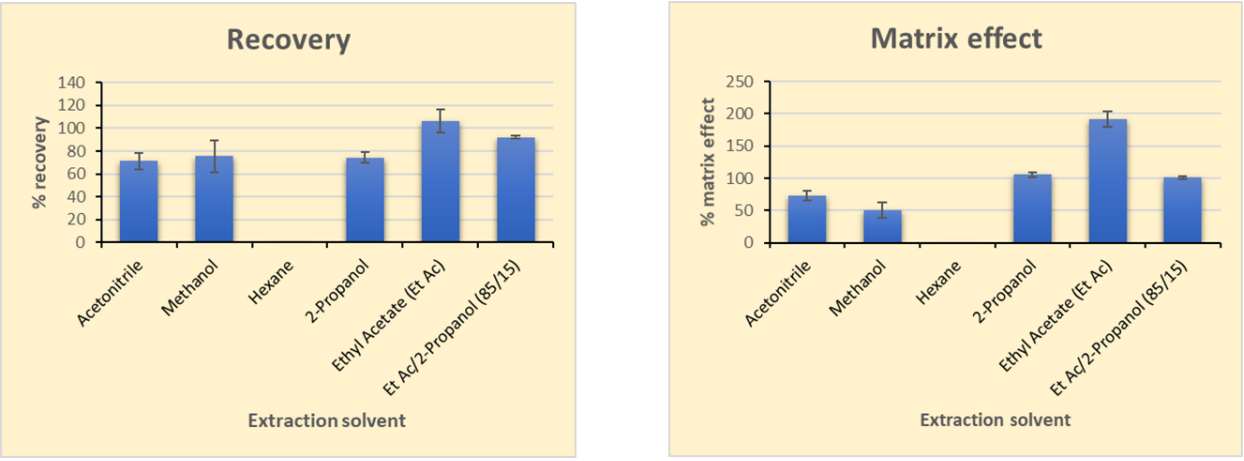

Figure 2-8. Recovery (%) and matrix effect (%) of carmofur with different solvents.

2.3.3. Method validation

2.3.3.1. Specificity and carryover

Specificity was evaluated by examining the mass chromatograms for blank mouse plasma, mouse plasma spiked with carmofur and internal standard, and mouse plasma collected after intraperitoneal injection of carmofur (figure 2-9). No endogenous components of the mouse plasma were found to interfere with the peak of carmofur at its retention time of carmofur indicating the specificity and selectivity of the method.

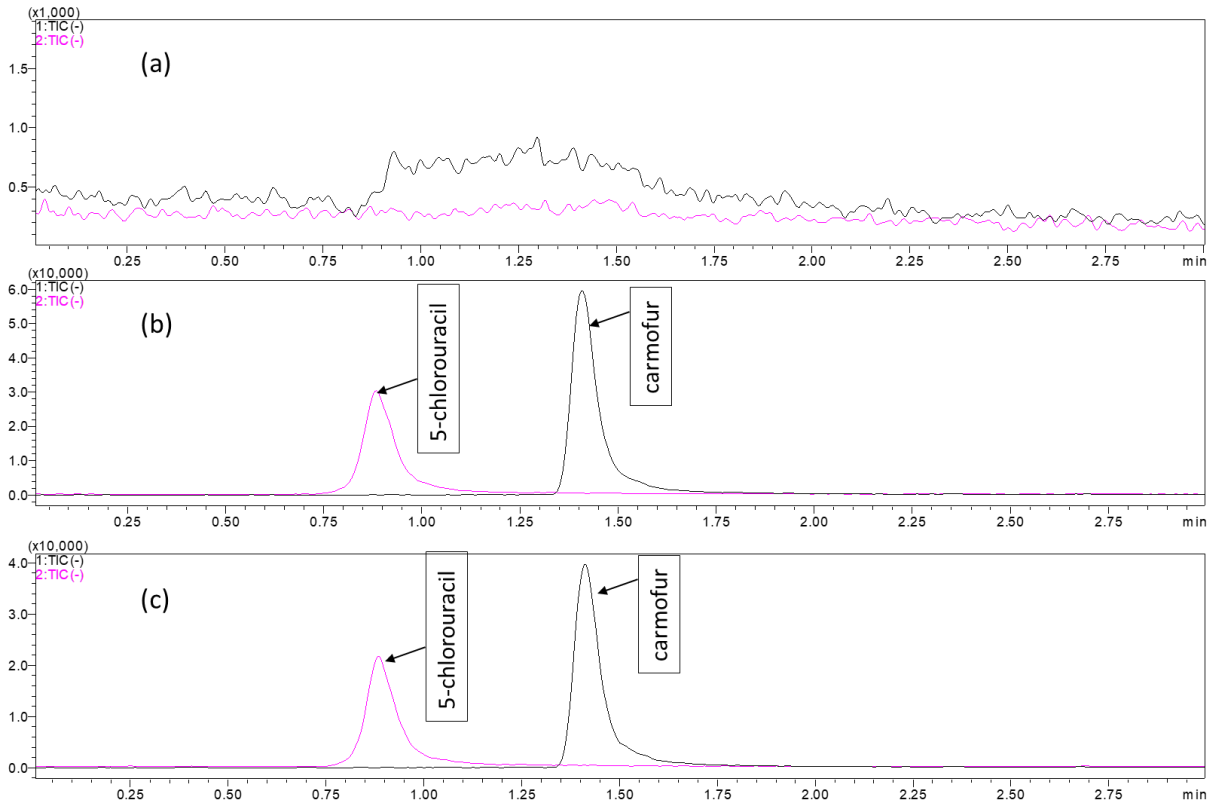

Figure 2-9. Representative chromatograms of a) extracted blank plasma b) blank plasma spiked with carmofur and IS c) plasma collected after i.p. administration of carmofur.

Carryover was evaluated by checking the blank mass chromatogram after running HQC (1000 ng.mL^{-1}) samples (figure 2-10). No significant carryover was observed. Although, running samples with concentrations that are over HQC showed considerable carryover, our observation found that increasing the post-run rinsing time for the autosampler needle decreases the carryover substantially.

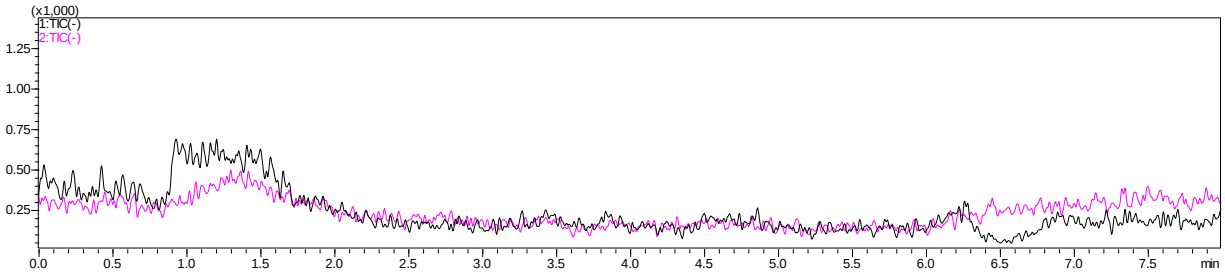

Figure 2-10. Representative mass chromatogram of a blank after running a HQC sample indicates the absence of carryover

2.3.3.2. Linearity and sensitivity

We found the LOD and LOQ to be 2 ng.mL^{-1} (appendix figure A-8)and 5 ng.mL^{-1} (appendix figure A-9), respectively. The LOQ could be lowered down with the injection of higher volume of samples. Nevertheless, we decided to keep the injection volume to 5 µL of samples to maintain optimum column performance. Acceptable linearity was achieved between the range of 5-1000 ng/mL with a correlation coefficient of 0.9948±0.003 for six replicate analyses. The regression equation was y = (78.1076±7.137)x - (0.0117±0.005) and a representative calibration curve is shown in figure 2-11.

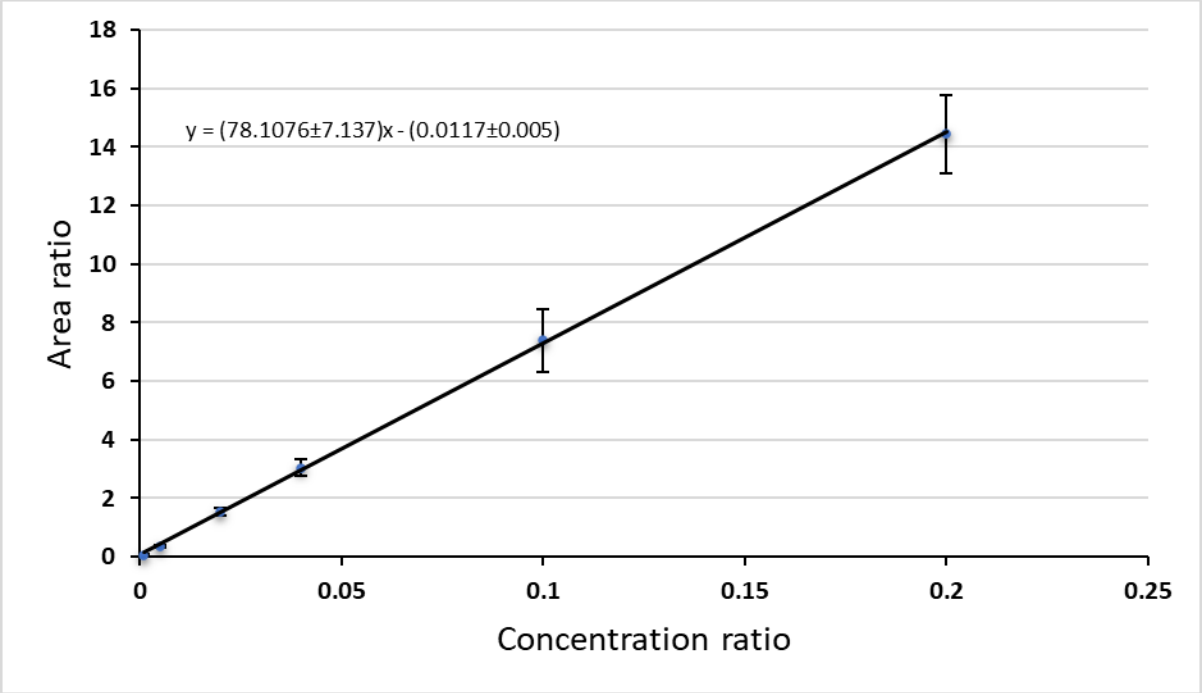

Figure 2-11. Calibration curve of carmofur in mouse plasma.

2.3.3.3. Matrix effect and recovery efficiency

Both matrix effect and recovery efficiency (figure 2-12) were evaluated for three QC samples: LQC (5 ng.mL^{-1}), MQC (100 ng.mL^{-1}), HQC (1000 ng.mL^{-1}). The matrix effect for the three QC samples were 111.87%, 113.21% and 112.48% respectively which indicates about 11-13% ion enhancement of carmofur by the matrix. The recovery was found between 81.64%-88.70% for the three QC samples. Regulatory guidelines require recovery to be consistent and precise and recovery that is greater than 70% is generally accepted[12]. Low percent relative standard deviation and reproducible recovery of carmofur in replicate analyses suggests a satisfactory recovery of carmofur employing the liquid-liquid extraction technique.

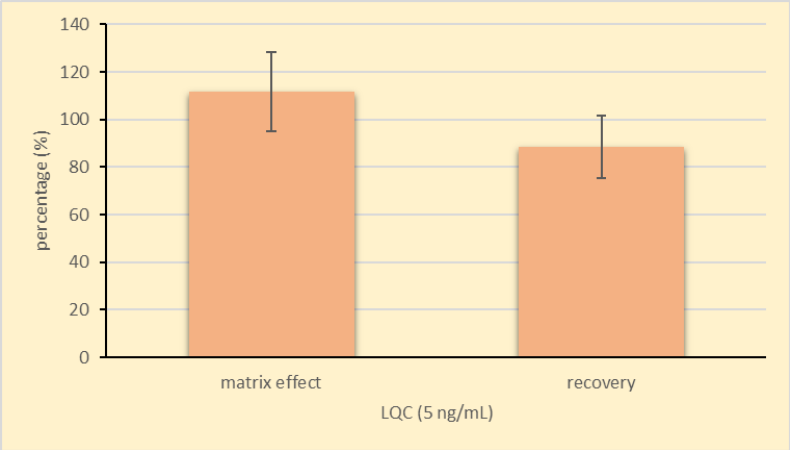

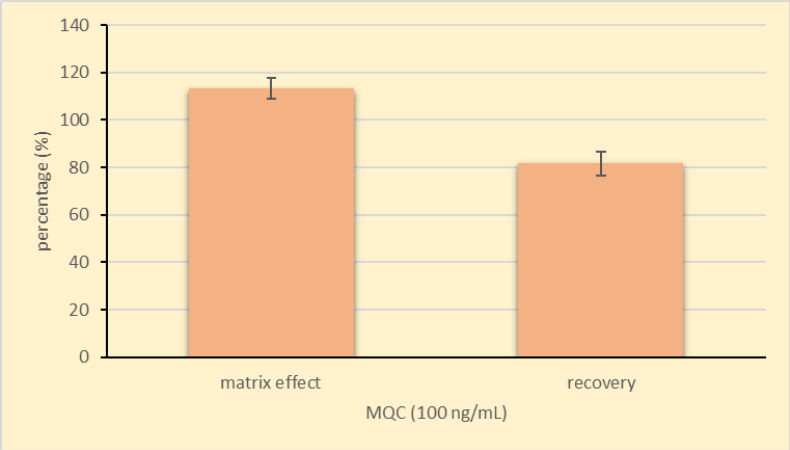

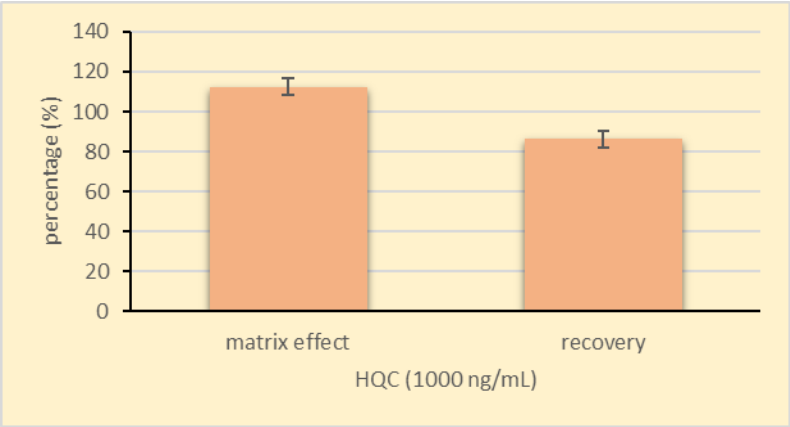

Figure 2-12. Matrix effect and recovery efficiency of carmofur (n=6).

2.3.3.4. Accuracy and precision

The three quality control samples (HQC, MQC, LQC) in six replicates were tested for intra- and inter-day accuracy and precision from the runs on three consecutive days (figure 2-13 and figure 2-14). The accuracy was between 102.40-110.24%, 98.72-107.20%, and 93.30-105.07% for day 1, 2 and 3, respectively. The precision (%CV) was between 1.75-3.55, 1.64-4.15, and 1.79-4.24 for day 1, 2, and 3, respectively. The data for three consecutive days were combined and the accuracy for the QC samples were 104.83% (LQC), 104.45% (MQC), and 98.14% (HQC). The inter-day precision (%CV) was 5.60, 3.37, and 4.24 for the LQC, MQC and HQC samples. Given that both intra- and inter-day accuracy are within ±15% of the desired concentration and the intra- and inter-day precision (%CV) is less than 15%, it indicates satisfactory quality assurance for accuracy and precision.

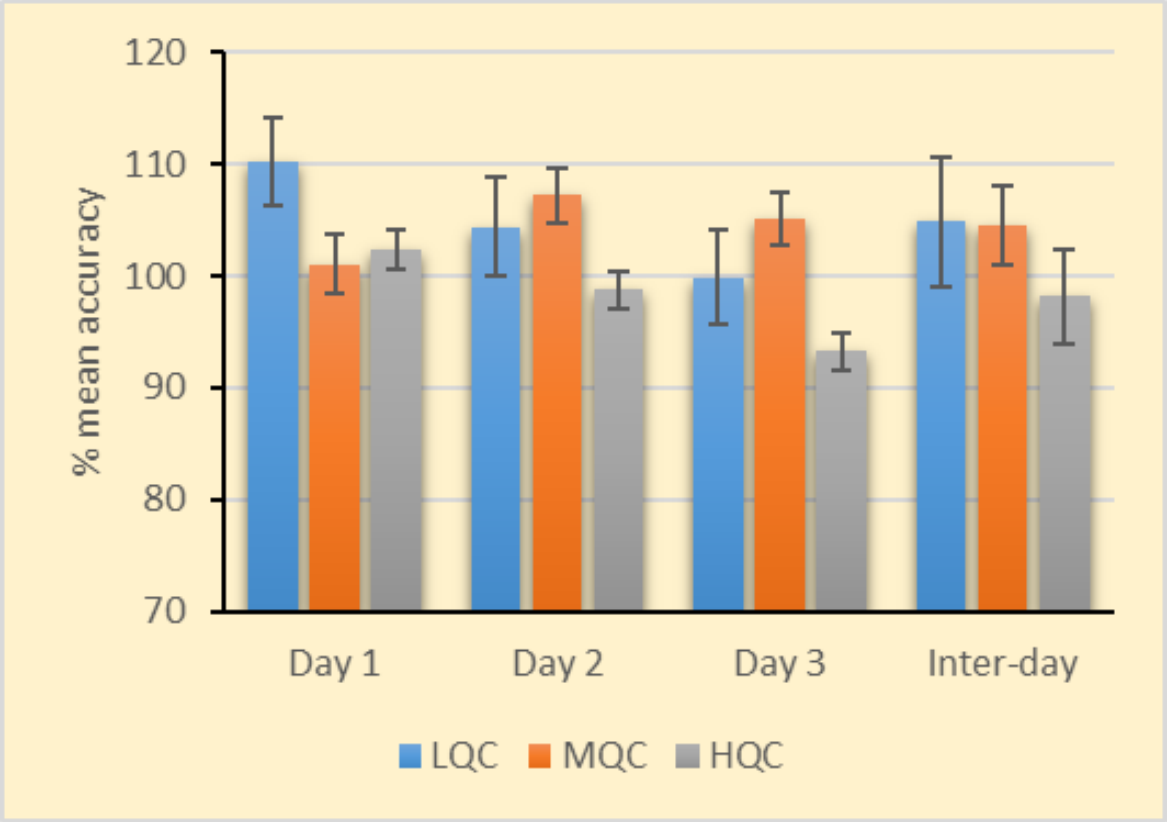

Figure 2-13. Intra- (n=6) and inter-day (n=18) accuracy of carmofur for three QC samples.

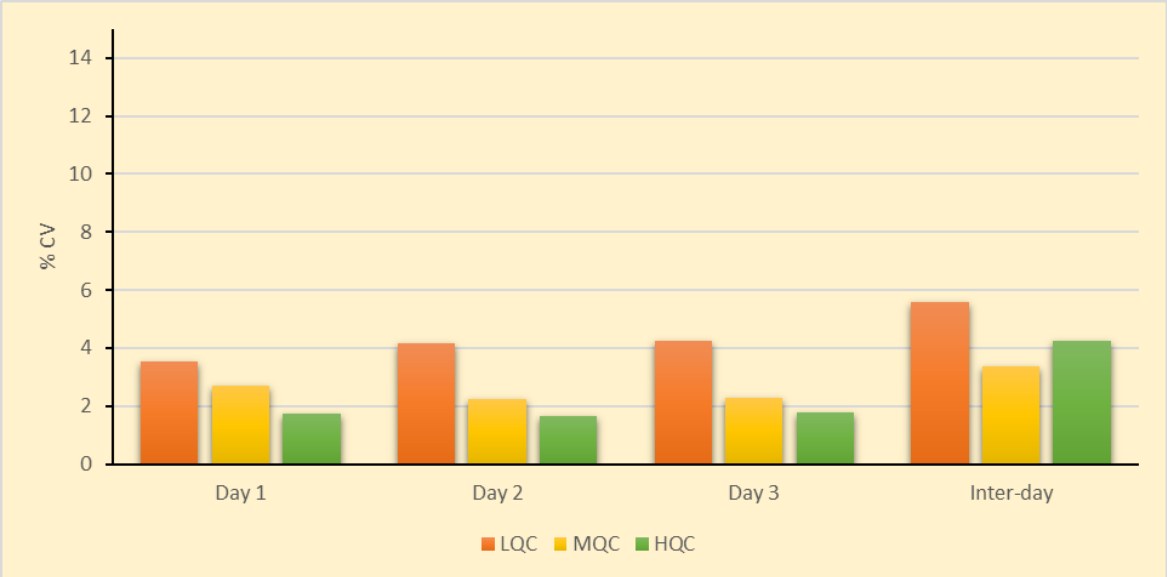

Figure 2-14. Intra-day (n=6) and inter-day (n=18) precision of carmofur for three QC samples.

2.3.3.5. Dilution Integrity

The dilution integrity quality control samples were diluted tenfold and twenty-fold in six replicates and analyzed. The accuracy of the test results were 97.48%, 94.66%, 86.95% and 110.32% for 2 $\mu g.mL^{-1}$ (10X dilution), 2 $\mu g.mL^{-1}$ (20X dilution), 10 $\mu g.mL^{-1}$ (10X dilution), and 10 $\mu g.mL^{-1}$ (20X dilution), respectively which indicates that the method is suitable and is not affected over dilution.

2.3.3.6. Stability

The stability of carmofur in mouse plasma is summarized in figure 2-15. We examined four experimental stability conditions at the three quality control concentrations. The mean accuracy (within ±15%) of the QC samples at different conditions such as long-term stability, freeze-thaw stability, autosampler stability, room temperature stability indicates that the method is appropriate and acceptable as a bioanalytical method.

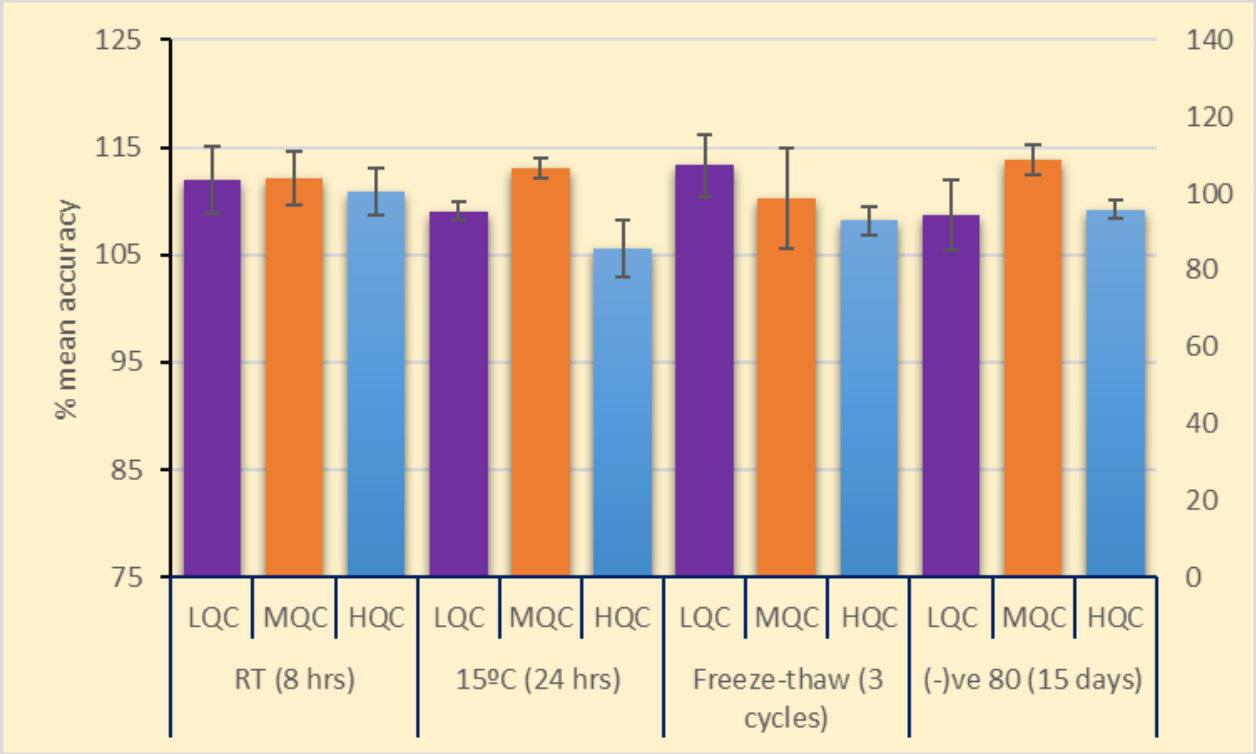

Figure 2-15. Stability of carmofur in mouse plasma (n=6).

2.3.4. Pharmacokinetic study

The developed and validated LC-MS/MS method was tested successfully for an *in-vivo* pharmacokinetic study. A total of 21 Swiss-Webster mice were injected intraperitoneally with carmofur at a dose of 10 $mg.kg^{-1}$. The plasma samples were collected immediately after drug administration and up to 4 hours. The samples were prepared using the protocol described in section 2.2.5. and the level of carmofur was quantified using the LC-MS/MS method. The time-plasma concentration data (figure 2-16) was imported in GraphPad Prism 9 software. The plasma concentration-time curve was generated by non-linear regression and the pharmacokinetic parameters were calculated by one-compartmental analysis. The peak plasma concentration (10279 $ng.ml^{-1}$) of carmofur reaches immediately after injection (T_{max} = 5 min) and elimination

half-life ($T_{1/2}$) was about 9.6 min. The areas under the curve (AUC) was 204795 min ng.mL^{-1}. The elimination rate constant (K_e) was 0.072 min^{-1}.

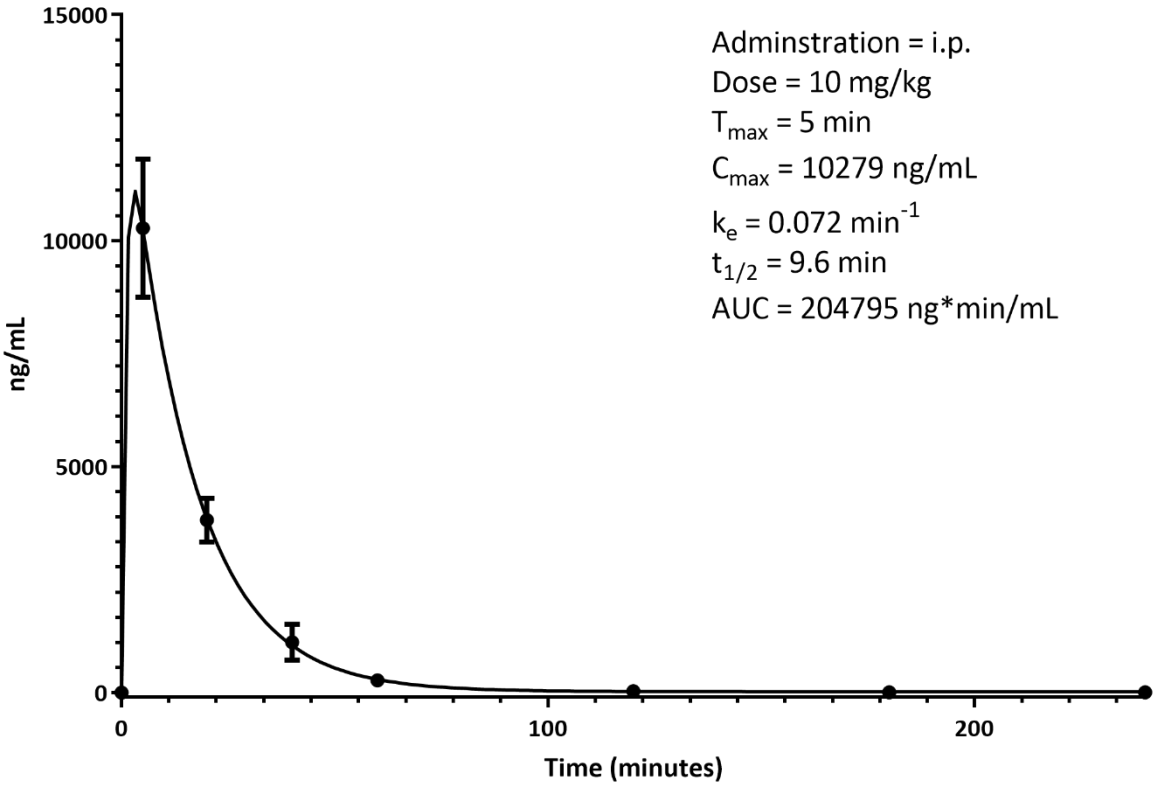

Figure 2-16. Mean plasma concentration-time plot of carmofur after intraperitoneal administration in mouse (n=3 each time point)

2.5. Conclusion

In this work, we have established an LC-MS/MS method for the quantitative bioanalysis of carmofur in mouse plasma. Our liquid-liquid extraction technique required only 100 µL of plasma whereas the past method used about 500 µL of it[9]. Moreover, the extraction technique was able to extract the analyte with least interferences. We have successfully constructed a calibration curve within the range of 5-1000 ng.mL^{-1}. We have also validated our method in terms of

specificity, sensitivity, accuracy, precision, recovery, matrix effect, carryover, dilution integrity and stability. Finally, we have analyzed carmofur concentration in mouse plasma for a pharmacokinetic study. We believe, our report on an LC/MS-MS method, the first one to our knowledge, for carmofur analysis will greatly help towards possible applicability in future preclinical and clinical setting.

References

1. Khojasteh, S. C.; Wong, H.; Hop, C. E. C. A., *Drug Metabolism and Pharmacokinetics Quick Guide*. Springer New York: New York, NY, 2011.
2. Li, L.; Feng, R.; Feng, X.; Chen, Y.; Liu, X.; Sun, W.; Zhang, L., The development and validation of an HPLC-MS/MS method for the determination of eriocitrin in rat plasma and its application to a pharmacokinetic study. *RSC Advances* **2020,** *10* (18), 10552-10558.
3. Yu, J.; Xiao, F.; Asenso, J.; Zhou, P.; Yang, X.-D.; Wang, C.; Wei, W., Simultaneous determination of paeoniflorin-6′-O-benzene sulfonate (CP-25) and its active paeoniflorin (Pae) metabolite in rat plasma using UPLC-MS/MS: an application for pharmacokinetic studies. *RSC Advances* **2016,** *6* (114), 113209-113218.
4. Kono, A.; Tanaka, M.; Eguchi, S.; Hara, Y.; Matsushima, Y., Determination of 1-hexylcarbamoyl-5-fluorouracil and its metabolites in biomedical specimens by high-performance liquid chromatography. *Journal of Chromatography B: Biomedical Sciences and Applications* **1979,** *163* (1), 109-113.
5. Iigo, M.; Nakamura, A.; kuretani, K.; Hoshi, A., Excretion of 1-hexylcarbamoyl-5-fluorouracil in urine of mice. *Journal of Pharmacobio-Dynamics* **1981,** *4* (7), 490-6.
6. Kobari, T.; Iguro, Y.; Ujiie, A.; Namekawa, H., Metabolism of 1-hexylcarbamoyl-5-fluorouracil (HCFU), a new antitumour agent, in rats, rabbits and dogs. *Xenobiotica* **1981,** *11* (1), 57-62.
7. Nakajima, O.; Yoshida, Y.; Isoda, T.; Takemasa, Y.; Imamura, Y.; Koyama, Y., Quantitative determination of 1-hexylcarbamoyl-5-fluorouracil and its metabolites in man. *Journal of Chromatography B: Biomedical Sciences and Applications* **1981,** *225* (1), 91-97.
8. Iigo, M.; Nakamura, A.; Kuretani, K.; Hoshi, A., Distribution of 1-hexylcarbamoyl-5-fluorouracil and 5-fluorouracil by oral administration in mice. *Journal of Pharmacobio-Dynamics* **1979,** *2* (1), 5-11.
9. Wu, K.; Xiu, Y.; Zhou, P.; Qiu, Y.; Li, Y., A New Use for an Old Drug: Carmofur Attenuates Lipopolysaccharide (LPS)-Induced Acute Lung Injury via Inhibition of FAAH and NAAA Activities. *Frontiers in Pharmacology* **2019,** *10*, 818-818.
10. Fda, Bioanalytical Method Validation Guidance for Industry. 2018.
11. Ananthula, S.; Janagam, D. R.; Jamalapuram, S.; Johnson, J. R.; Mandrell, T. D.; Lowe, T. L., Development and validation of sensitive LC/MS/MS method for quantitative bioanalysis of levonorgestrel in rat plasma and application to pharmacokinetics study. *Journal of Chromatography B* **2015,** *1003*, 47-53.
12. Kosovec, J. E.; Egorin, M. J.; Gjurich, S.; Beumer, J. H., Quantitation of 5-fluorouracil (5-FU) in human plasma by liquid chromatography/electrospray ionization tandem mass spectrometry. *Rapid Communications in Mass Spectrometry* **2008,** *22* (2), 224-230.
13. Neervannan, S., Preclinical formulations for discovery and toxicology: physicochemical challenges. *Expert Opinion on Drug Metabolism & Toxicology* **2006,** *2* (5), 715-731.
14. Woo, Y.; Kim, G.; Jeong, E.; Kim, C., Simultaneous determination of doxifluridine and 5-fluorouracil in monkey serum by high performance liquid chromatography with tandem mass spectrometry. *Journal of Chromatography B* **2008,** *875* (2), 487-492.
15. Remaud, G.; Boisdroncelle, M.; Morel, A.; Gamelin, A., Sensitive MS/MS–liquid chromatography assay for simultaneous determination of tegafur, 5-fluorouracil and 5-fluorodihydrouracil in plasma. *Journal of Chromatography B* **2005,** *824* (1-2), 153-160.
16. Li, W.; Zhang, J.; Tse, F. L. S., *Handbook of LC-MS Bioanalysis*. John Wiley & Sons Inc.: Hoboken, NJ, USA, 2013.
17. Liu, G. W.; Aubrey, A. F., Best Practices in Biological Sample Preparation for Lc-Ms Bioanalysis. *Handbook of Lc-Ms Bioanalysis: Best Practices, Experimental Protocols, and Regulations* **2013**, 165-184.

18. Polson, C.; Sarkar, P.; Incledon, B.; Raguvaran, V.; Grant, R., Optimization of protein precipitation based upon effectiveness of protein removal and ionization effect in liquid chromatography-tandem mass spectrometry. *J Chromatogr B* **2003,** *785* (2), 263-275.

Chapter-3

Development and Validation of LC-MS/MS method with application to parallel artificial membrane permeability assay (PAMPA) and permeability assessment of acid ceramidase inhibitors

3.1. Introduction

Parallel artificial membrane permeability assay (PAMPA) is a technique that has been developed to mimic passive and transcellular transmission in vitro[1]. The PAMPA was coined by Kansy et al. in 1998 using artificial egg lecithin/dodecane membrane to simulate gastrointestinal permeability[2]. Later on many variations of PAMPA were developed such as PAMPA-skin (skin penetration)[3], BBB-PAMPA (blood-brain-barrier penetration)[4] etc. The various forms of PAMPA were developed based on the nature/composition of the membrane substance, pH of PAMPA matrix (donor/acceptor wells) and the incubation time etc[5]. Since inception, PAMPA has been established as a better technique in terms of permeation predictability and high-throughput analysis.

Assessing BBB permeability is one of the most important considerations at early-stage drug discovery especially for disorders of the central nervous system (CNS) such as glioblastoma[6]. It is also important for drugs targeting peripheral organs. A limited CNS penetration would limit the exhibition of side effects associated with the drug exposure.

The-blood-brain barrier is a physiological barrier that separates the interstitial fluid of the brain from the blood. It is composed of tight junctions between the endothelial cells resulting in a superior barrier compared to what is found in peripheral endothelium. In addition to that, the presence of several enzymes such as glutamyl transpeptidase, alkaline phosphatase and aromatic acid decarboxylase makes the formation of a metabolic barrier. Due to this unique and selective morphology, the penetration of the BBB is primarily transcellular[7-8].

Efficacy of glioblastoma chemotherapy can also be limited by the BBB permeability of the therapeutic agents. Therefore, assessing the selectivity of BBB penetration is the foremost evaluation before doing further studies. It is known that carmofur, an acid ceramidase inhibitor can cross the blood brain barrier; however, to what extent is not well known[9-10]. No information for another potential acid ceramidase inhibitor ARN14988 for BBB permeability is found in the literature.

Assessing the in vivo BBB permeability at an early stage drug discovery is expensive and can become infeasible for a wide array of compounds under screening. Particularly, the introduction of combinatorial chemistry has enabled the synthesis of hundreds of potential drug candidates in a short period of time[8].

In contrast to cell-based assays, PAMPA is cheap, provides high-throughput accurate analysis, avoids the complexity of active transport and ranks the test compounds based on permeability property alone[11]. Although cell-based assays such as Caco-2 permeability have some advantages such as active transport predictability, but they take longer to perform, less throughput and are expensive[8].

PAMPA kit is composed of two parts, a donor plate and an acceptor plate (figure 3-1), and estimates the permeability from donor to acceptor plate over an incubation period[12]. An artificial membrane, aligned with the donor plate, usually composed of lecithin, phosphatidylcholine, hexadecane or porcine brain lipid extract, represents the passive diffusion which is the principle mechanism of small molecule transfusion through BBB[13-14]. An important consideration while doing PAMPA is to use multiple controls ranging from low to high BBB permeability in order to evaluate the membrane integrity and validation of study results[15].

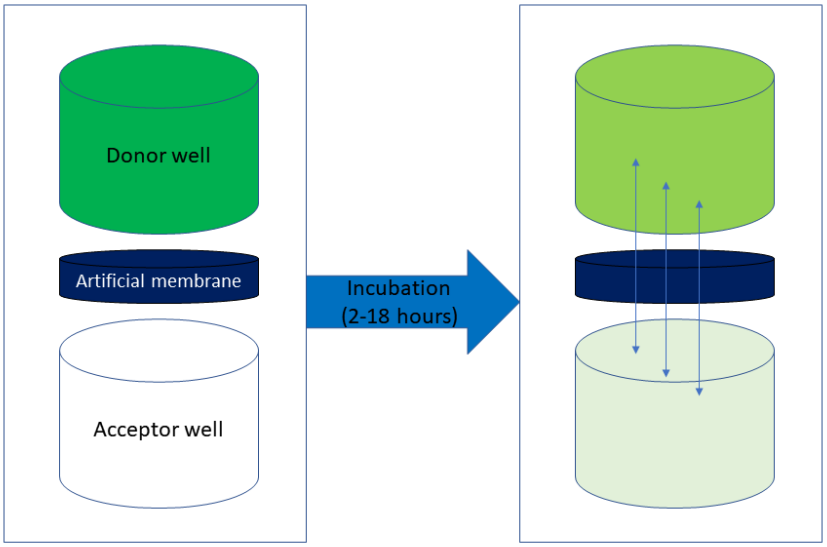

Figure 3-1. Schematic of Parallel artificial membrane permeability assay (PAMPA)[14].

PAMPA samples from acceptor and donor wells are analyzed using either UV-vis spectrophotometry, high-performance liquid chromatography or liquid chromatography-mass spectrometric technique. The disadvantage of using UV-vis spectrophotometric technique is that it can falsely report a result if multiple compounds in the solution absorbs at the same wavelength. This particularly becomes a problem when the test compounds are unstable. Therefore, we developed liquid chromatography-tandem mass spectrometry methods to determine three controls (verapamil, ranitidine, and naproxen) and test compounds (carmofur, ARN14988-M) (figure 3-2) in PAMPA matrix. Furthermore, we validated the methods in terms of selectivity, linearity, accuracy, precision, and stability. Finally, we evaluated the PAMPA-BBB permeability of the test compounds using the LC-MS/MS methods we developed.

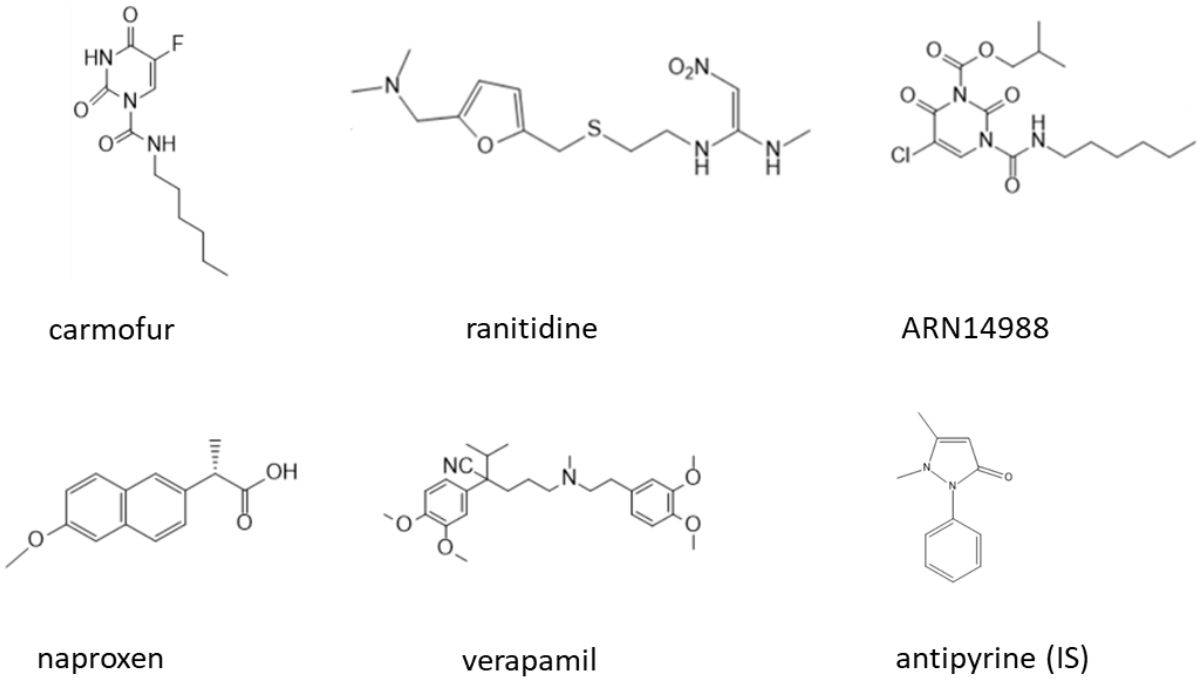

Figure 3-2. Structures of the compounds used in this work.

3.2. Experimental

3.2.1. Chemicals and reagents

Carmofur and ARN14988 are the two acid ceramidase inhibitors that were used as test compounds. Carmofur was obtained from Tokyo Chemical Co. Ltd (Portland, OR, USA). ARN-14988 (CAS No. 1502027-70-4) was synthesized in-house by Vilashini Rajaratnam (Mirza lab) with the assistance of Cook group at the University of Wisconsin-Milwaukee according to the procedure described[16]. Antipyrine (CAS No. 60-80-0) was used as an internal standard and was obtained from Millipore-Sigma (St. Louis, MO, USA). Ranitidine, verapamil and naproxen were used as positive controls representing different degrees of BBB permeability. Ranitidine (CAS No. 66357-59-3), verapamil (CAS No. 152-11-4), and naproxen (CAS No. 22204-53-1) were purchased from Millipore-Sigma (St. Louis, MO, USA).

All solvents and buffers used were of analytical grade. PBS solution at pH 7.4 and n-hexadecane were procured from Thermo-Fisher Scientific (MA, USA). Dimethyl sulfoxide (DMSO) and n-hexane were purchased from Millipore-Sigma (St. Louis, MO, USA). LC-MS grade mobile phase solvents (water, acetonitrile, methanol, formic acid) were purchased from Fisher chemical (USA).

Donor plate (MAIPNTR10) and acceptor plates (MATRNPS50) for the PAMPA assay were purchased from Millipore-Sigma (St. Louis, MO, USA).

3.2.2. Instrumentation

Liquid chromatography was performed on a Shimadzu Nexera X2 UPLC system consisting of binary pumps (Shimadzu LC-30AD), degasser units (Shimadzu DGU-20A 5R), autosampler (Shimadzu SIL-30AC MP) and column oven (Shimadzu CTO20A). The UPLC system was interfaced with a Shimadzu 8040 triple quadrupole mass spectrometer. The LCMS 8040 instrument is equipped with dual ionization source (Electrospray + Atmospheric Pressure Chemical Ionization). For supplying nitrogen gas to the mass spectrometer, we used an in-house nitrogen generator (NM32LA) purchased from Peak Scientific (Glasgow, UK). The CID gas Argon (Ar) was purchased from Airgas (PA, USA).

The analytes were retained, and chromatographic separation was achieved on a XBridge BEH C18 XP column (100 mm X 3 mm, 2.5 µm, Waters Corporation, MA, USA). 10 mM ammonium acetate in water was used as mobile phase A and methanol was used as mobile phase B for the analysis of carmofur, ARN14988, ranitidine and naproxen while 0.1% formic acid in water was used as mobile phase A and 0.1% formic acid in acetonitrile was used as mobile phase B for the analysis of verapamil. The total runtime was 9 min with the gradient elution program as follows: 45% of B from 0-0.50 min, a linear gradient from 45% B to 95% B from 0.50 - 3.00 min, 95% B to 100% B from 3.00-3.50 min, 100% of B from 3.50 -6.00 min, a linear gradient of 100% B to 45% B from 6.00 - 6.50 min and 45% B from 6.50 to 9 min. The column oven was kept at 40°C.

All analytes were ionized by electrospray ionization (ESI) technique and the quantification was achieved in multiple reaction monitoring (MRM) mode. The desolvation line and ion source temperature were kept at 250°C and 400°C, respectively. The drying gas and nebulizing gas flow

rate were 15 L/min and 2 L/min, respectively. The dwell time of analysis for all analytes was 100 msec. Data were acquired and post-acquisition data processing were performed in LabSolutions software (Shimadzu Corporation, Japan) and Microsoft Excel (Microsoft, USA) software packages.

3.2.3. Preparation of standard solutions and quality control samples

Stock solutions for each compound were prepared in DMSO. Standard solutions were prepared by matrix matching with the prepared samples. Quality control (QC) samples were prepared at three different concentrations (low QC, LQC; medium QC, MQC; high QC, HQC). The LQC/MQC/HQC concentrations were verapamil (0.1 µM/1.2 µM/4.0 µM), naproxen (0.9 µM/4.5 µM/18 µM), ranitidine (0.225 µM/1.8 µM/4.5 µM), ARN14988 (0.9 µM/4.5 µM/9 µM). Each of the samples had a final composition of 5% DMSO in PBS at pH 7.4 except for verapamil which was diluted further 2.5 times with acetonitrile. Antipyrine was used as an internal standard at 1 µM level for carmofur, ARN14988, ranitidine and naproxen analysis and at 1.2 µM level for verapamil analysis.

3.2.4. Sample preparation

Stock solution was diluted with PBS and DMSO as needed to prepare the donor well concentration. The assay was performed following the procedure as described in section 3.2.6. For LC-MS/MS analysis, IS solution was added before analysis.

3.2.5. LC-MS/MS Method validation

The developed method was evaluated to validate for selectivity, linearity, accuracy, precision, and stability in accordance with Analytical Procedures and Methods Validation for Drugs and Biologics guideline and ICH Q2(R1)[17-18].

3.2.5.1. Selectivity/Specificity

Selectivity was examined to evaluate the ability of the method to differentiate and quantify the analytes and internal standards in presence of other components in the sample (ICH Q2(R1)). Selectivity was determined by comparing blank matrix and standard solutions- spiked with the analytes and pooled PAMPA samples.

3.2.5.2. Carryover

Carryover was evaluated by injecting a blank sample after the injection of HQC sample for each analyte.

3.2.5.3. Sensitivity and linearity

Instrument sensitivity was assessed at the lower limit of quantification (LOQ). LOQ was evaluated at the lowest point in the calibration with a minimum signal to noise (S/N) ratio of 10. A series of calibration standards were prepared including the LOQ in order to determine the linearity. The calibration curves were prepared by weighted least square linear regression analysis with a weighing factor of $1/concentration^2$ and the linearity was considered acceptable with a correlation coefficient (R^2) of 0.99 or greater.

3.2.5.4. Intra- and inter-day accuracy and precision

The samples at three different concentrations (LQC, MQC, HQC) were prepared separately in six replicates for three consecutive days and analyzed for intra-day accuracy and precision. The data obtained from intra-day accuracy and precision were re-analyzed to determine inter-day accuracy and precision. The precision was expressed as the percent coefficient of variance (%CV) and the accuracy was expressed as the percent mean accuracy. It was considered acceptable if the %CV is <15% and % mean accuracy is within ±20% respectively.

3.2.5.5. Stability

The stability of the analytes at the three QC concentrations (LQC, MQC, and HQC) were assessed over a period of 24 hours.

3.2.6. PAMPA assay

The PAMPA assay was performed according to the methodology published in literature[11, 14, 19]. In brief, 15 µL of 5% (v/v) n-hexadecane in n-hexane was added to the donor plate well and allowed to evaporate to form an artificial BBB membrane. 300 µL of 5% (v/v) DMSO in PBS solution (pH 7.4) was added into the acceptor well followed by 150 µL of analyte solution in 5% (v/v) DMSO in PBS solution into the donor well. The donor well plate was then placed on top of the acceptor well plate and incubated on a reciprocal shaker for 2-18 hours with agitation at 100 rpm. After incubation, 100 µL of acceptor well solution and 100 µL of donor well solution was transferred for analysis. The assay was performed in triplicate. The apparent permeability, P_{app}, for the analytes was calculated using the following equation:

$$P_{app} = C \times -\ln\left(1 - \frac{[Drug_{acceptor}]}{[Drug_{equilibirum}]}\right)$$

and,

$$C = \frac{V_A \times V_D}{(V_A + V_D)A \times t}$$

where, $Drug_{acceptor}$ and $Drug_{equilibrium}$ is the concentration of the analyte from the acceptor well and equilibrium solution (if the donor and acceptor wells were combined) respectively, V_A and V_D are the volumes in acceptor well and donor well respectively, t is the incubation time (seconds), and A is the active surface area (0.283 cm^2) of the membrane.

3.3. Results and discussion

3.3.1. Method development

Herein, we aimed at developing accurate and sensitive LC-MS/MS method with little to no sample pre-treatment. In addition to our test compounds, it is also essential to select multiple controls of varying Biopharmaceutical Classification System (BCS) category. Addition of controls to PAMPA evaluate the membrane integrity and validate the study results[15]. In order to represent the entire spectrum of BBB permeability, we selected three compounds based on their different degree of permeability (verapamil, high permeability; naproxen, medium-high permeability; ranitidine, low permeability). Verapamil and naproxen are BCS class II drugs - indicating high solubility and high permeability. Ranitidine is BCS class III drug-indicating good solubility but poor permeability.

The differences in their permeability come from the differences in their chemical structure, presence of functional groups and their relevant physio-chemical properties. During method development, highest ionization efficiency and linearity was prioritized with reasonable resolution and peak shape of the compounds. Mass spectrometry conditions were optimized by both manual tuning and optimization tool built in with the LabSolutions software. Initially Q3 scans were performed for all compounds to identify the precursor ions. MRM transitions were optimized from product ion scans. Compounds were ionized in both polarities. Furthermore, other mass spectrometric conditions like collision energy (CE), needle position, desolvation line temperature, ion source temperature, dwell time, and drying gas flow rate were optimized manually for maximum sensitivity. 1 µL of sample injection gave good results without salt deposition in ESI chamber. Optimized mass spectrometric parameters are listed in table 3-1.

Compound	Precursor ion (m/z)	Product ion (m/z)	Q1 Pre-Bias (V)	CE (V)	Q3 Pre-Bias (V)
Carmofur	256.25	129.05	11	9	23
ARN14988	264.10	147.10	-24	-11	-14
Ranitidine	315.15	176.10	-14	-18	-17
Verapamil	455.30	165.10	-12	-29	-28
Naproxen	229.25	169.05	10	28	30
Antipyrine (IS)	189.05	56.10	-12	-34	-21

Table 3-1. Optimized mass spectrometric conditions used for the analytes in PAMPA study.

Among the compounds, carmofur decomposes to 5-FU in presence of physiologic basic pH in a time-dependent manner[20]. Because of the instability of carmofur in physiologic pH (figure 3-3), it has not been pursued for intra-day and inter-day accuracy, precision, and stability in method validation. However, the compound was linear within the range of quantification in six replicate analyses with freshly prepared standards.

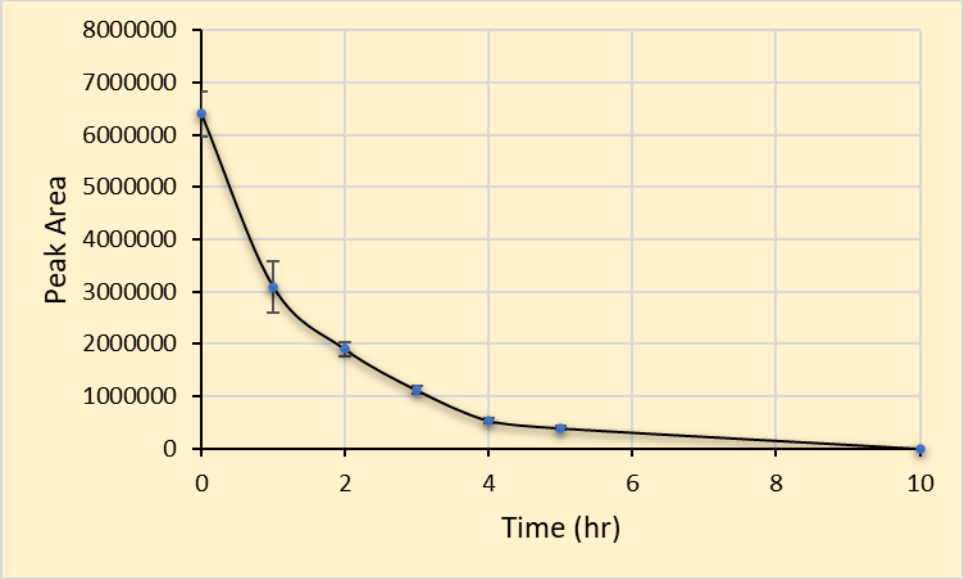

Figure 3-3. Degradation of carmofur over time in 5% DMSO in PBS solution (n=3).

On the other hand, Q3 scan in +ve mode (figure 3-4) of ARN14988 in neat solvent yields two peaks (m/z 391 and m/z 264). We hypothesize that m/z 391 is the ammonium adduct of ARN14988 and m/z 264 is the ammonium adduct of the remaining moiety after the loss of 1-hexylcarbamoyl group.

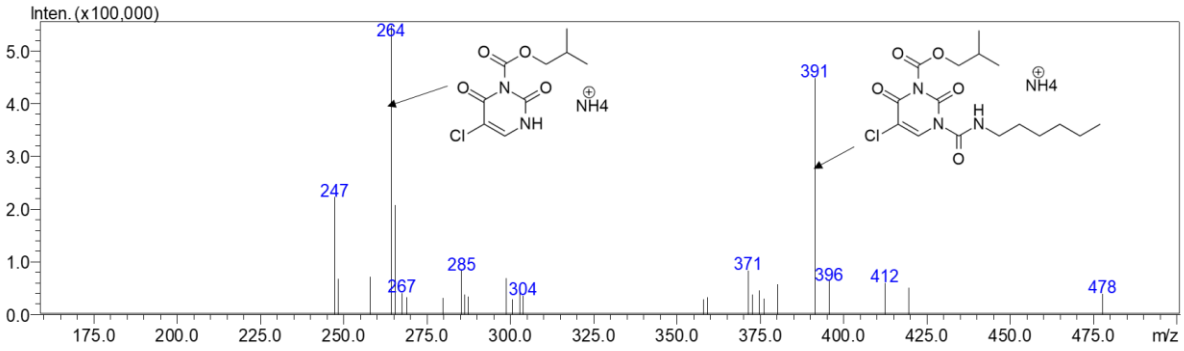

Figure 3-4. Q3 (+ve mode) scan of ARN14988.

We investigated the MRM transition for both m/z 391 and m/z 264. We found that both of these ions produces m/z 147 as the fragment fragment or product ion (figure 3-5).

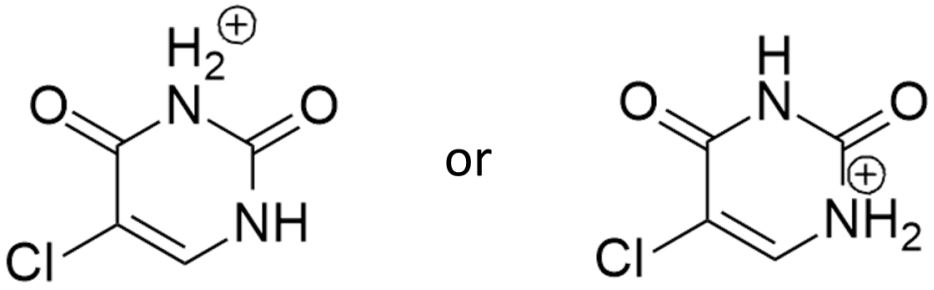

Figure 3-5. Probable structure of the fragment m/z 147.

Thereafter, we investigated the stability of m/z 391 and m/z 264 in presence of PBS in 5% DMSO. We found that, ARN14988 (m/z 391) is not stable in PBS and readily decomposes in the moiety that ionizes as m/z 264 (figure 3-6). The instability of ARN14988 appears to be greater than it is for carmofur in PBS solution.

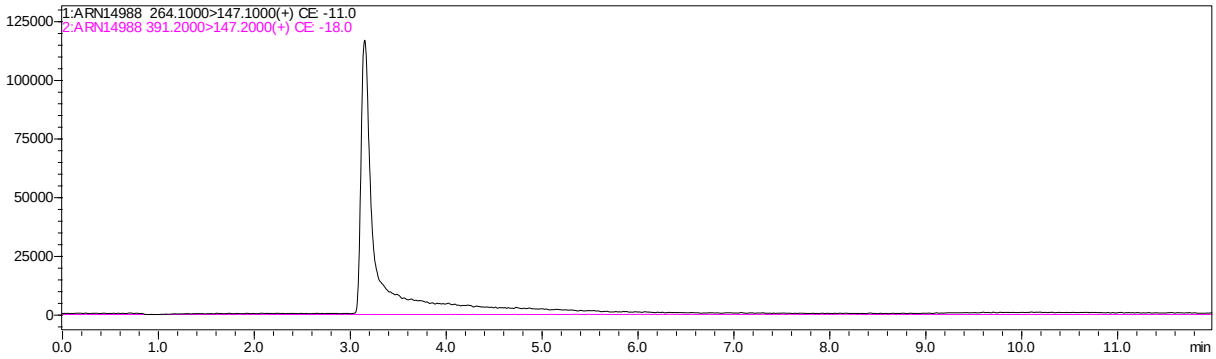

Figure 3-6. Absence of m/z 391 to m/z 147 transition (pink) in ARN14988 solution in PBS with 5% DMSO at time 15 min.

We also studied the stability of m/z 264 over a period of 24 hours before performing further studies. The stability study indicates that m/z 264 is fairly stable over the period of 24 hours.

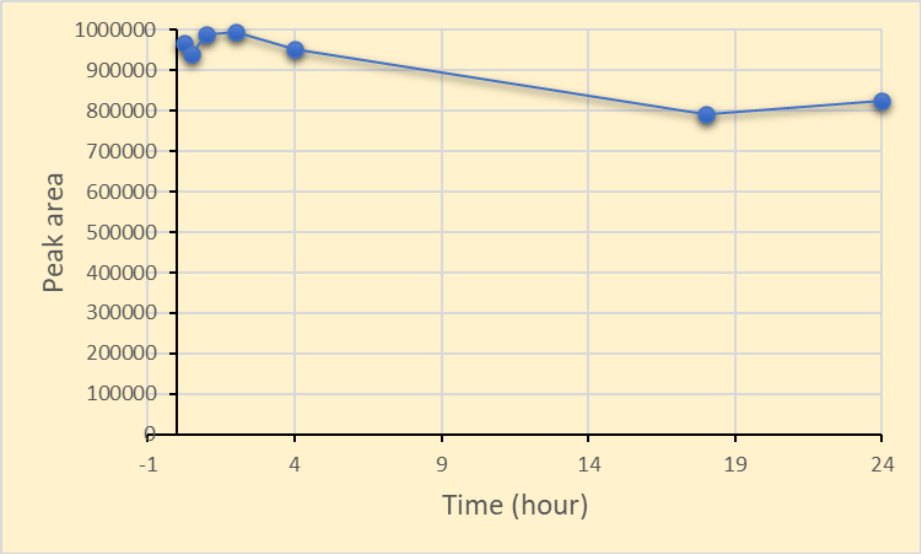

Figure 3-7. Stability of m/z 264 to m/z 147 transition over a period of 24 hours (n=1).

It is important to mention that ARN14988 is found very cytotoxic in melanoma and glioblastoma cell lines[16, 21]. ARN14988 inhibits adult glioblastoma cell line U87MG more efficiently than FDA approved drug temozolomide over a period of 24 hours. Given the instability of AR14988 in basic pH, the cytotoxic activity of ARN14988 could be due to the activity of the moiety that corresponds to m/z 264. Although the cytotoxicity of m/z 264 is yet to be tested, we decided to study the in vitro BBB permeability of m/z 264 (referred as ARN14988-M from hereon) by PAMPA.

During the method development, we also observed significant carryover (figure B1) and lack of linearity (figure B2) with verapamil analysis.

We tested the effect of diluent and mobile phase on verapamil ionization and carryover. Presence of acetonitrile as diluent in verapamil solution provides higher peak area compared to verapamil solution prepared in PBS which indicates the effect of diluent in verapamil ionization (figure 3-8). Investigation around the two sets of mobile phases reveals that 0.1% formic acid in methanol

and 10 mM ammonium acetate in water gives better peak area and hence, better ionization of verapamil. However, 0.1% formic acid in water and 0.1% formic acid in acetonitrile provides less peak area but solves the carryover issue. Therefore, we decided to use 0.1% formic acid in water as mobile phase A and 0.1% formic acid in acetonitrile as mobile phase B for verapamil analysis.

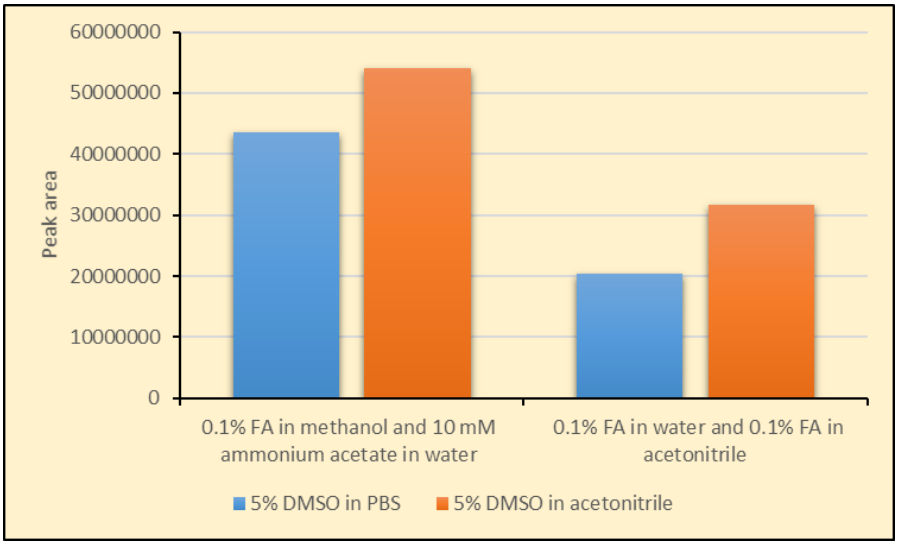

Figure 3-8. Effect of diluent and mobile phase on ionization of verapamil (n=1).

Our investigation on diluent continued and we tested different ratios of PBS and acetonitrile (ACN) and their impact on linearity. Presence of acetonitrile in the PAMPA matrix resolves the issue of lack of linearity and we decided to use PBS: ACN (40:60) ratio for analyzing the verapamil samples (figure 3-9). In order to do so, the collected pooled PAMPA samples for verapamil were diluted 2.5 times with 5% DMSO in acetonitrile before MS analysis.

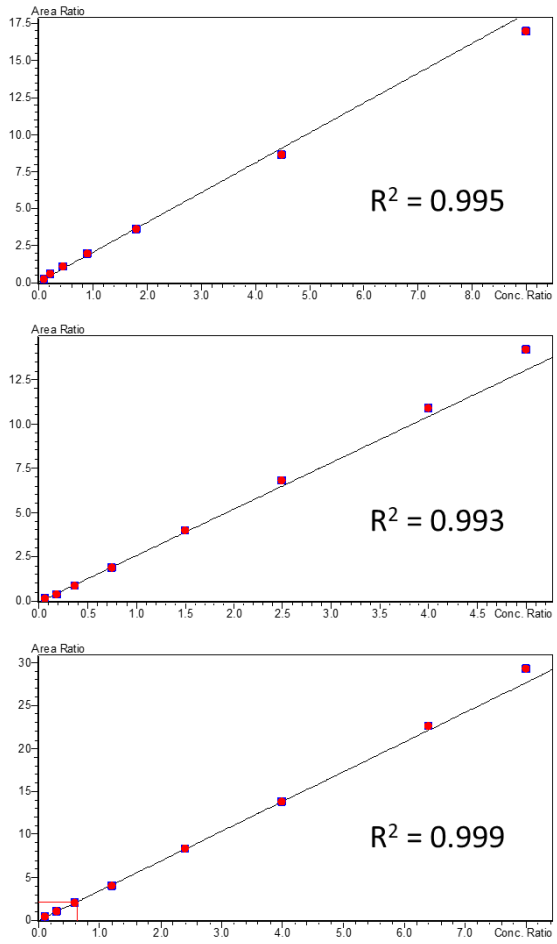

Range: 0.09 µM-9.00 µM
PBS:ACN (0:100)

Range: 0.0625 uM-9.00 µM
PBS: ACN (25:75)

Range: 0.09 uM-9.00 µM
PBS: ACN (40:60)

Figure 3-9. Effect of diluent on linearity of verapamil (n=1).

It was also observed that the sensitivity of naproxen significantly gets diminished in presence of formic acid in mobile phase. Therefore, we opted to use two different sets of mobile phases as mentioned in section 3.2.2.

We also divided the data acquisition into segments to increase the sensitivity of the analysis. Antipyrine, ranitidine, ARN14988-M, naproxen, and carmofur were monitored between 0-2, 0-4, 2-4, 2-4, and 4-7 min respectively.

The retention time was 5.35 min for carmofur, 1.4 min for antipyrine, 1.1 min for ranitidine, 2.4 min for ARN14988-M, 2.88 min for naproxen and 2.35 min for verapamil. Figure 3-10 shows some representative chromatograms for the analytes.

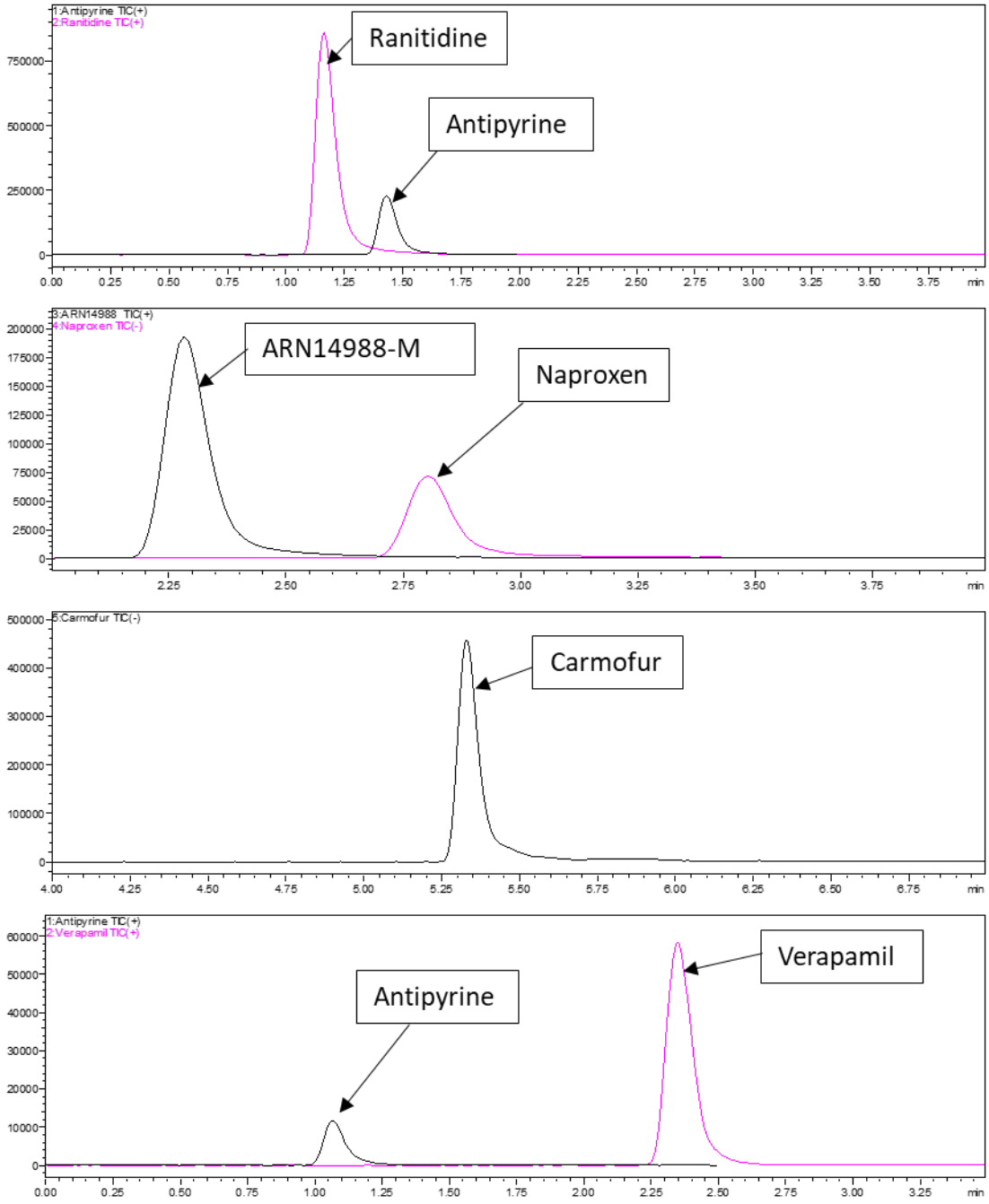

Figure 3-10. Representative chromatograms for the analytes under study.

3.3.2. Method validation

3.3.2.1. Selectivity

The selectivity was evaluated by examining the chromatograms of blank matrix, standard solution spiked with the analytes and IS, and pooled PAMPA sample spiked with IS. No interfering peaks were detected, suggesting that the method was selective.

3.3.2.2. Carryover

Carryover was evaluated based on the presence or absence of analyte peak in blank after running the HQC samples. Figure 3-11 shows that our method shows no carryover.

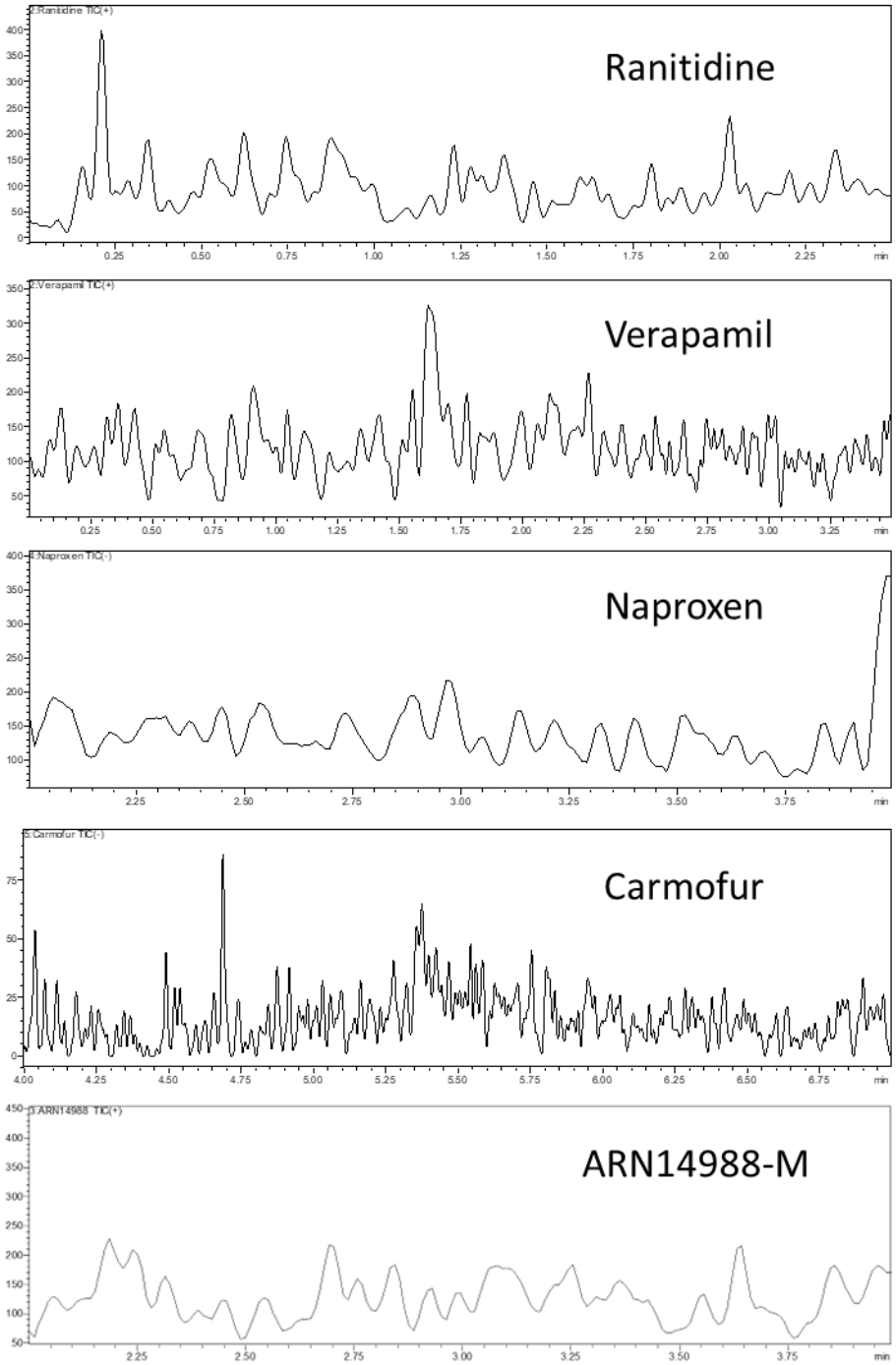

Figure 3-11. Absence of carryover in blanks after running the HQC samples.

3.3.2.3. Linearity

According to our literature search, there were no reported LOQ for the compounds under study in PAMPA matrix. In this work, a stock solution of the analytes was serially diluted in order to determine the LOQ. In addition to high sensitivity, the developed method also showed good linearity for all compounds over the quantification range. We also studied six replicates for the calibration curves which also indicated the good reproducibility of our method. The calibration standards for verapamil were prepared at 0.1 µM, 0.3 µM, 0.6 µM, 1.2 µM, 2.4 µM, and 4.0 µM concentrations. The calibration standards for carmofur were prepared at 0.45 µM, 1.8 µM, 9.0 µM, 18.0 µM, 45.0 µM, and 90.0 µM concentrations. The calibration standards for ARN14988-M were prepared at 0.45 µM, 0.90 µM, 1.80 µM, 4.50 µM, 7.20 µM, and 9.0 µM concentrations. The calibration standards for naproxen were prepared at 0.45 µM, 0.90 µM, 1.80 µM, 4.50 µM, 9.0 µM, and 18.0 µM concentrations. The calibration standards for ranitidine were prepared at 0.045 µM, 0.090 µM, 0.225 µM, 0.450 µM, 0.900 µM, 1.800, and 4.500 µM concentrations.

The LOQ, linear range of quantification, linear fit equation, and their corresponding correlation co-efficient are reported in table 3-2. Representative calibration curves are shown in figure 3-12.

Compound	Linearity	Linear fit equation	Correlation co-efficient (R^2)
Carmofur	0.45 µM - 90 µM	y = (0.1732±0.0127)x + 0.0062±0.0056	0.9933±0.0021
ARN14988-M	0.45 µM - 9 µM	y = (0.0899±0.0008)x - 0.0009±0.0024	0.9986±0.0008
Ranitidine	0.045 µM - 4.5 µM	y = (4.1111±0.7038)x + 0.0177±0.0149	0.9965±0.0017
Verapamil	0.1 µM - 4.0 µM	y = (3.8444±0.1772)x - 0.0776±0.0120	0.9967±0.0013
Naproxen	0.45 µM - 18 µM	y = (0.0466±0.0028)x - 0.0024±0.0020	0.9953±0.0010

Table 3-2. Linearity, and calibration curve data (n=6) for the five analytes.

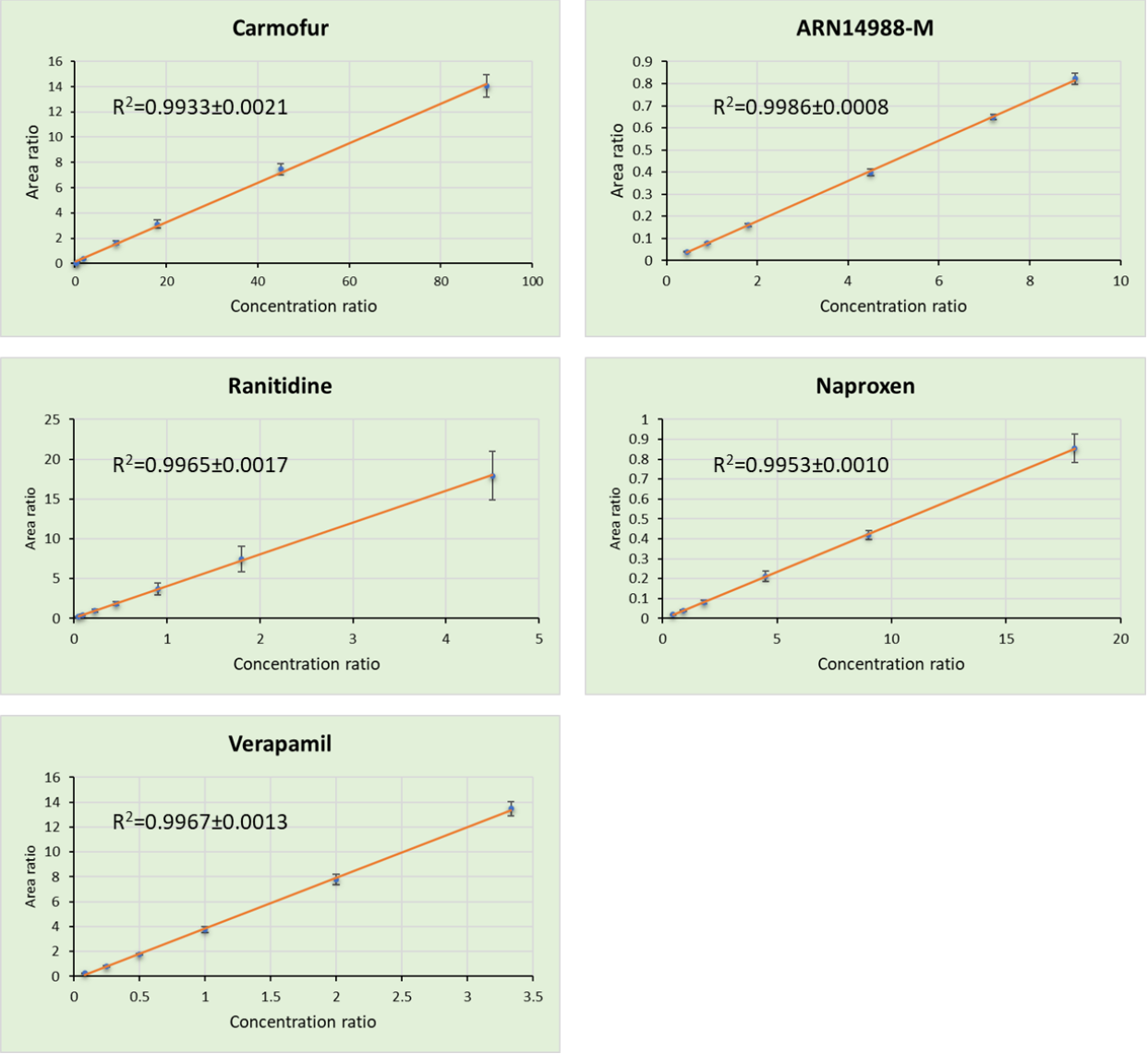

Figure 3-12. Calibration curves of carmofur, ARN14988-M, ranitidine, naproxen, and verapamil.

3.3.2.4. Intra- and inter-day accuracy and precision

Three QC samples for each compound were tested for their intra-day and inter-day accuracy and precision. All analytes at these concentrations showed excellent intra-day and inter-day accuracy and precision. The resulting data are summarized in figure 3-13 and figure 3-14 respectively. The

results of intra-day and inter-day accuracy and precision were within the range defined for accuracy and precision under section 3.2.5.4.

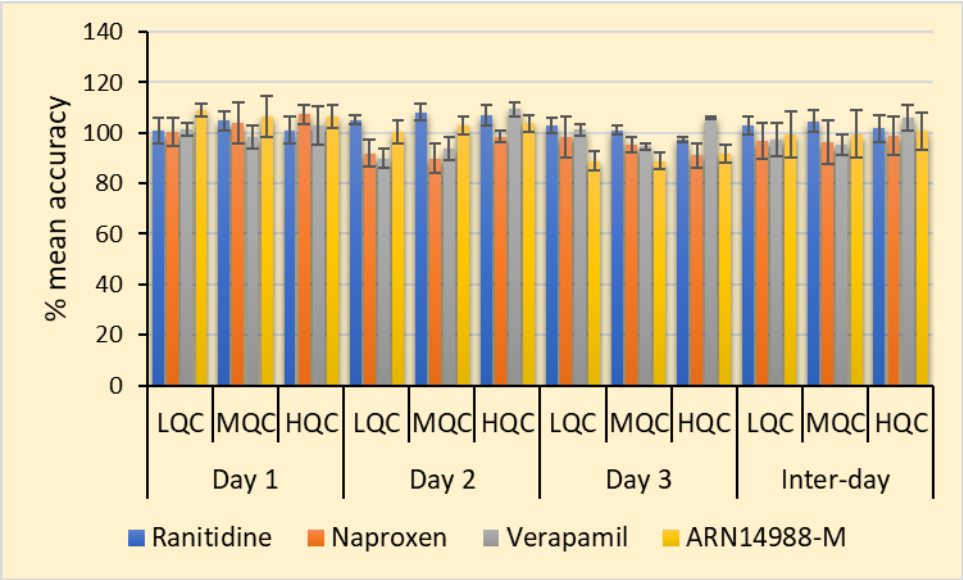

Figure 3-13. Summary of intra- (n=6) and inter-day (n=18) accuracy study.

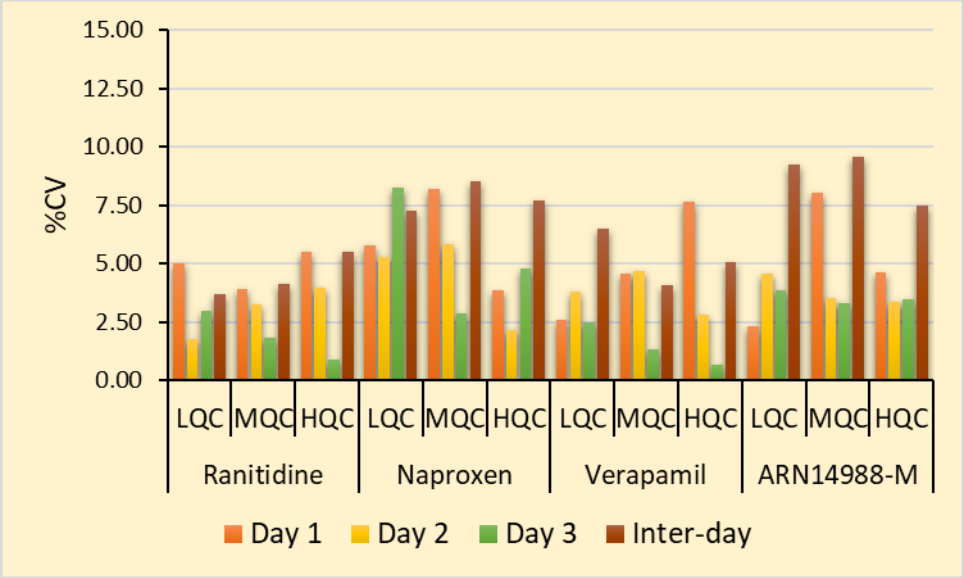

Figure 3-14. Summary of intra- (n=6) and inter- (n=18) day precision study.

3.3.2.5. Stability

Stability of the analytes of interest in test solution over the course of analysis is important to get reliable and reproducible results. We determined the stability of the compounds at room temperature for 24 hours at different time points, given that PAMPA samples are expected to analyze immediately without any storage. The stability data are summarized in figure 3-15, indicating the stability of the compounds; therefore, making the method suitable for application to PAMPA assay.

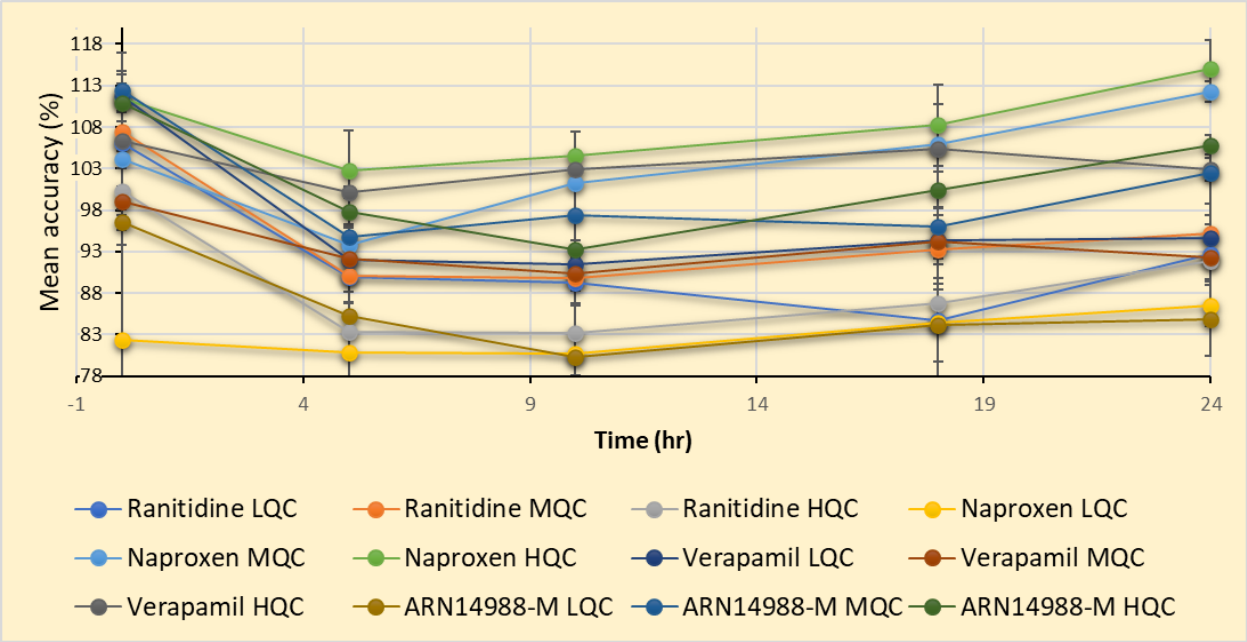

Figure 3-15. Summary of the stability (n=3) study over a period of 24 hours.

3.3.3. Application to PAMPA assay

Finally, we determined the applicability of the method by analyzing the PAMPA samples. The PAMPA assay was performed in triplicate. After the incubation period, the samples from acceptor well and the donor well were analyzed by LC-MS/MS. The results were summarized in table 3-3. Based on the measured Log $P_{app,}$ it is noticeable that the Log P_{app} for carmofur and ARN14988-M is in between the Log P_{app} for ranitidine and verapamil which is a strong indication that both of this two test compounds are likely to cross the blood brain barrier

Compound	**Log P_{app}**	
	Experimental	Literature[22]
Verapamil	-4.92	-3.80
Naproxen	-7.02	-5.04
Ranitidine	-6.98	-6.88
Carmofur	-6.11	-
ARN14988-M	-6.50	-

Table 3-3. Summary of the PAMPA study for the test compounds.

3.4. Conclusion

This study presents simple, quick and sensitive liquid chromatography and mass spectrometric method for the determination of two acid ceramidase inhibitors and three controls in PAMPA matrix. The method was also successfully applied for the analysis of PAMPA samples. To the best of our knowledge, this is the first report of BBB permeability for carmofur, ARN14988-M in terms of transcellular passive diffusion assay using a high-throughput technique. The results from this analysis will pave the way towards further in vivo study for carmofur and ARN14988-M. It is also important to mention that this study reports validated LC-MS/MS method for the analysis of controls which will aid drug discovery researchers for permeability assays in choosing appropriate control compounds and with the ease of method development.

References

1. Graverini, G.; Piazzini, V.; Landucci, E.; Pantano, D.; Nardiello, P.; Casamenti, F.; Pellegrini-Giampietro, D. E.; Bilia, A. R.; Bergonzi, M. C., Solid lipid nanoparticles for delivery of andrographolide across the blood-brain barrier: in vitro and in vivo evaluation. *Colloids and Surfaces B: Biointerfaces* **2018,** *161*, 302-313.
2. Kansy, M., Physicochemical high throughput screening: parallel artificial membrane permeation assay in the description of passive absorption processes. *J Med Chem* **1998,** *41*, 1007-1010.
3. Ottaviani, G.; Martel, S.; Carrupt, P. A., Parallel artificial membrane permeability assay: a new membrane for the fast prediction of passive human skin permeability. *J Med Chem* **2006,** *49* (13), 3948-54.
4. Di, L.; Kerns, E. H.; Fan, K.; McConnell, O. J.; Carter, G. T., High throughput artificial membrane permeability assay for blood-brain barrier. *Eur J Med Chem* **2003,** *38* (3), 223-32.
5. Faller, B., Artificial membrane assays to assess permeability. *Curr Drug Metab* **2008,** *9* (9), 886-92.
6. Bennion, B. J.; Be, N. A.; McNerney, M. W.; Lao, V.; Carlson, E. M.; Valdez, C. A.; Malfatti, M. A.; Enright, H. A.; Nguyen, T. H.; Lightstone, F. C.; Carpenter, T. S., Predicting a Drug's Membrane Permeability: A Computational Model Validated With in Vitro Permeability Assay Data. *J Phys Chem B* **2017,** *121* (20), 5228-5237.
7. Mensch, J.; Jaroskova, L.; Sanderson, W.; Melis, A.; Mackie, C.; Verreck, G.; Brewster, M. E.; Augustijns, P., Application of PAMPA-models to predict BBB permeability including efflux ratio, plasma protein binding and physicochemical parameters. *Int J Pharm* **2010,** *395* (1-2), 182-97.
8. Ciura, K.; Dziomba, S., Application of separation methods for in vitro prediction of blood-brain barrier permeability-The state of the art. *J Pharm Biomed Anal* **2020,** *177*, 112891.
9. Nguyen, H.; Awad, A.; Shabani, S.; Doan, N., Molecular Targeting of Acid Ceramidase in Glioblastoma: A Review of Its Role, Potential Treatment, and Challenges. *Pharmaceutics* **2018,** *10* (2), 45-45.
10. Tea, M. N.; Poonnoose, S. I.; Pitson, S. M., Targeting the Sphingolipid System as a Therapeutic Direction for Glioblastoma. *Cancers* **2020,** *12* (1), 111-111.
11. PAMPA Assay.
12. Naik, P.; Cucullo, L., In vitro blood-brain barrier models: current and perspective technologies. *J Pharm Sci* **2012,** *101* (4), 1337-54.
13. Wong, A. D.; Ye, M.; Levy, A. F.; Rothstein, J. D.; Bergles, D. E.; Searson, P. C., The blood-brain barrier: An engineering perspective. 2013.
14. McCallum, M., High-Throughput Approaches for the Assessment of Factors Influencing Bioavailability of Small Molecules in Pre-Clinical Drug Development. *Theses and Dissertations* **2013**.
15. Hu, L.; Liu, Y.; Cheng, S., Simultaneous determination of six analytes by HPLC-UV for high throughput analysis in permeability assessment. *Journal of Chromatographic Science* **2011**.
16. Realini, N.; Palese, F.; Pizzirani, D.; Pontis, S.; Basit, A.; Bach, A.; Ganesan, A.; Piomelli, D., Acid ceramidase in melanoma: Expression, localization, and effects of pharmacological inhibition. *Journal of Biological Chemistry* **2016**.
17. Fda; Cder; Beers; Donald *Analytical Procedures and Methods Validation for Drugs and Biologics Guidance for Industry*; 2015.
18. *INTERNATIONAL CONFERENCE ON HARMONISATION OF TECHNICAL REQUIREMENTS FOR REGISTRATION OF PHARMACEUTICALS FOR HUMAN USE ICH HARMONISED TRIPARTITE GUIDELINE VALIDATION OF ANALYTICAL PROCEDURES: TEXT AND METHODOLOGY Q2(R1)*.
19. Schmidt, D.; Lynch, J., Evaluation of the reproducibility of Parallel Artificial Membrane Permeation Assays (PAMPA) | Sigma-Aldrich.

20. Domracheva, I.; Muhamadejev, R.; Petrova, M.; Liepinsh, E.; Gulbe, A.; Shestakova, I.; Duburs, G.; Arsenyan, P., 1,2-Dimyristoyl-sn-glycero-3-phosphocholine (DMPC) increases Carmofur stability and in vitro antiproliferative effect. *Toxicology Reports* **2015,** *2*, 377-383.
21. Doan, N. B.; Alhajala, H.; Al-Gizawiy, M. M.; Mueller, W. M.; Rand, S. D.; Connelly, J. M.; Cochran, E. J.; Chitambar, C. R.; Clark, P.; Kuo, J.; Schmainda, K. M.; Mirza, S. P., Acid ceramidase and its inhibitors: a de novo drug target and a new class of drugs for killing glioblastoma cancer stem cells with high efficiency. *Oncotarget* **2017,** *8* (68), 112662-112674.
22. Parallel artificial membrane permeability assay (PAMPA). https://www.cyprotex.com/admepk/in-vitro-permeability/pampa (accessed 5/5/2022).

Chapter-4

Simultaneous quantitative bioanalysis of carmofur and 5-fluorouracil by LC-MS/MS with an application to drug distribution study in mouse

4.1. Introduction

As mentioned in previous chapters, carmofur, also known as 1-hexylcarbamoyl-5-fluorouracil (HCFU) is a pyrimidine-analog anticancer compound. It was first synthesized by Ozaki et al. as a pro-drug of 5-fluorouracil (5-FU) with better gastrointestinal stability for oral delivery and the activity was evaluated by Hoshi, Kuretani and co-workers at the National Cancer Center Research Institute, Japan in 1976[1-3]. Carmofur has a higher LD50 (median lethal dose) value in different animals than it is for 5-FU. Initial studies on experimental murine tumor models of leukemia L-1210 and C-1498, Nakahara-Fukuoka sarcoma, adenocarcinoma 755, ascites sarcoma 180, and Ehrlich ascites carcinoma confirmed the antitumor activity of carmofur after oral administration[1, 4]. Following that, a multicenter phase I clinical study was initiated by National Cancer Center Hospital in Japan in 1977 targeting a spectrum of cancers such as stomach, colorectal, breast, liver, lung, uterus, pancreas, esophagus, larynx, brain, and neuroblast etc[2]. The Phase II clinical trial began in 1978[2]. Of all the cancers tested, a high-response rate (39.4%) of carmofur therapy was found in colorectal cancer[5]. Eventually in 1981, carmofur was approved in Japan for the treatment of colorectal cancer. Later on, carmofur was approved in China, Korea and Finland as well[6].

Studies demonstrated that carmofur is stable in acidic environment, specifically at pH lower than 5. However, it degrades over time to 5-FU in neutral and alkaline environment. In phosphate buffer, carmofur (di-keto form) converts into 2- and 4-hydroxy tautomers with the increase in pH and then it hydrolyzes into 5-FU (Figure 4-1)[7].

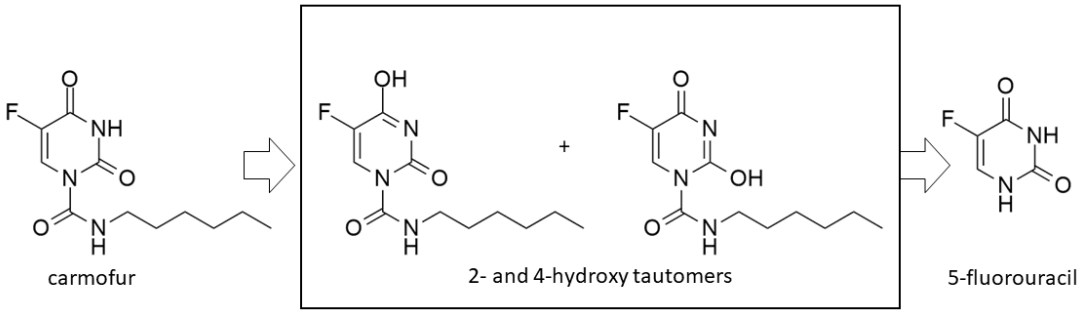

Figure 4-1. Conversion of carmofur into 5-fluorouracil in Phosphate buffer[7].

Carmofur shows both 5-FU dependent and 5-FU independent anticancer activity. The inhibition of carmofur by acid ceramidase and subsequent release of 5-FU is shown in figure 4-2[8]. In biological system, carmofur is directly metabolized into 5-FU or carmofur converts into HHCFU, OHCFU, CPEFU, CPRFU which eventually converts into 5-FU. 5-FU can be excreted in the urine or converts into the inactive form FBAL and excretes out from the body (Figure 4-3)[9-14].

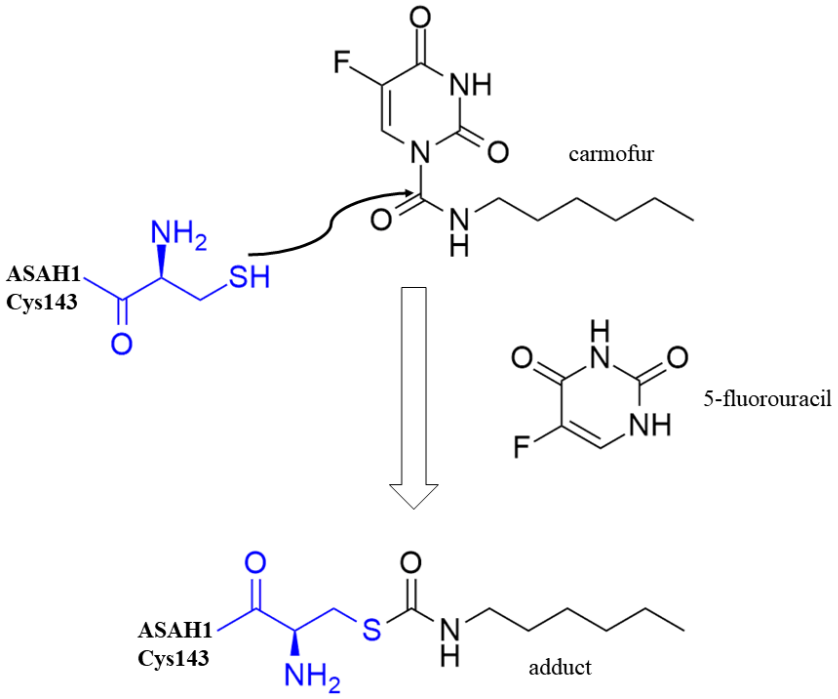

Figure 4-2. Inhibition of acid ceramidase by carmofur and release of 5-fluorouracil[8].

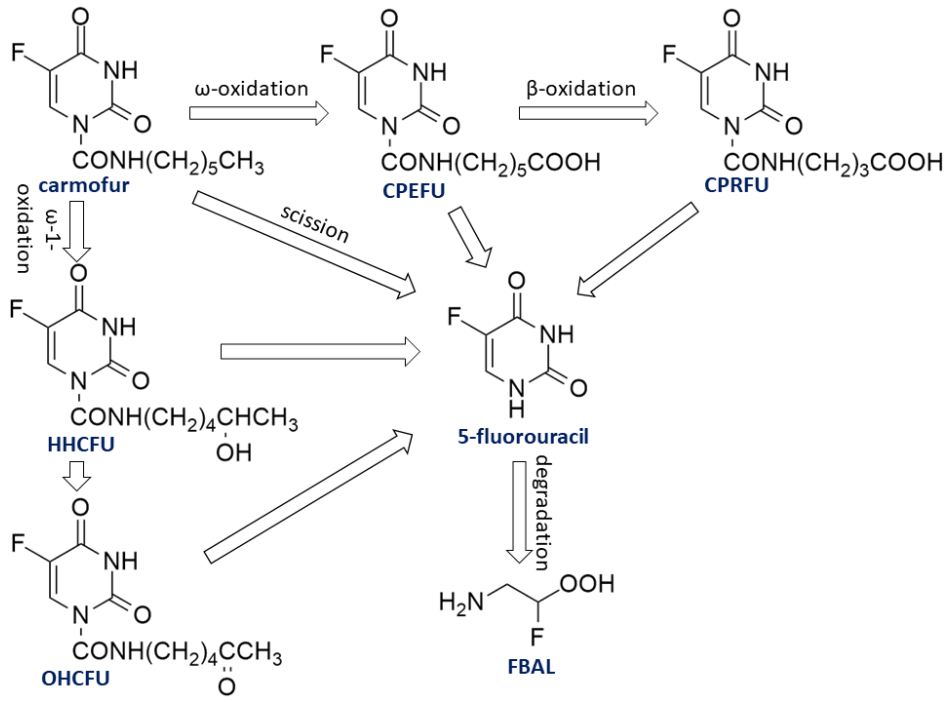

Figure 4-3. Metabolism of carmofur into 5-fluorouracil[9-10].

5-FU is an uracil derivative and one of the oldest anticancer drug that is still in use[15]. The injection and topical formulations of 5-FU are approved for the treatment of a number of diseases such as breast cancer, colorectal cancer, gastric (stomach) cancer, pancreatic cancer, skin cancer and actinic keratosis. A few pro-drugs of 5-FU were developed to have greater in-vivo stability against degradation, better cytotoxic effect and to facilitate oral administration[16]. Among the pro-drugs, the most studied are capecitabine[17], doxifluridine[18], ftorafur[19], carmofur[20] etc. with anti-cancer efficacy. The therapeutic uses of carmofur have been described in chapter 1.

There are two major ways 5-FU acts as cytotoxic agent and exerts it's effect as an anticancer agent. 5-FU is an inhibitor of thymidylate synthase (TS). It is rapidly taken up by the cells and converts into several active metabolites such as fluorodeoxyuridine monophosphate, fluorodeoxyuridine triphosphate and fluorouridine triphosphates. The presence of these active metabolites incorporates into RNA and disrupts the transcription process. They also interrupt the action of TS and disrupts the intracellular deoxynucleotide pools required for DNA replication[21-22].

Being an active metabolite of carmofur, it is important to monitor the level of 5-FU after carmofur administration. Previously 5-FU was determined in biological specimen after oral administration of carmofur using less selective and sensitive bioanalytical techniques such as radio-chromatography[14], high performance liquid chromatography[13, 23], and gas chromatography-mass spectrometry[24].

To the best of our knowledge, there is no LC-MS/MS based method for quantifying carmofur in biological tissues such as liver, kidney, and brain. According to our literature review, there is also no LC-MS/MS method to quantify 5-FU in the biological tissue specimens after the administration of carmofur. We also did not find any method that can simultaneously quantify carmofur and 5-fluorouracil in a single run in vivo.

In chapter 2, quantification of carmofur in mouse plasma has been described. Herein, we performed LC-MS/MS-based quantification of 5-FU in mouse plasma after the administration of carmofur. We also report LC-MS/MS method to simultaneously quantify carmofur and 5-FU in mouse brain, liver, and kidney. Finally, we showed the applicability of our method by analyzing carmofur and 5-FU in a biodistribution study in mouse model.

4.2. Materials and methods

4.2.1. Chemicals and reagents

Carmofur was obtained from Tokyo Chemical Co. Ltd (Portland, OR, USA). 5-FU (CAS No. 51-21-8) and 5-CU were obtained from Millipore-Sigma (St. Louis, MO, USA). All solvents and buffers used in mobile phase were of analytical grades. LC-MS grade water, acetonitrile, and ammonium acetate used in this work were obtained from Fisher Chemical (USA). Glacial acetic acid was purchased from Merck KGaA (Germany). Ethyl acetate was procured from BeanTown Chemical (NH, USA). DMSO was obtained from Honeywell International Inc. (MI, USA). PBS at pH 7.4 buffer was obtained from Corning (VA, USA). PEG E 400 was procured from Millipore-Sigma (St. Louis, Mo, USA). Tween 80 was obtained from MP Biomedicals (Illkirch, France). 1 mL tuberculin syringe with 25 G × 5/8" needles/syringes were purchased from Covidien (Dublin, Ireland).

4.2.2. Animal handling

All animal experimentation performed in this work was approved by the University of Wisconsin Milwaukee's (UWM) Institutional Animal Care and Use Committee (IACUC) (protocol reference no. 20-21#53). Six-eight weeks old female Swiss Webster mice were purchased from Charles River Laboratories (MA, USA). The animals were housed for at least seven days in the Lapham Animal Resource Center (ARC) of UWM before performing the experiment. While housed, they were provided with free access to food and water and maintained on a 12 h light (7:00 to 19:00) and dark cycle (19:00 to 07:00) at a temperature of 22±2°C and 60±5% humidity.

4.2.3. Instruments and conditions

For the sample preparation, we used the following: Orbital Shaker M60 (Labnet, NJ, USA), Centrifuge 5430R (Eppendorf, Germany), TurboVap Evaporator (Biotage, Sweden) and Pressure + 48 Positive pressure Manifold (Biotage, Sweden). For tissue homogenization, we used BeadBug^{TM} 3 position Bead Homogenizer (Benchmark Scientific, Sayreville, NJ, USA).

Liquid chromatography was performed on a Shimadzu Nexera X2 UPLC system that consisting of binary pumps (Shimadzu LC-30AD), degasser units (Shimadzu DGU-20A 5R), autosampler (Shimadzu SIL-30AC MP) and column oven (Shimadzu CTO20A). The UPLC system was interfaced with a Shimadzu LCMS 8040 triple quadrupole mass spectrometer. The LCMS 8040 instrument is equipped with dual ionization source (Electrospray + Atmospheric Pressure Chemical Ionization). For supplying nitrogen gas to the mass spectrometer, we used an in-house nitrogen generator (NM32LA) purchased from Peak Scientific (Glasgow, UK). The CID gas Argon (Ar) was purchased from Airgas (PA, USA).

The analytes were retained, and chromatographic separation was achieved on a XBridge BEH C18 XP column (100 mm X 3 mm, 2.5 µm, Waters Corporation, MA, USA). The data acquisition and post-run analysis were performed using LabSolutions (Shimadzu, Japan) and Microsoft Excel (Microsoft, USA) software packages.

Mass spectrometric ionization carried out in negative electrospray ionization technique and the quantification in multiple reaction monitoring (MRM) mode. The desolvation line and ion source temperature were kept at 275°C and 420°C, respectively. The drying gas and nebulizing gas flow

rate were 16 $L.min^{-1}$ and 2.5 $L.min^{-1}$, respectively. The dwell time of analysis for all analytes was 100 msec.

10 mM ammonium acetate in water at pH 6.8 was used as mobile phase A and acetonitrile was used as mobile phase B. The injection volume was 5 µL. The total runtime was 9 min with the gradient elution program as follows: 50% of B from 0-0.50 min, a linear gradient from 50% B to 95% B from 0.50 - 3.50 min, 95% of B from 3.50 - 5.50 min, a linear gradient of 95% B to 50% B from 5.50 - 6.00 min and 50% B from 6.00 to 9 min. The column oven was kept at 32°C.

4.2.4. Preparation of calibration and quality control standards

Appropriate amount of carmofur and 5-FU were weighed using weighing by difference technique and dissolved in DMSO to prepare the stock solutions at 5000 $\mu g.mL^{-1}$ concentration. The stock solutions were further diluted with acetonitrile to prepare the working stock solutions. Each of the working stock solutions were further diluted in blank plasma or tissue homogenates to prepare the calibration standards. The calibration standards for carmofur were prepared at concentrations 5, 25, 50, 100, 200, 500, and 1000 $ng.mL^{-1}$. The calibration standards for 5-FU were prepared at concentrations 200, 500, 1000, 2000, 5000, and 10,000 $ng.mL^{-1}$. Three quality control (QC) samples: low QC (LQC), medium QC (MQC) and high QC (HQC) were prepared at concentrations 5, 200, and 1000 $ng.mL^{-1}$ respectively for carmofur and 200, 2000, and 10,000 $ng.mL^{-1}$ respectively for 5-FU. The QC working stock solutions were subjected to spiking in plasma or tissue homogenate in a similar way as the standards. Thereafter, standards and QC samples underwent liquid-liquid extraction before analyzing by mass spectrometry as described in section 4.2.5.

4.2.5. Sample preparation

Tissue samples were homogenized using stainless steel beads in BeadBug homogenizer. About 1000 µL water is added to 40 mg of tissue sample and bead beaten at high speed for about 30-60 seconds. Upon homogenization, they were centrifuged at high speed (18,000 × g at 4°C) for 5 min for clarification before performing liquid-liquid extraction. Collected blood samples were centrifuged for 10 min at 18,000 × g to separate the plasma.

On the assay day, 10 µL of 5-chlorouracil internal standard (IS) (50 $\mu g.mL^{-1}$) was added to 100 µL plasma/tissue homogenate sample. The sample is then acidified by adding 10 µL of glacial acetic acid. 1 mL of extraction solvent (ethyl acetate) was added and vortexed for 5 min. The sample tubes were then centrifuged at 18,000 × g at 4°C for 15 min. 800 µL of the supernatant was transferred into another tube and dried under compressed air flow at room temperature. The dried residue is then reconstituted in 100 µL of acetonitrile and 5 µL of the prepared sample was injected for LC-MS/MS analysis.

4.2.6. LC-MS/MS method validation

The developed LC-MS/MS was validated in terms of specificity, carryover, linearity, intra- and inter-day accuracy and precision, matrix effect, recovery efficiency and stability according to the United States Food and Drug Administration's (FDA) guideline for bioanalytical method validation[25].

4.2.6.1. Specificity and carryover

i) Blank plasma and blank tissue homogenates, ii) blank plasma and tissue homogenate spiked with carmofur, 5-FU and IS, and iii) plasma and tissue homogenate collected from the mice after intraperitoneal injection of carmofur were treated according to the extraction procedure described in section 4.2.5. before analyzing with LC-MS/MS. Specificity was evaluated by comparing the presence or absence of mass chromatograms for carmofur, 5-FU, and IS in their respective peak regions.

Carryover was evaluated by injecting a blank sample after the injection of HQC samples. Peak area below 20% of LQC for carmofur and 5-FU and below 5% for IS was considered acceptable in the blank sample.

4.2.6.2. Linearity and sensitivity

A series of diluted solutions of the standards were prepared to identify the lower limit of detection (LOD) and the lower limit of quantification (LOQ). A minimum signal to noise (S/N) ratio of 3 was considered for the LOD and a minimum S/N ratio of 10 was considered for LOQ. Seven calibration standards (5, 25, 50, 100, 200, 500, 1000 ng/mL) within the range of 5-1000 $ng.mL^{-1}$ including both upper and lower limit of quantification were used for generating the calibration curve for carmofur. Calibration curve for 5-FU was prepared within the range of 200-10,000 $ng.mL^{-1}$ with six calibration standards (200, 500, 1000, 2000, 5000, 10000 $ng.mL^{-1}$). Each calibration standard was spiked with the IS at 5 $\mu g.mL^{-1}$ concentration. The calibration curves were constructed by plotting the peak area ratio (y) against the concentration ratio (x) of the analyte and IS. The curves were fitted for weighted least square linear regression analysis with a

weighing factor of $1/x^2$ and the linearity was considered acceptable with a correlation coefficient (r^2) of 0.99 or greater.

4.2.6.3. Matrix effect and recovery efficiency

Matrix effect was investigated both for carmofur and 5-FU for three QC samples (low, medium, and high) and calculated based on the ratio of peaks areas of the post-extracted spiked sample to the peak areas of neat standard samples[26].

$$\text{Matrix effect (\%)} = \frac{\text{Peak area of post extracted spiked sample}}{\text{Peak area of neat standard sample}} \times 100$$

A matrix effect of 100% indicates no contribution of extracted matrix substances on the ionization of the analytes while less 100% indicates ion suppression and greater than 100% indicates ion enhancement.

Recovery efficiency of the analytes was also evaluated at the three QC (LQC, MQC, HQC) samples by comparing the peaks areas of the spiked sample in blank matrix and extracted with the extraction solvent (ethyl acetate) with those peak areas of the post extracted spiked sample[26].

$$\text{Recovery efficiency (\%)} = \frac{\text{Peak area of extracted spiked sample}}{\text{Peak area of post extracted spiked sample}} \times 100$$

4.2.6.4. Accuracy and precision

Accuracy implies the ability of the method to measure close to the true value. And precision indicates the agreement between subsequent measurements.

Three QC samples for carmofur and 5-FU were prepared in three replicates and analyzed for intra-day accuracy and precision for three consecutive days. The data obtained from intra-day

accuracy and precision were reanalyzed for inter-day accuracy and precision at all three QC sample concentrations.

The accuracy was expressed as the percent mean accuracy. The precision was expressed as the percent coefficient of variance (%CV). Mean accuracy in considered acceptable if it is within ±15% and the %CV should be less than 15%.

$$\%CV = \frac{\text{Standard deviation}}{\text{Mean measured concentration}} \times 100$$

4.2.6.5. Stability

The stability of carmofur and 5-FU was evaluated in mouse plasma/tissue homogenate and in the final reconstituted solvent at different stability conditions. Long term stability was assessed by the accuracy of the measured carmofur and 5-FU concentration at three QC (LQC, MQC, HQC) concentration after storing for 15 days at -80°C. In process stability was studied after three cycles of freeze-thaw from -80°C to room temperature. Post-operative stability was studied with the final reconstituted sample at three QC concentration by storing at room temperature for 8 hours and at the autosampler (15°C) for 24 hours. Carmofur and 5-FU were considered stable with an accuracy of ±15% of the desired concentration.

4.2.7. Tissue distribution study of carmofur and 5-FU

Finally, we tested the applicability of our validated method in a rodent model. A total of 21 female Swiss Webster mice were selected for doing the pharmacokinetic study. Carmofur was injected at a dose of 10 $mg.kg^{-1}$ intraperitoneally[27]. Blood, brain, liver, kidney samples were collected at the following time points: immediate after administration (5 min), 20 min, 40 min, 60 min, 120

min, 180 min, and 240 min. Collected blood samples were immediately centrifuged at 18,000 × g for 10 min. Separated plasma and the tissue organs was collected in microcentrifuge tubes and stored at -80°C until analysis. The concentration-time curve for carmofur and 5-FU was prepared using GraphPad Prism 9. The pharmacokinetic parameters such as C_{max}, T_{max}, $T_{1/2}$, AUC, K_e were calculated by one-compartmental model.

4.3. Results and Discussion

4.3.1. Development of the LC-MS/MS method

The mass spectrometer parameters for carmofur and IS was developed and optimized in chapter 2. Herein, we incorporated the conditions for 5-FU analysis. The optimized MS parameters used in this method are listed in table 4-1. At first, we did a Q3 scan (figure 4-4) of 5-FU to identify the precursor ion peak. 5-FU ionized in negative mode with a m/z of 129 $[M-H]^-$. After we have identified the precursor ion, we did a product ion scan (figure 4-5) to identify the product ions of 5-FU utilizing the built in 'optimization for method' tool in the LabSolutions software to optimize the voltages for the MRM transitions. We identified one transition m/z 129 → m/z 42 which similar to what reported in the literature[17-18, 28].

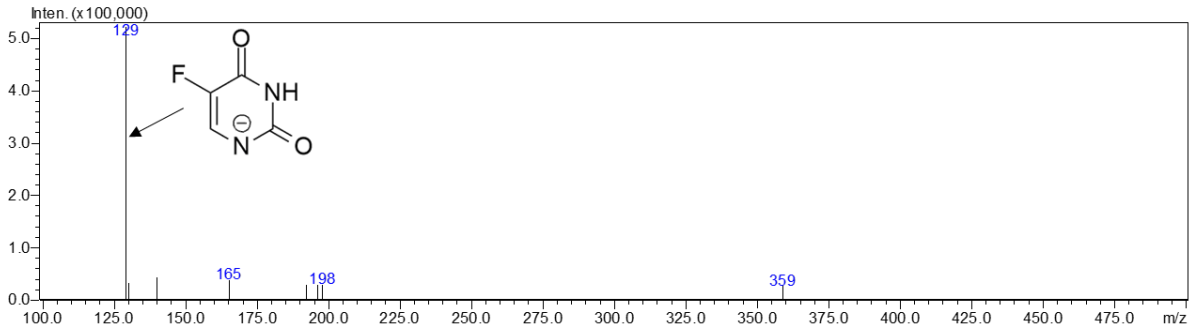

Figure 4-4. Negative mode Q3 scan of 5-FU solution at a concentration of 100 µg.mL^{-1}.

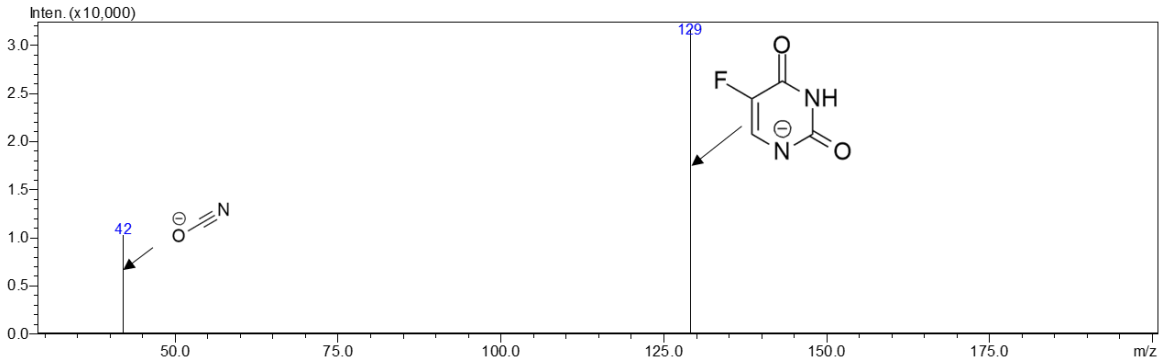

Figure 4-5. Product ion scan of 5-FU.

Analyte	Precursor ion	Product ion	Q1 pre-bias (V)	CE (V)	Q3 pre-bias (V)
Carmofur	256.25	129.00	16.00	8.00	23.00
Carmofur	256.25	86.00	28.00	40.00	28.00
Carmofur	256.25	42.00	27.00	31.00	16.00
5-FU	129.10	42.00	17.00	17.00	16.00
5-CU	145.10	42.00	25.00	16.00	16.00

Table 4-1. Optimized MS parameters used in this method.

During the liquid chromatography separation two peaks (figure 4-6) that corresponds to the m/z 129 → m/z 42 transition were observed. The first one co-eluting with 5-CU peak is the 5-FU peak. The second m/z 129 → m/z 42 transition peak co-elutes with the carmofur peak. This is due to the breakdown of carmofur during the ionization. While there are two m/z 129 → m/z 42 transition peaks in the mass chromatogram, we used a slower gradient in the mobile phase to

separate these two peaks completely. The optimized gradient elution program is described in section 4.2.3.

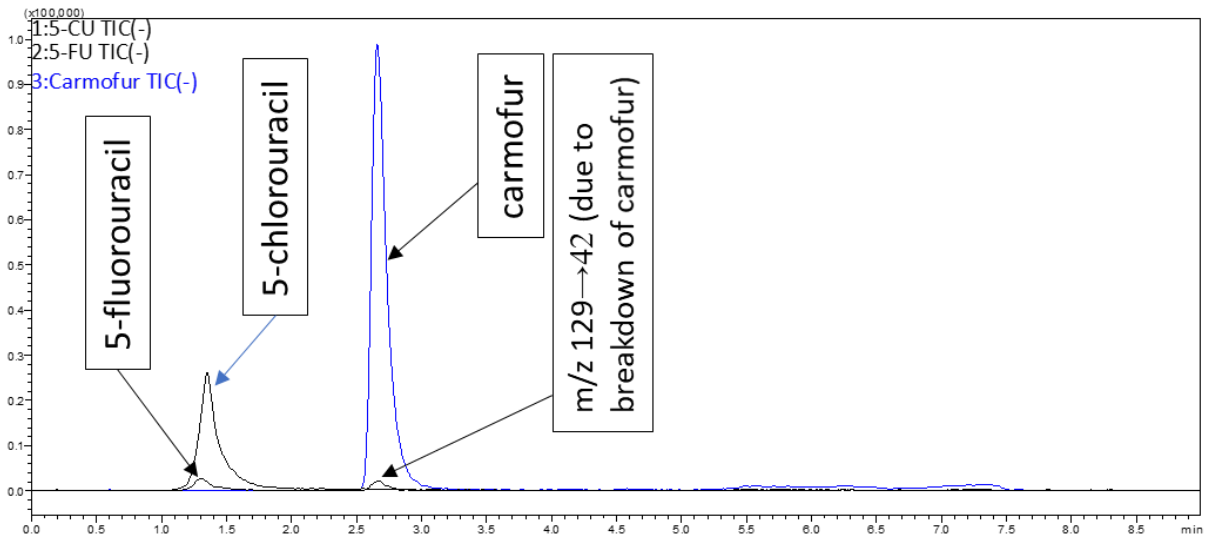

Figure 4-6. A representative mass chromatogram. 5-FU and 5-CU co-elutes because of only slight difference in their polarity.

4.3.2. Development of the sample preparation technique

In chapter 2, we utilized a combination of ethyl acetate and 2-propanol at the 85/15 ratio. In literature, 5-FU was extracted from plasma using 100% ethyl acetate[26]. Therefore, we decided to do a trial in duplicate of extraction efficiency at three ratio of ethyl acetate and 2-propanol (100/0, 85/15, 50/50) to find out the proper extraction solvent for extracting carmofur and 5-FU in a single analysis. The results of the trial are summarized in table 4-2. This is no surprising that carmofur has the better extraction using ethyl acetate/2-propanol (85/15) as described in chapter 2. However, 5-FU shows greater ion suppression using ethyl acetate/2-propanol (85/15) in the extraction solvent. Ion suppression is least observed using 100% ethyl acetate as the

extraction solvent. Therefore, we decided to use 100% ethyl acetate as our extraction solvent for plasma and the tissue sample analysis.

Analyte	**Ethyl acetate/2-propanol (100/0)**		**Ethyl acetate/2-propanol (85/15)**		**Ethyl acetate/2-propanol (50/50)**	
	Matrix effect (%)	Recovery efficiency (%)	Matrix effect (%)	Recovery efficiency (%)	Matrix effect (%)	Recovery efficiency (%)
Carmofur (100 $ng.mL^{-1}$)	112.53	64.73	99.44	87.00	100.56	52.21
5-FU (1 $\mu g.mL^{-1}$)	70.65	61.13	42.27	74.78	10.04	53.26

Table 4-2. Recovery and matrix effect of carmofur and 5-FU at different extraction solvent ratio in plasma.

4.3.3. Method validation

We have validated our method in terms of selectivity, carryover, linearity, matrix effect, recovery efficiency, intra-and inter-day accuracy and precision and stability. The results of the method validation are described in this section.

4.3.3.1. Specificity and carryover

Specificity was evaluated by examining the mass chromatograms for blank mouse plasma and tissue homogenate, mouse plasma and tissue homogenate spiked with carmofur, 5-FU and IS, and mouse plasma and tissue homogenate collected after intraperitoneal injection of carmofur (figure C1-C4). No endogenous components of the mouse plasma were found to interfere with the peak of 5-FU at the retention time of 5-FU. No endogenous components of the tissue homogenate were also found to interfere with the peak of carmofur and 5-FU at their respective retention time indicating the specificity and selectivity of the method.

Carryover was evaluated by checking the blank mass chromatogram after running HQC (1000 $ng.mL^{-1}$ for carmofur and 10,000 $ng.mL^{-1}$ for 5-FU) samples (figure C5-C6). No significant carryover was observed.

4.3.3.2. Linearity

We found the LOD and LOQ to be 2 $ng.mL^{-1}$ and 5 $ng.mL^{-1}$ respectively for carmofur. The LOD and LOQ was 50 $ng.mL^{-1}$ and 200 $ng.mL^{-1}$ respectively for 5-FU. Acceptable linearity was achieved for carmofur between the range of 5-1000 $ng.mL^{-1}$ with a correlation coefficient of 0.9941±0.0028, 0.9935±0.0016, and 0.9915±0.0017 in brain, liver and kidney tissue homogenate respectively for

three replicate analyses. The regression equation was y = (32.7382±6.1777)x + (0.0014±0.0063) (brain), y = (32.6676±4.3489)x + (0.0010±0.0054) (liver), and y = (26.7814±10.9393)x + (0.0058±0.0117) (kidney) and representative calibration curves are shown in figure 4-7. The acceptable linearity was 200-10,000 ng.mL^{-1} for 5-FU in three replicate analyses with a correlation coefficient of 0.9944±0.0012 (plasma), 0.9955±0.0016 (brain), 0.9975±0.0013 (liver), and 0.9935±0.0040 (kidney). The regression equation was y = (1.0928±0.1878)x + (0.0046±0.0088) (plasma), y = (0.7512±0.0918)x + (0.0059±0.0065) (brain), y = (0.6986±0.1096)x + (0.0038±0.0084) (liver), and y = (0.5399±0.2616)x + (0.0025±0.0036) (kidney). Representative calibration curves are shown in figure 4-8.

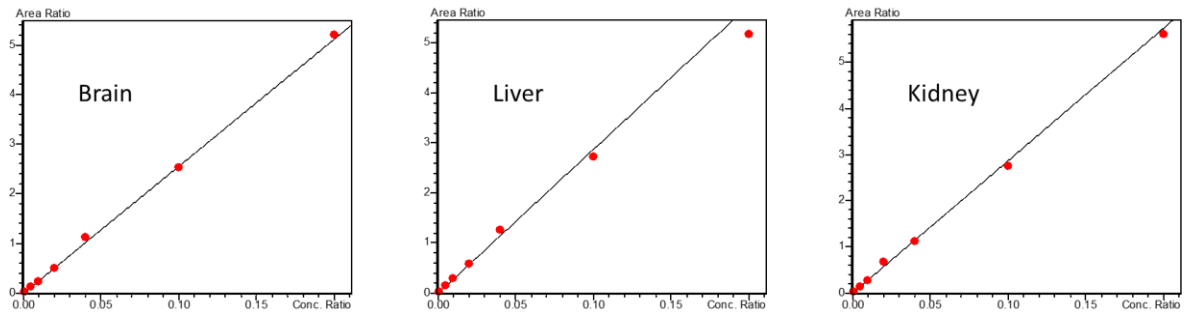

Figure 4-7. Representative calibration curves for carmofur in different tissue homogenates.

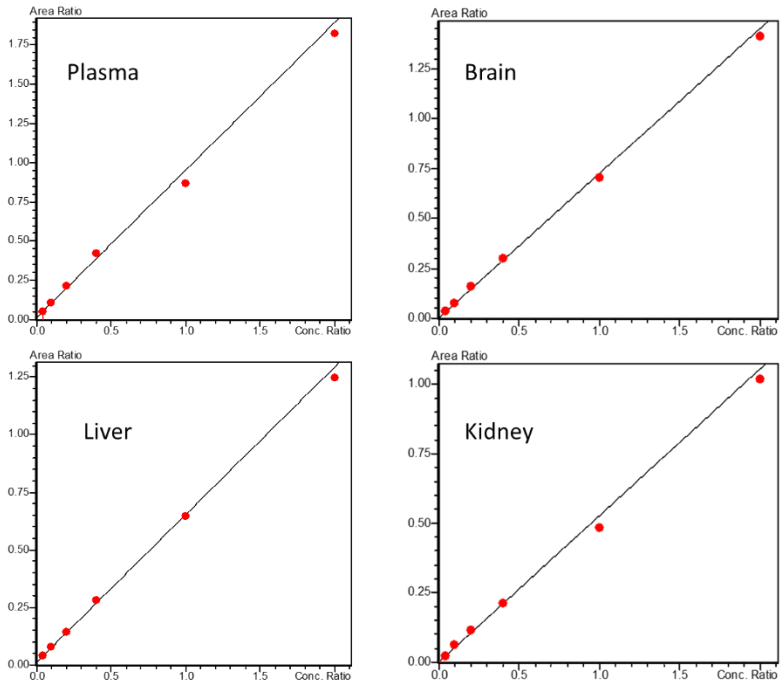

Figure 4-8. Representative calibration curves for 5-FU in mouse plasma and other tissues.

4.3.3.3. Matrix effect and recovery efficiency

Matric effect and recovery efficiency were evaluated for three QC samples: LQC (5 ng.mL^{-1}), MQC (100 ng.mL^{-1}), HQC (1000 ng.mL^{-1}) for carmofur and LQC (200 ng.mL^{-1}), MQC (2000 ng.mL^{-1}), HQC (10,000 ng.mL^{-1}) for 5-FU. The matrix effect was between 103.36% to 124.70%, 105.78% to 121.51%, 107.25% to 126.34% in brain, liver, and kidney homogenates for carmofur. The average matrix effect was found between 68.89% to 85.15%, 67.05% to 79.20%, 51.77% to 64.75%, and 63.73% to 77.45% in plasma, brain, liver and kidney homogenates for 5-FU. Recovery was found between 98.09% to 100.80%, 84.39% to 87.41%, and 93.24% to 102.63% in brain, liver and kidney homogenates for carmofur. The recovery for 5-FU was found between 68.17% to 78.43%, 53.52% to 71.59%, 65.95% to 73.41%, and 64.11% to 76.39% in plasma, brain, liver and kidney tissue

homogenates. The summary of matrix effect and recovery efficiency is shown in figures 4-9 and 4-10.

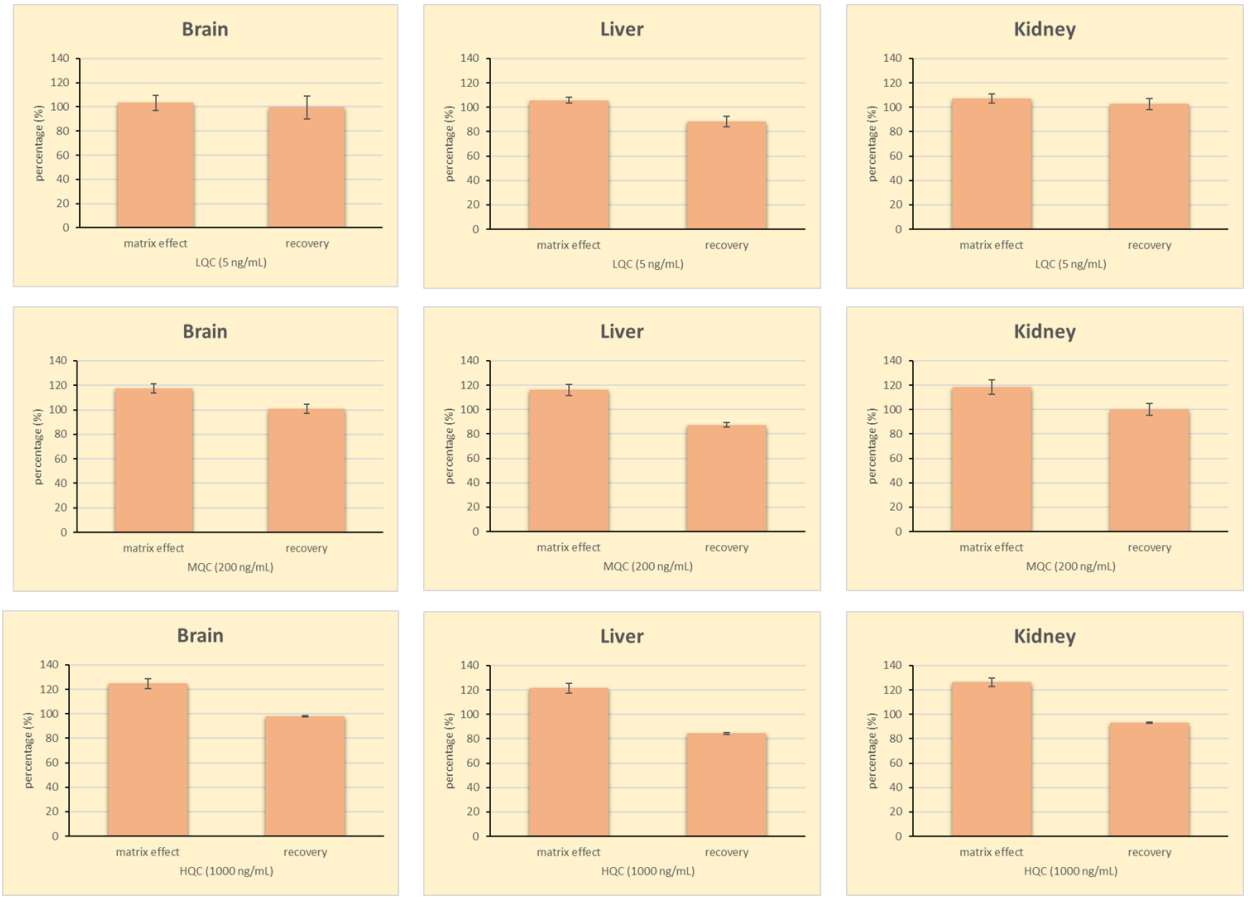

Figure 4-9. Matrix effect and recovery efficiency of carmofur (n=3) in mouse tissues.

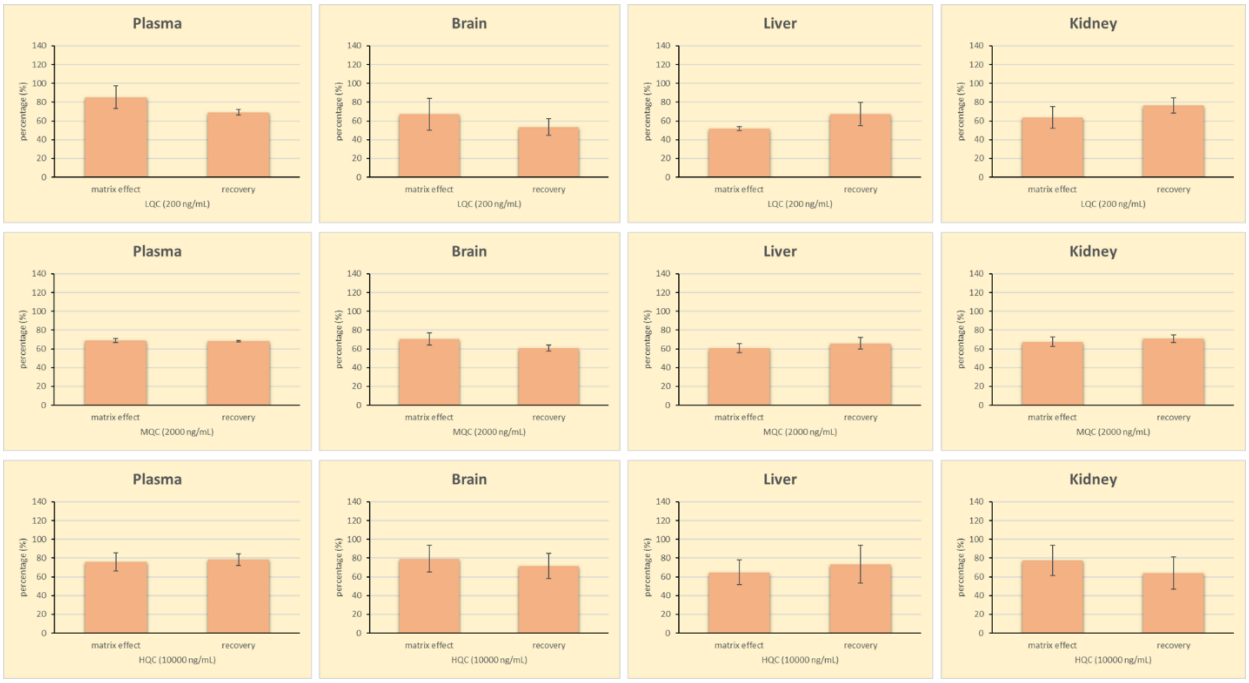

Figure 4-10. Matrix effect and recovery efficiency of 5-FU (n=3) in mouse plasma and other tissues.

4.3.3.4. Intra-day and Inter-day accuracy and precision

The three quality control samples for carmofur and 5-FU (HQC, MQC, LQC) were tested in three replicates for intra- day accuracy and precision for three consecutive days. The data obtained were combined and recalculated for inter-day accuracy and precision. The mean accuracy was found to be within ±15% and the precision (%CV) was found to be <15% for all three quality samples in all sample types which indicates the accuracy and precision of our developed method. The summary of the intra- and inter-day accuracy and precision are summarized in figures 4-11 and 4-12.

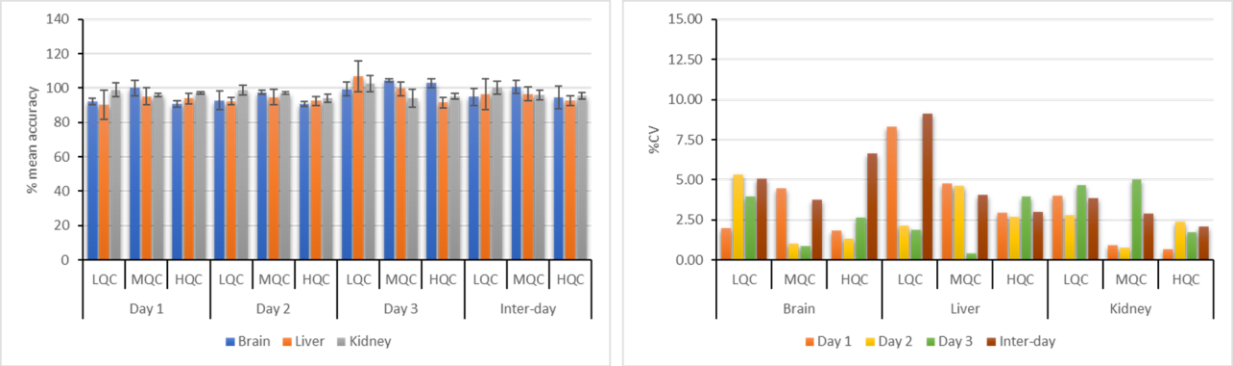

Figure 4-11. Intra- and inter-day accuracy and precision for carmofur in mouse tissues.

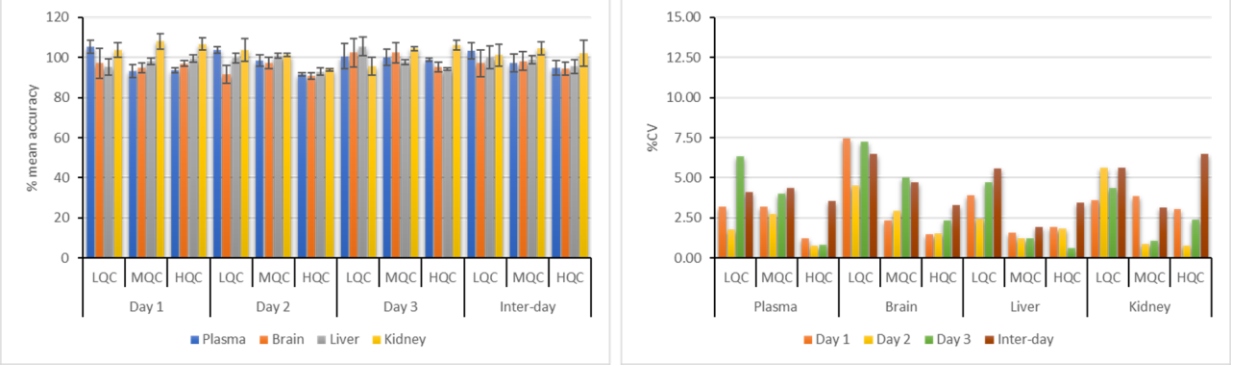

Figure 4-12. Intra- and inter-day accuracy and precision for 5-FU in mouse plasma and other tissues.

4.3.3.5. Stability

The stability of carmofur in mouse brain, liver, and kidney tissue homogenate and the stability of 5-FU in mouse plasma, brain, liver, and kidney tissue homogenate is summarized in figure 4-13. We examined four experimental stability conditions at the three quality control (LQC, MQC, HQC) concentrations. The mean accuracy (within ±15%) of the QC samples at different conditions such as long-term stability (15 days at -80°C), freeze-thaw stability (3 cycles), autosampler stability (24

hours), room temperature stability (8 hours) indicates that the method is appropriate and acceptable as a bioanalytical method for a tissue drug distribution study.

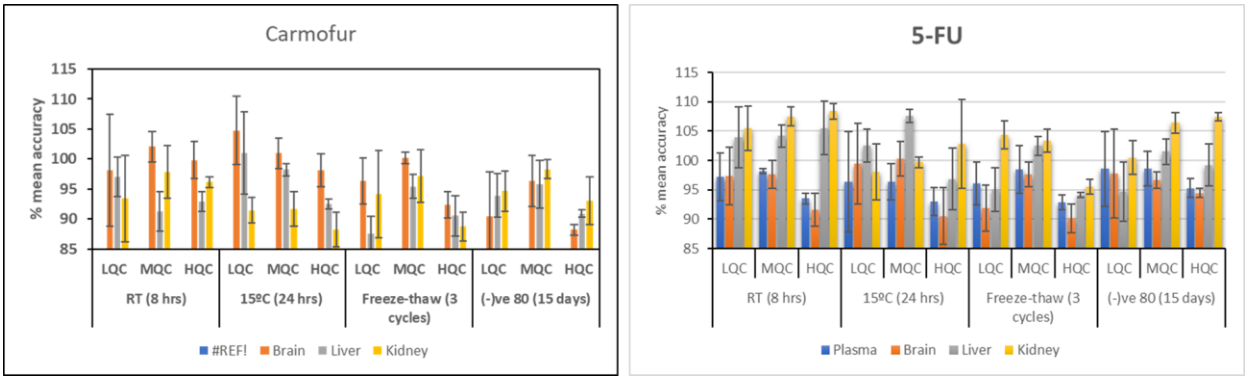

Figure 4-13. Stability of carmofur and 5-FU in terms of accuracy at different test conditions in mouse tissues.

4.3.4. Biodistribution study of carmofur and 5-FU in mouse model

The developed and validated LC-MS/MS method was tested successfully for an in vivo drug biodistribution study. A total of 21 Swiss-Webster mice were injected intraperitoneally with carmofur at a dose of 10 $mg.kg^{-1}$. The blood, brain, liver and kidney samples were collected at the following time points: immediate, (5 min), 20 min, 40 min, 60 min, 120 min, 180 min, and 240 min. The samples were prepared using the procedure described in section 4.2.5. The prepared samples were quantified against freshly prepared calibration curves using the LC-MS/MS method. The time-concentration data was imported into GraphPad Prism 9 to prepare the pharmacokinetic plots (figure 4-14 to figure 4-20). The tissue pharmacokinetic parameters for carmofur and 5-FU were calculated by one-compartmental analysis.

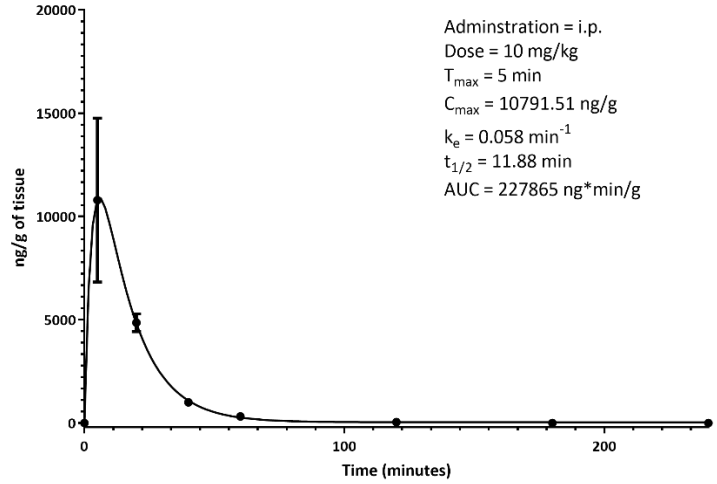

Figure 4-14. Concentration-time curve of carmofur in mouse brain after i.p. injection of carmofur (10 $mg.kg^{-1}$).

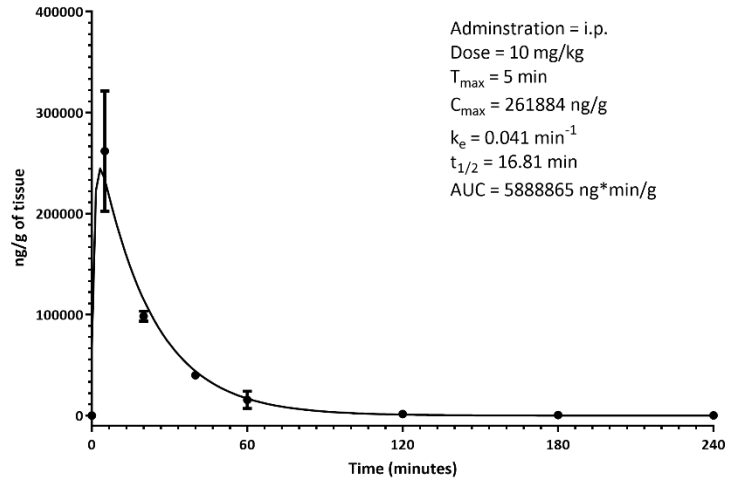

Figure 4-15. Concentration-time curve of carmofur in mouse liver after i.p. injection of carmofur (10 $mg.kg^{-1}$).

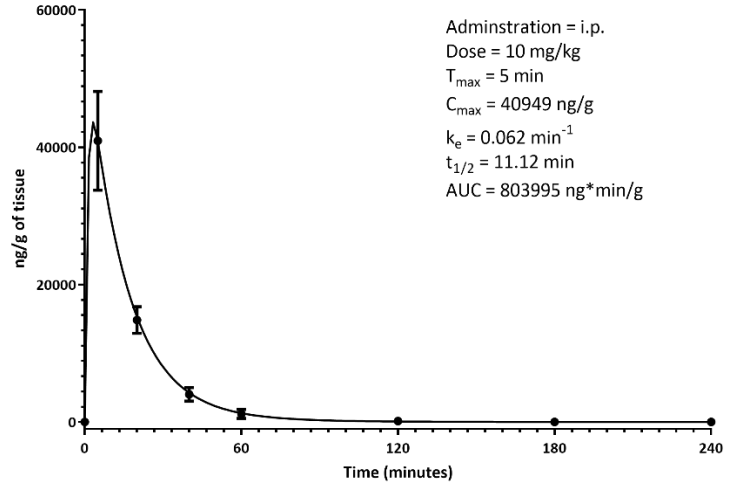

Figure 4-16. Concentration-time curve of carmofur in mouse kidney after i.p. injection of carmofur (10 $mg.kg^{-1}$).

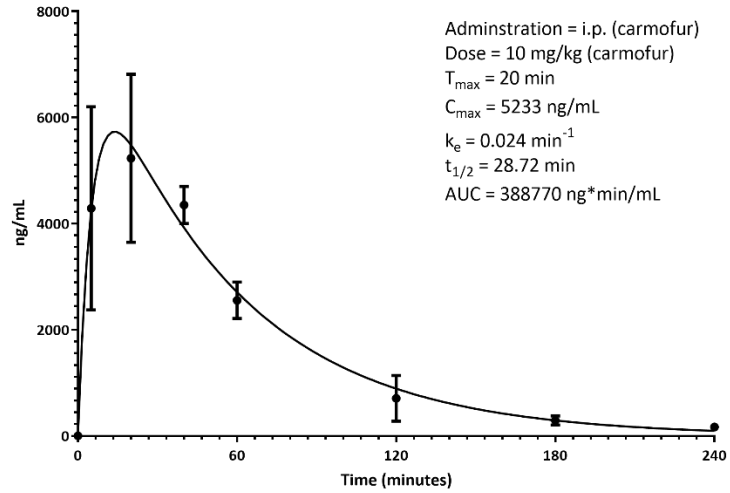

Figure 4-17. Concentration-time curve of 5-FU in mouse plasma after i.p. injection of carmofur (10 $mg.kg^{-1}$).

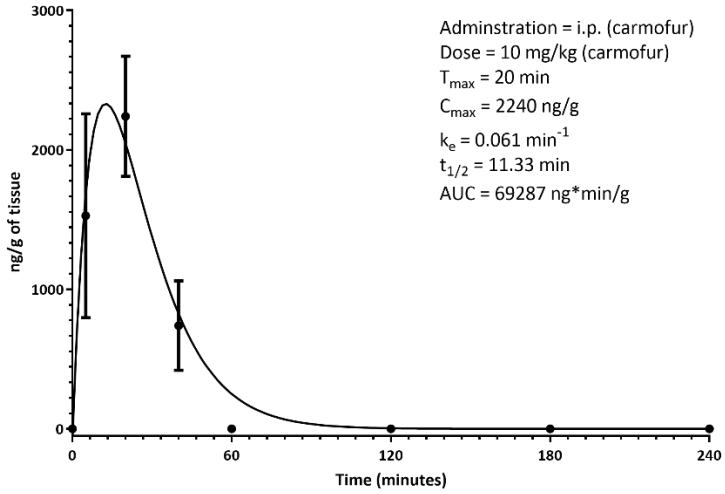

Figure 4-18. Concentration-time curve of 5-FU in mouse brain after i.p. injection of carmofur (10 $mg.kg^{-1}$).

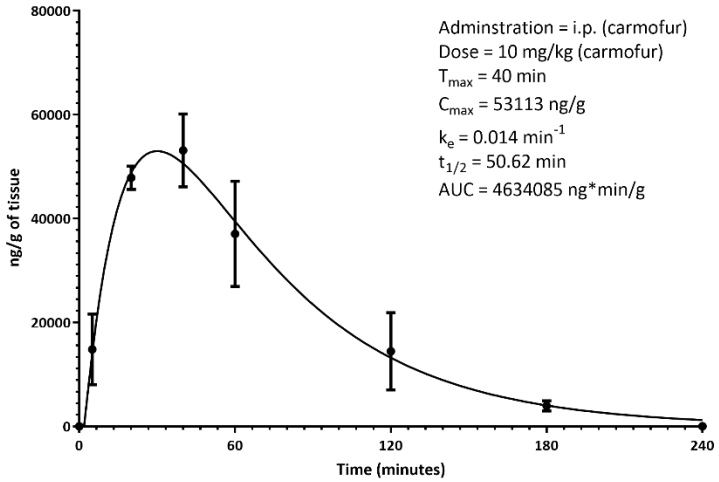

Figure 4-19. Concentration-time curve of 5-FU in mouse liver after i.p. injection of carmofur (10 $mg.kg^{-1}$).

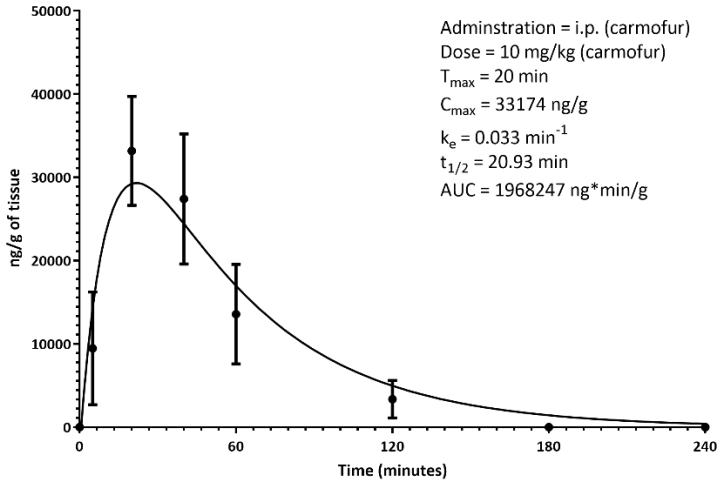

Figure 4-20. Concentration-time curve of 5-FU in mouse kidney after i.p. injection of carmofur (10 $mg.kg^{-1}$).

4.4. Conclusion

In this chapter, we have developed a liquid-liquid extraction technique which only require 100 µL of plasma or tissue homogenate to simultaneously extract carmofur and 5-FU. We have also developed a sensitive and accurate LC-MS/MS method to quantify carmofur and 5-FU in biological samples. Thereafter, we have validated our method in terms of specificity, sensitivity, accuracy, precision, and stability in a variety of mouse tissues. Finally, we have shown the applicability for a drug biodistribution study in mouse plasma, brain, liver, and kidney.

To the best of our knowledge, this is the first report of carmofur quantification in mouse brain, liver, and kidney tissues using an LC-MS/MS method. Herein we also first report to quantify 5-FU after the administration of carmofur using an LC-MS/MS method. This is also the first report to simultaneously quantify carmofur and 5-FU after the administration of carmofur using a single LC-MS/MS run.

We believe our method will help researchers in the field who are interested to perform further in vitro and in vivo studies with carmofur using LC-MS/MS method. This chapter will also assist in analyte extraction technique development and LC-MS/MS analysis for further pre-clinical and clinical studies with carmofur. Researchers who are interested to monitor carmofur and 5-FU in biological specimens can also get valuable insights from our study.

References

1. Hoshi, A.; Iigo, M.; Nakamura, A.; Yoshida, M.; Kuretani, K., Antitumor activity of 1-hexylcarbamoyl-5-fluorouracil in a variety of experimental tumors. *Gan* **1976,** *67* (5), 725-31.
2. Koyama, Y., 1-Hexylcarbamoyl-5-fluorouracil (HCFU)--a masked 5-fluorinated pyrimidine. *Cancer Treat Rev* **1981,** *8* (2), 147-56.
3. Ozaki, S.; Ike, Y.; Mizuno, H., 5-Fluorouracil derivatives. I. The synthesis of 1-carbamoyl-5-fluorouracils. *Bulletin of the Chemical Society of Japan* **1977,** *50* (9), 2406-2412.
4. Iigo, M.; Hoshi, A.; Nakamura, A.; Kuretani, K., Antitumor activity of 1-alkylcarbamoyl derivatives of 5-fluorouracil in a variety of mouse tumors. *Cancer Chemother Pharmacol* **1978,** *1* (4), 203-8.
5. Inokuchi, K., Prolonged survival of stomach cancer patients after extensive surgery and adjuvant treatment: an overview of the Japanese experience. *Semin Surg Oncol* **1991,** *7* (6), 333-8.
6. Doan, N. B.; Nguyen, H. S.; Montoure, A.; Al-Gizawiy, M. M.; Mueller, W. M.; Kurpad, S.; Rand, S. D.; Connelly, J. M.; Chitambar, C. R.; Schmainda, K. M.; Mirza, S. P., Acid ceramidase is a novel drug target for pediatric brain tumors. *Oncotarget* **2017,** *8* (15), 24753-24761.
7. Domracheva, I.; Muhamadejev, R.; Petrova, M.; Liepinsh, E.; Gulbe, A.; Shestakova, I.; Duburs, G.; Arsenyan, P., 1,2-Dimyristoyl-sn-glycero-3-phosphocholine (DMPC) increases Carmofur stability and in vitro antiproliferative effect. *Toxicology Reports* **2015,** *2*, 377-383.
8. Dementiev, A.; Joachimiak, A.; Nguyen, H.; Gorelik, A.; Illes, K.; Shabani, S.; Gelsomino, M.; Ahn, E.-Y. E.; Nagar, B.; Doan, N., Molecular Mechanism of Inhibition of Acid Ceramidase by Carmofur. *Journal of Medicinal Chemistry* **2019,** *62* (2), 987-992.
9. Iigo, M.; Nakamura, A.; kuretani, K.; Hoshi, A., Excretion of 1-hexylcarbamoyl-5-fluorouracil in urine of mice. *Journal of Pharmacobio-Dynamics* **1981,** *4* (7), 490-6.
10. Kobari, T.; Iguro, Y.; Ujiie, A.; Namekawa, H., Metabolism of 1-hexylcarbamoyl-5-fluorouracil (HCFU), a new antitumour agent, in rats, rabbits and dogs. *Xenobiotica* **1981,** *11* (1), 57-62.
11. Kobari, T.; Tan, K.; Kumakura, M.; Watanabe, S.; Shirakawa, I.; Kobayashi, H.; Ujiie, A.; Miyama, Y.; Namekawa, H.; Yamamoto, H., Metabolic fate of 1-hexylcarbamoyl-5-fluorouracil in rats. *Xenobiotica* **1978,** *8* (9), 547-556.
12. Kono, A.; Hara, Y.; Eguchi, S.; Tanaka, M.; Matsushima, Y., Determination of two new metabolites of 1-hexylcarbamoyl-5-fluorouracil in biomedical specimens by high-performance liquid chromatography. *Journal of Chromatography B: Biomedical Sciences and Applications* **1980,** *182* (1), 125-129.
13. Nakajima, O.; Yoshida, Y.; Isoda, T.; Takemasa, Y.; Imamura, Y.; Koyama, Y., Quantitative determination of 1-hexylcarbamoyl-5-fluorouracil and its metabolites in man. *Journal of Chromatography B: Biomedical Sciences and Applications* **1981,** *225* (1), 91-97.
14. Iigo, M.; Nakamura, A.; Kuretani, K.; Hoshi, A., Metabolic fate of 1-hexylcarbamoyl-5-fluorouracil after oral administration in mice. *Xenobiotica* **1980,** *10* (11), 847-854.
15. de Oliveira, B. E.; Amorim, O. H. J.; Lima, L. L.; Rezende, R. A.; Mestnik, N. C.; Bagatin, E.; Leonardi, G. R., 5-Fluorouracil, innovative drug delivery systems to enhance bioavailability for topical use. *J Drug Deliv Sci Tec* **2021,** *61*.
16. Malet-Martino, M.; Jolimaitre, P.; Martino, R., The prodrugs of 5-fluorouracil. *Curr Med Chem Anticancer Agents* **2002,** *2* (2), 267-310.
17. Siethoff, C.; Orth, M.; Ortling, A.; Brendel, E.; Wagner-Redeker, W., Simultaneous determination of capecitabine and its metabolite 5-fluorouracil by column switching and liquid chromatographic/tandem mass spectrometry. *J Mass Spectrom* **2004,** *39* (8), 884-889.
18. Woo, Y.; Kim, G.; Jeong, E.; Kim, C., Simultaneous determination of doxifluridine and 5-fluorouracil in monkey serum by high performance liquid chromatography with tandem mass spectrometry. *Journal of Chromatography B* **2008,** *875* (2), 487-492.

19. Remaud, G.; Boisdroncelle, M.; Morel, A.; Gamelin, A., Sensitive MS/MS–liquid chromatography assay for simultaneous determination of tegafur, 5-fluorouracil and 5-fluorodihydrouracil in plasma. *Journal of Chromatography B* **2005,** *824* (1-2), 153-160.
20. Takenaka, K.; Kanematsu, T.; Shimada, M.; Sugimachi, K., Low dose 1-hexylcarbamoyl-5-fluorouracil (HCFU) recommended for cirrhotic patients with hepatocellular carcinoma. *European Journal of Cancer and Clinical Oncology* **1989,** *25* (8), 1191-1195.
21. Longley, D. B.; Harkin, D. P.; Johnston, P. G., 5-fluorouracil: mechanisms of action and clinical strategies. *Nature reviews cancer* **2003,** *3* (5), 330-338.
22. Vodenkova, S.; Buchler, T.; Cervena, K.; Veskrnova, V.; Vodicka, P.; Vymetalkova, V., 5-fluorouracil and other fluoropyrimidines in colorectal cancer: Past, present and future. *Pharmacology & therapeutics* **2020,** *206*, 107447.
23. Kono, A.; Tanaka, M.; Eguchi, S.; Hara, Y. *Determination of l-hexylcarbamoyld-fluorouracil and its metabolites in biomedical specimens by high-performance liquid chromatography*; Biomedical Applications @ EIsevier Scientific Publishing Company: 1979; pp 109-113.
24. Isomura, H.; Higuchi, S.; Kawamura, S., GAS CIIROMATOGRAPHIC-MASS SPECTROMETRIC DETERMINATION OF PLASMA 5-FLUOROURACIL AFTER ADMINISTRATION OF l-HEXYLCARRAMOYL5-FLUOROURACIL TO DOGS AND HUMANS. *Journal of Chromatography* **1981,** *224*, 423-429.
25. Fda, Bioanalytical Method Validation Guidance for Industry. 2018.
26. Ananthula, S.; Janagam, D. R.; Jamalapuram, S.; Johnson, J. R.; Mandrell, T. D.; Lowe, T. L., Development and validation of sensitive LC/MS/MS method for quantitative bioanalysis of levonorgestrel in rat plasma and application to pharmacokinetics study. *Journal of Chromatography B* **2015,** *1003*, 47-53.
27. Neervannan, S., Preclinical formulations for discovery and toxicology: physicochemical challenges. *Expert Opinion on Drug Metabolism & Toxicology* **2006,** *2* (5), 715-731.
28. Kosovec, J. E.; Egorin, M. J.; Gjurich, S.; Beumer, J. H., Quantitation of 5-fluorouracil (5-FU) in human plasma by liquid chromatography/electrospray ionization tandem mass spectrometry. *Rapid Communications in Mass Spectrometry* **2008,** *22* (2), 224-230.

Chapter-5

Development of an imaging mass spectrometry (IMS) method for bioanalysis of carmofur/5-fluorouracil in mouse brain

5.1. Introduction

Matrix assisted laser desorption ionization (MALDI) is a soft ionization technique widely known for its ability to ionize intact biomolecules such as proteins which is unlikely with conventional mass spectrometry ionization techniques[1]. The inception of MALDI has enabled to perform label-free bioanalysis to visualize the spatial distribution of biomolecules, pharmaceuticals, and other xenobiotics in tissue sections[2]. MALDI-MS was first introduced in late 1980s but the first successful imaging was performed by the Caprioli group in 1997[3]. Over the next decades, MALDI technology has improved in terms of sensitivity, application, spatial resolution, reproducibility, and speed[4-5]. Now-a-days, MALDI-IMS is applicable in organ or biopsy tissue section analysis to whole-body imaging[4, 6-9].

The analysis of biodistribution of drugs in different organs and tissues is an important consideration during the pre-clinical and clinical development of drugs. Traditional techniques such as whole-body autoradiography (WBA) or microautoradiography (MARG) and liquid chromatography-mass spectrometry (LC-MS/MS) provides quantitative information about the presence of a drug in an organ. Nevertheless, WBA/MARG though very sensitive it suffers from the lack of selectivity. LC-MS/MS overcomes the issue of selectivity. However, due to tissue homogenization and extraction, no substantial information is achieved in terms of the

localization and spatial distribution of the drugs in a tissue sample[4, 10]. Another technique, positron emission tomography (PET) also uses radiolabeling drug compounds prior to administration. It provides real-time in vivo imaging. Again, specificity is a concern due to its inability to distinguish between the parent drug compound and the metabolites[10-11]. MALDI-IMS provides complementary data that overcomes the lack of selectivity of WBA/MARG/PET and the loss of tissue construct by homogenization during LC-MS/MS analysis and hence, very useful in screening potential drug analogs during the early stages of drug development.

Although, there are a few different ionization methods that have been employed in imaging mass spectrometric techniques such as secondary ion mass spectrometry (SIMS)[12], desorption electrospray ionization (DESI)[13], laser ablation electrospray ionization (LAESI)[14], laser desorption ionization (LDI)[15], nanostructure initiator mass spectrometry (NIMS)[16] etc., MALDI-IMS is primarily the most widely used because of it's enhanced sensitivity over other techniques[10]. In a typical MALDI-IMS experiment, a matrix-substance is spray-coated on the surface of thin (5-20μm) tissue sections. Matrix substances are small organic compounds such as organic acids or bases with high UV-absorptivity. Sinapinic acid (SA), α-cyano-4-hydroxycinnamic acid (CHCA), 9-aminoacridine (9-AA), and 2,5-dihydroxybenzoic acid (DHB) are some of the commonly used MALDI matrices used in the laboratory[1, 17]. SA is typically used for ionizing high molecular weight biomolecules such as proteins, CHCA is used for low-molecular weight proteins or peptides, and DHB is used for small molecular weight compounds such as lipids, carbohydrates, and drug molecules. 9-AA is used for negative mode ionization[18-19]. Recently, nanoparticles such as gold nanoparticle and silver nanoparticles have been reported as MALDI matrices with low background interferences[20]. The selection of a MALDI matrix is dependent on the type of analyte,

the mode of ionization desired, wavelength of the UV laser, and lastly by trial and error. Sometimes addition of additives (e.g. acids such as trifluoroacetic acid or inorganic salts) can also aid the ionization of the target analytes. The matrix can be applied using automated coating instrument such as iMLayer (Shimadzu, Japan) and HTX TM-Sprayer (HTX, USA) or manually using a thin-layer chromatography (TLC) sprayer. Application of matrix in solution with organic solvent allows extraction of the analytes from the tissue section in the organic solvent and then, the analytes and the matrix co-crystallize upon evaporation of the solvent.

Sample preparation is followed by ionization of the analytes and ion detection. IMS is performed by rastering an beam throughout the surface of the tissue section. The irradiated ions are separated using a high-resolution mass analyzer or multiple analyzers in tandem (QqTOF or TOF-TOF etc.). The separated ions are recorded in collected mass spectra at defined x, y coordinates. A separate imaging software is used to generate an image or ion map from the dataset of mass spectrum wherein each pixel consists of a spectrum[10]. Images can be generated for any particular m/z from either MS1 or MS/MS transition.

In this work, we used Shimadzu 7090 MALDI-TOF-TOF-MS instrument to understand the spatial distribution of carmofur/5-FU in mouse brain. In our previous chapters, we have described LC-MS/MS based methods to understand the quantitative distribution of carmofur and 5-FU in different tissues including the brain. Given our interest in glioblastoma, we are interested to understand the tissue localization of carmofur and 5-FU inside the brain in a mouse model. To the best of our knowledge, there is no reported MALDI-TOF-MS based method for carmofur and 5-FU. So herein, we report for the first time a MALDI-TOF-MS based method to understand the spatial distribution of carmofur and 5-FU in brain tissue.

5.2. Materials and methods

5.2.1. Chemicals and reagents

Carmofur was obtained from Tokyo Chemical Co. Ltd (Portland, OR, USA). 5-FU was purchased from Millipore Sigma (St. Louis, USA). Different matrix substances such as DHB, CHCA, SA, 9-AA, 2',6'-dihydroxyacetophenone (DHAP), 2,4,6- trihydroxyacetophenone (THAP), 2-picolinic acid (2-PA), 3-hydroxycoumarin (3-HC) and universal MALDI matrix were purchased from Millipore-Sigma (St. Louis, MO, USA). Standard calibration standard TOF mix kit was obtained from Shimadzu Corporation (Kyoto, Japan). All solvents and buffers used were of analytical grades. LC-MS grade water, acetonitrile, ethanol, and methanol used in this work were obtained from Fisher Chemical (MA, USA). Trifluoroacetic acid was procured from Millipore-Sigma (St. Louis, USA). Dimethyl sulfoxide (DMSO) was purchased from Millipore Sigma (St. Louis, USA). PEG E 400 was procured from Millipore-Sigma (St. Louis, Mo, USA). Tween 80 was obtained from MP Biomedicals (Illkirch, France). Tissue freezing medium (TFM) was purchased from General Data Healthcare (OH, US). Phosphate buffered saline (PBS) at pH 7.4 was obtained from Thermo-Fisher Scientific (MA, USA).

5.2.2. Animal handling

All animal experimentation was approved by the University of Wisconsin Milwaukee's (UWM) Institutional Animal Care and Use Committee (IACUC) (protocol reference no. 20-21#53). Six-eight weeks old female Swiss Webster mice was purchased from Charles River Laboratories (MA, USA). The animals were housed for at least 3-4 weeks in the Lapham Animal Resource Center (ARC) of UWM before performing the experiment. While housed, they were provided with free access to food and water and maintained on a 12 h light (7:00 to 19:00) and dark cycle (19:00 to 07:00) at a temperature of 22±2°C and 60±5% humidity.

5.2.3. Instruments and conditions

The collected brain tissue was cryo-sectioned horizontally into 12 µm sections using a Leica C3050 S Research cryostat (Leica Biosystems, Germany). During the cryosectioning of the tissues the cryochamber was set to -20°C and the specimen temperature was kept at between -14°C to -17°C. The tissue sections were collected into FlexiMass-SRO#TO-432R00 stainless steel MALDI-MS slides (Shimadzu corporation, Japan) for matrix application and analysis. A 10 mL TLC sprayer (Millipore-Sigma, St. Louis, USA) was used for matrix deposition.

Imaging spectra were collected in reflectron negative mode with a laser power of 90. Acquired spectra were converted into cube files and analyzed for images using IonView software (Shimadzu corporation, Japan). Images were generated by normalizing to the total matrix ion current (m/z 193.38)

For the method development, spot analysis was performed by spotting the drug-matrix solution on FlexiMass-SR48 #TO-431R00 stainless steel MALDI-MS slides (Shimadzu corporation, Japan). The mass spectrometry data acquisition was performed using Shimadzu 7090 MALDI-TOF/TOF instrument (Shimadzu corporation, Japan) equipped with 2 KHz solid-state ultraviolet (UV) laser at 355 nm wavelength. The laser diameter was 100 µm and the laser power was scanned between 40 to 90. The collusion induced gas (CID) used for MS/MS analysis was helium.

5.2.4. Preparation of tissue samples

On the assay day, carmofur was administered intraperitoneally at 50 mg/kg (20% DMSO, 10% PEG E 400, 5% Tween 80, 65% PBS) concentration. The mouse was euthanized immediately using carbon dioxide (CO_2) and spinal cord dislocation. The brain tissue was harvested in dry ice and brought into cryo-sectioning facility without delay. The tissue was allowed to equilibrate with the chamber temperature of the cryo-sectioning instrument before starting cryosectioning. The sections were cut into 12 µm thickness and mounted into the MALDI slides using thaw-mount technique. The matrix solution (15 mg/mL 9-aminoacridine at 80% v/v in ethanol and water, 10-15 mL/plate) was sprayed into the tissue sections using a TLC sprayer before analyzing by the IMS.

5.3. Results and discussions

5.3.1. Selection of a MALDI matrix

Selection of an appropriate MALDI matrix is crucial in MALDI IMS to obtain high quality images with high spatial resolution[21]. Initially we tried all the available matrix substances in our laboratory to find the right matrix with highest ionization for carmofur. We prepared matrix solutions for DHB, CHCA, SA, DHAP, THAP, 2-PA, 3-HC and universal MALDI matrix at a concentration of 50 mg/mL in 70% acetonitrile in water with 0.1% TFA. 9-AA matrix solution was prepared without TFA and in 70% ethanol solution in water. Saturated solutions with undissolved matrix components were centrifuged at 18000 rpm for 5 min and the clear top layer was used for matrix application. The carmofur stock solution was prepared at 5000 $\mu g.mL^{-1}$ in DMSO which was further diluted in acetonitrile to 100 $\mu g.mL^{-1}$ for spot analysis. The carmofur and the matrix solutions were pre-mixed at 1:1 (v/v) ratio and 1 µL of it was spotted on the MALDI plate. It was then allowed to air-dry for matrix-analyte co-crystal formation before MS analysis. Given the low molecular weight of our analyte, we chose reflectron mode and scanned between the range m/z 30-600. Both the positive and negative mode ionization was assessed. Sample MS spectra was compared to the matrix MS spectra in search for the analyte peak (Appendix D, Figure D1-D8). We found only 9-AA was able to ionize carmofur in negative mode and two distinct peaks at m/z 256 and m/z 129 were identified for carmofur. MS spectra for carmofur in 9-AA is shown in figure 5-1. Peak m/z 256 is observed due to the loss of a proton $[M-H]^-$. Peak m/z 129 was found to be the dominant peak and that could be attributed to the breakdown of the compound upon laser irradiation and releasing the fluorouracil group.

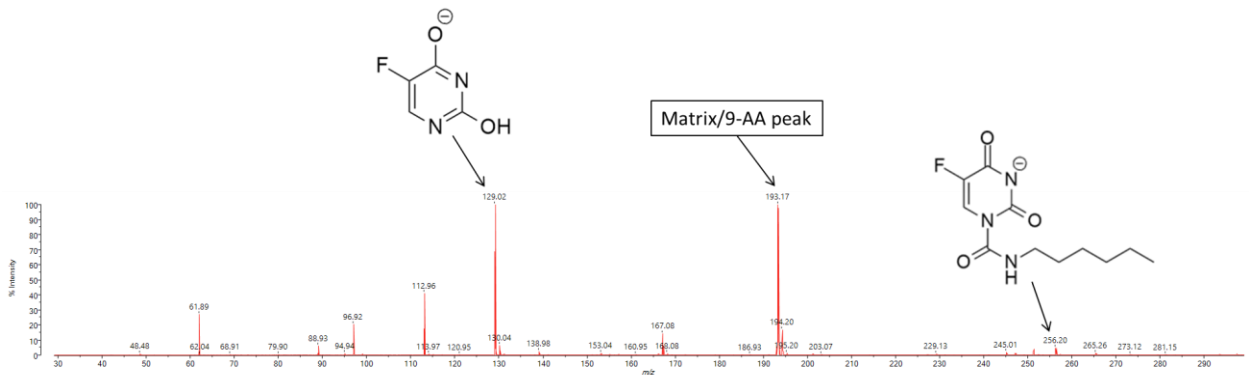

Figure 5-1. Mass spectra of carmofur in 9-AA in negative reflectron mode.

The peak m/z 129 coincides with the 5-FU peak in negative mode analysis (figure 5-2). 5-FU is also ionized using 9-AA as the matrix substance.

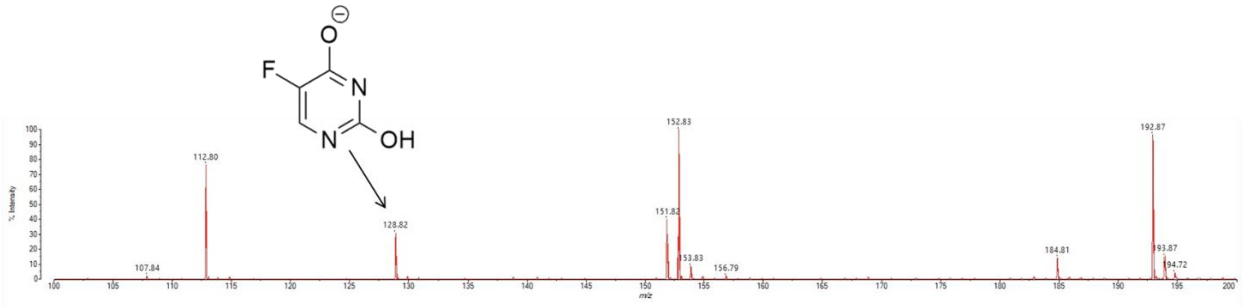

Figure 5-2. Mass spectra of 5-FU in 9-AA in negative reflectron mode.

5.3.2. Optimization of instrument parameters

A successful MALDI method also needs to be optimized for other sample preparation and instrument parameters. We have optimized for matrix concentration, laser power, laser diameter, spacing between the raster points, mass analyzer modes.

5.3.2.1. Matrix concentration

Typically, MALDI matrix is used at a concentration between 10-50 mg/mL. We looked into the optimal matrix concentration that we can use. Previous report from our group used at 15 mg/mL of 9-AA in ethanol/water (70/30, v/v) and the solution was needed to be centrifuged at 14,000 rpm for 5 min to remove the undissolved solids[22]. Therefore, we initially prepared the matrix solution at 10 mg/mL concentration to avoid wasting matrix material due to improper dissolution. Later on, we found that the matrix solution can be prepared at 15 mg/mL without the need of centrifugation step. To prevent having undissolved solids, the matrix substance needs to be dissolved in 100% ethanol first. Upon dissolution, an appropriate amount of water can be added to make the final solution with the desired ethanol/water ratio. 20 mg/mL concentration can be prepared but then the matrix component precipitates out of the solution over time. Therefore, we decided to use 15 mg/mL as the matrix concentration; however, we increased the ethanol/water ratio to 80/20 while spraying the tissue section for faster drying and co-crystallization.

5.3.2.2. Mass analyzer mode

During the method development, we explored and evaluated the feasibility of two mass analyzer modes ‘reflectron negative’ and ‘refelctron negative MSMS’ to understand the MS and MSMS scan of the analytes. While MS analysis for carmofur and 5-FU produces identical m/z 129 peak, a successful MSMS analysis can differentiate them. Therefore, during the MSMS scan, we selected both m/z 256 & m/z 129 peaks for fragmentation. We identified a m/z 256 to m/z 129 transition (figure 5-3); however, we could not see the fragment peak during MSMS analysis of

the tissue section analysis. This is due to the low signal intensity of the m/z 256 peak and potential fragmentation to m/z 129 upon laser irradiation before entering the fragmentation chamber. MSMS analysis of m/z 129 parent ions did not produce any fragment peak for imaging (figure 5-4). Finally, we decided to use the MS scan for the m/z 129 for imaging purposes due to its consistent high intensity among samples and the lack of reproducible signal and low intensity of m/z 256.

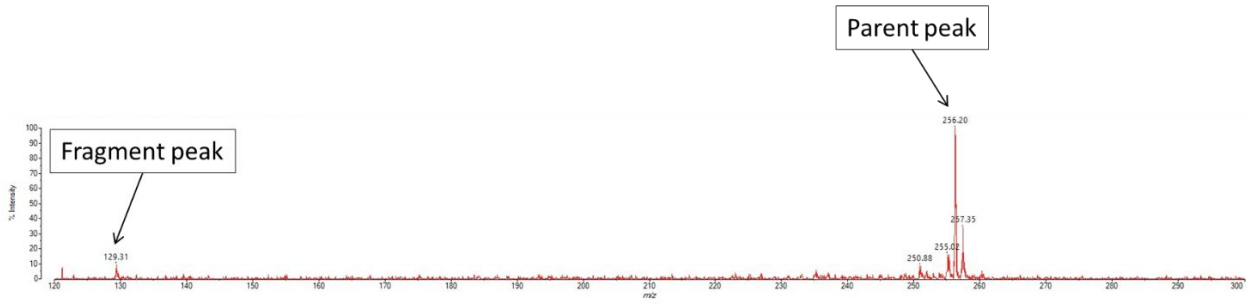

Figure 5-3. MSMS scan for m/z 256.

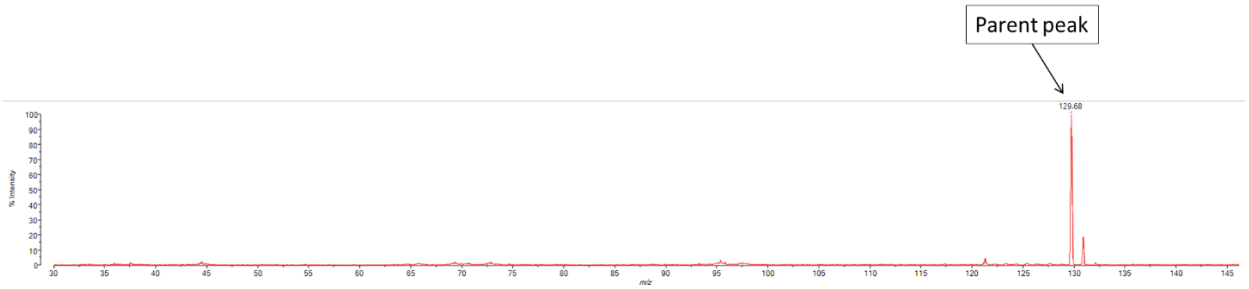

Figure 5-4. MSMS scan for m/z 129.

5.3.2.3. Laser power

We investigated the impact of laser power on the ionization of the m/z 129. We explored laser power between 40 to 90 with an increment of 10. Intensity of the analyte signal increases with the increase of the laser power. It also increases the presence of the background noise level. We found laser power 90 works best for ionizing m/z 129 for carmofur spot analysis (figure 5-5) and laser power 50 works best for ionizing m/z 129 in 5-FU spot analysis (figure 5-6). Spot analysis is performed in the absence of complex mixture of analytes; however, tissue sections are attended by lots of endogenous and interfering substances. Therefore, we further optimized laser power for tissue analysis. Laser power as low as 50 for tissue section analysis is not enough for good signal intensity of compound of interest (carmofur), hence, we investigated laser power 70, 80, and 90 for their impact on tissue section analysis (figure 5-7). Finally, we optimized the laser power to 90 for rastering the tissue sections. This adjustment in laser power was made due to the influence of the tissue components on the ionization of the analyte.

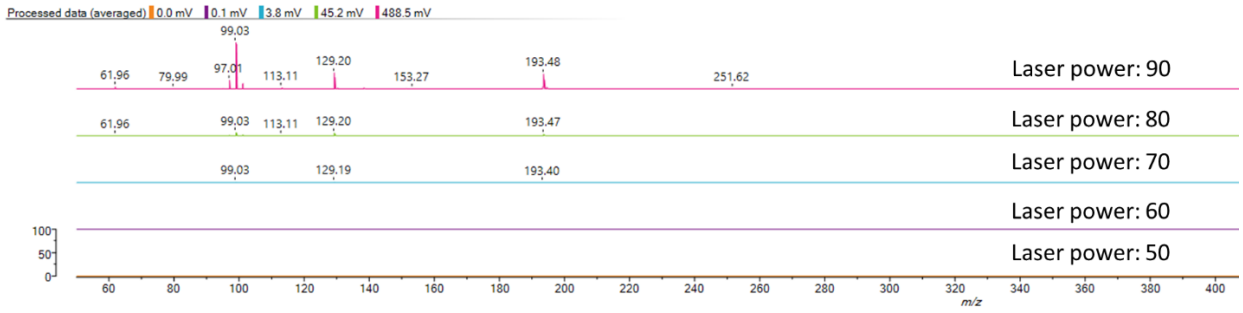

Figure 5-5. Impact of laser power on carmofur (m/z 129) spot analysis.

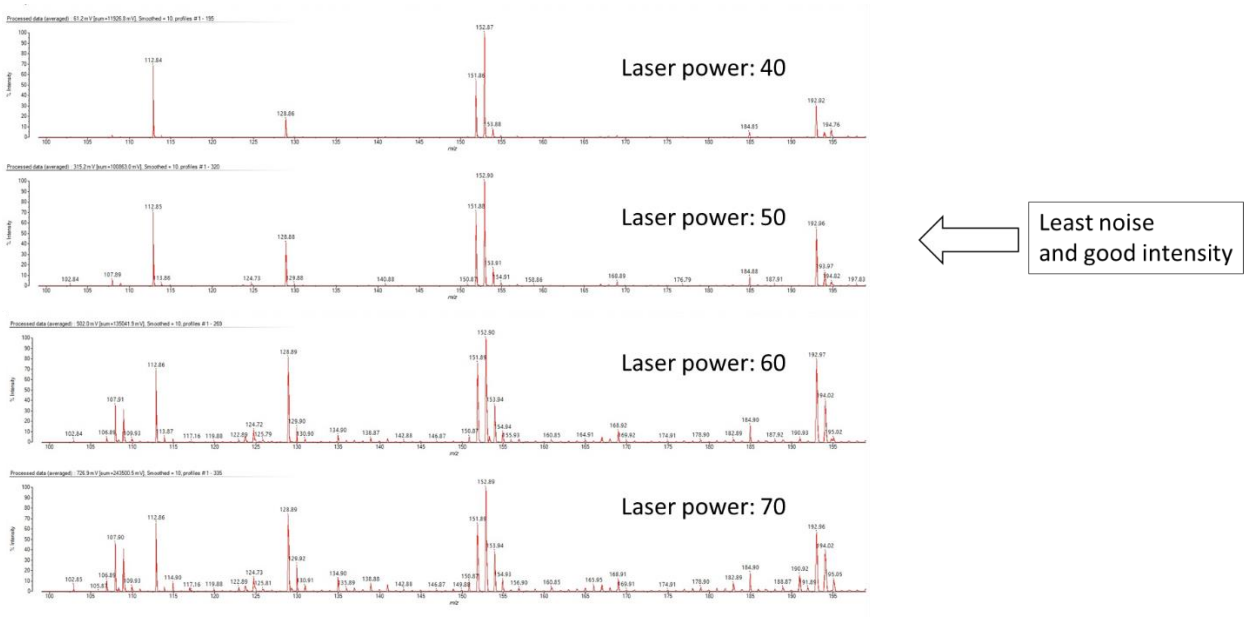

Figure 5-6. Impact of laser power on 5-FU (m/z 129) spot analysis.

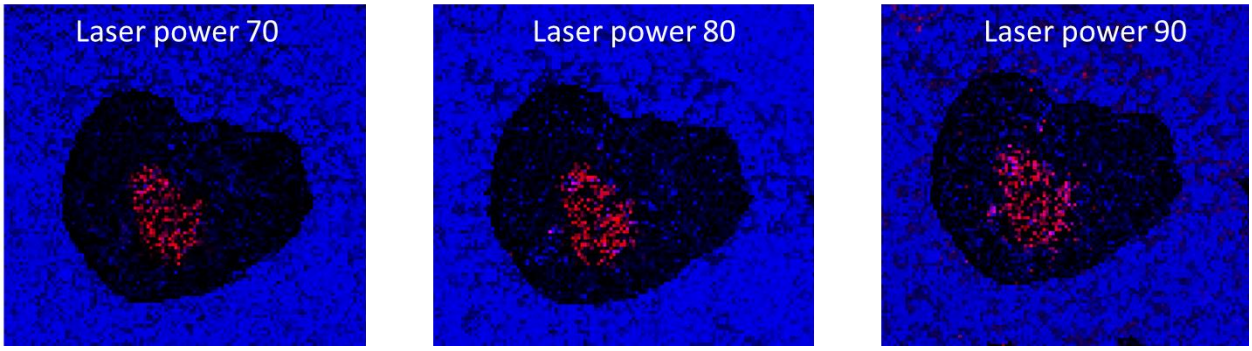

Figure 5-7. Impact of laser power on tissue section analysis. The same tissue section is irradiated at laser power 70, 80 and 90 where laser power 90 provides greater ionization and hence, better images for m/z 129 (red). Blue represents the 9-AA matrix (m/z 193.38).

5.3.2.4. Laser diameter and spacing between the raster points

We used laser diameter of 100 µm for our analysis. We also defined the spacing (X = 100 µm, Y = 100 µm) between the raster points. Decreasing the laser diameter and the distances between the raster points considerably increases the number of points for laser irradiation in the tissue section, and hence, it takes substantial long time for data acquisition and post-acquisition data analysis. Although it increases the spatial resolution of the images, it comes at a huge cost for running the instrument for a long period of time and not feasible when there are a lot of tissue sections for analysis. Besides, the set parameters of our method were able to identify and generate images during the tissue analysis.

5.3.3. System suitability check

We checked the system suitability in terms of selectivity and sensitivity of our proposed method.

5.3.3.1. Selectivity and sensitivity

Selectivity is an important consideration of bioanalytical methods because of the presence of other endogenous substances. It is important that there are no interfering peaks in the target tissue. In order to check the selectivity, we compared i) brain tissue harvested from mouse that received no carmofur ii) brain tissue harvested from mouse that received no carmofur-but underwent carmofur spiking after cryosectioning, and iii) brain tissue harvested from mouse after carmofur administration. The absence of ion m/z 129 in the blank tissues indicates the selectivity of our developed method (figure 5-8).

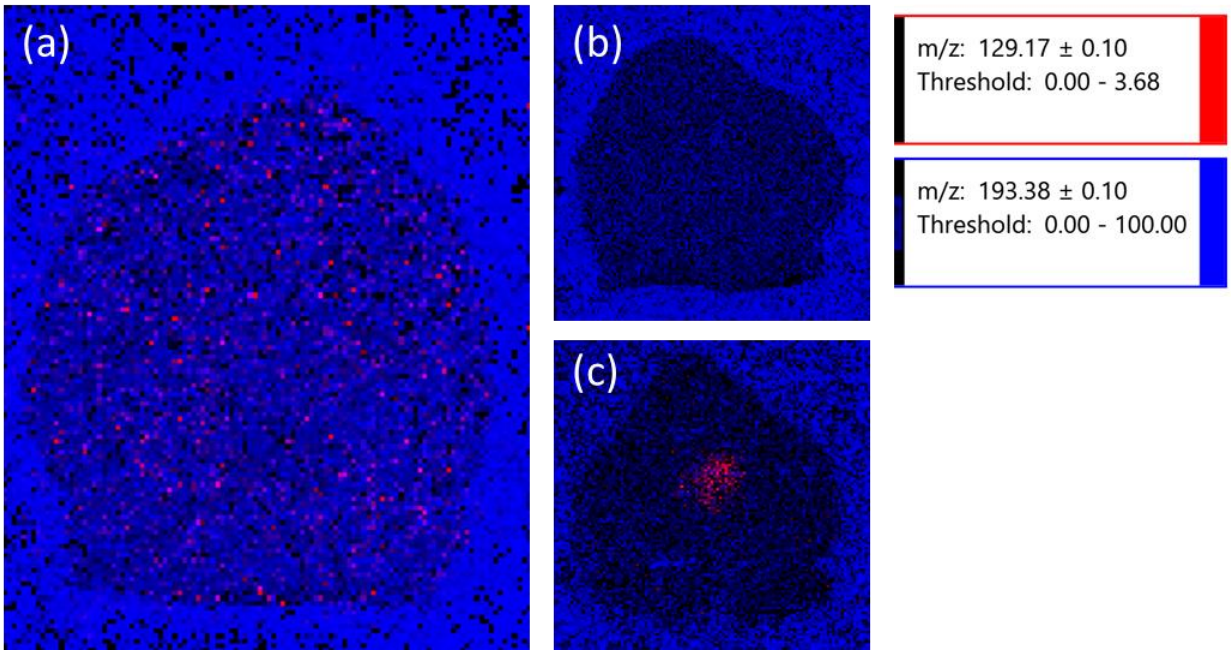

Figure 5-8. (a) brain tissue section from mouse after carmofur administration (b) brain tissue section that received no carmofur (c) Blank brain tissue spiked with carmofur. m/z 129.17 is in red. m/z 193.38 (blue) represents the 9-AA matrix.

Sensitivity of the method was evaluated by spiking carmofur solution on top of the 12 µm sections of the blank brain tissue. We spiked at different concentrations of carmofur to understand the instrument sensitivity with regard to concentration gradient (figure 5-9). Given that it is a qualitative method, we did not aim at finding the limit of detection.

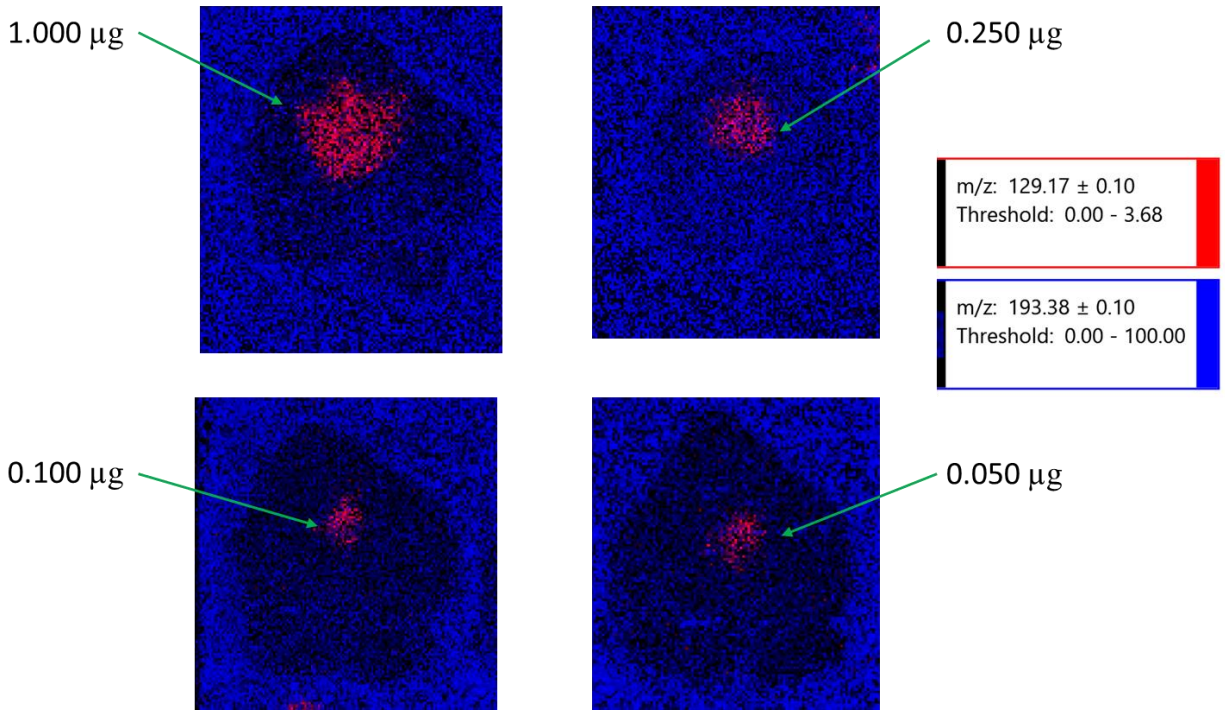

Figure 5-9. Sensitivity of m/z 129 (red) over concentration gradient spiked on tissue section. m/z 193.38 (blue) represents the 9-AA matrix.

5.3.4. Analysis of the brain tissue

Finally, we showed the applicability of our method in analyzing the spatial distribution of carmofur/5-FU in mouse brain. Carmofur was administered in three mice intraperitoneally at a concentration of 50 mg/kg. The animals were sacrificed immediately after the administration because the highest concentration of carmofur was previously observed from LC-MS/MS analysis (chapter 4) at this time point. Figure 5-10 represents the distribution of m/z 129 throughout the brain.

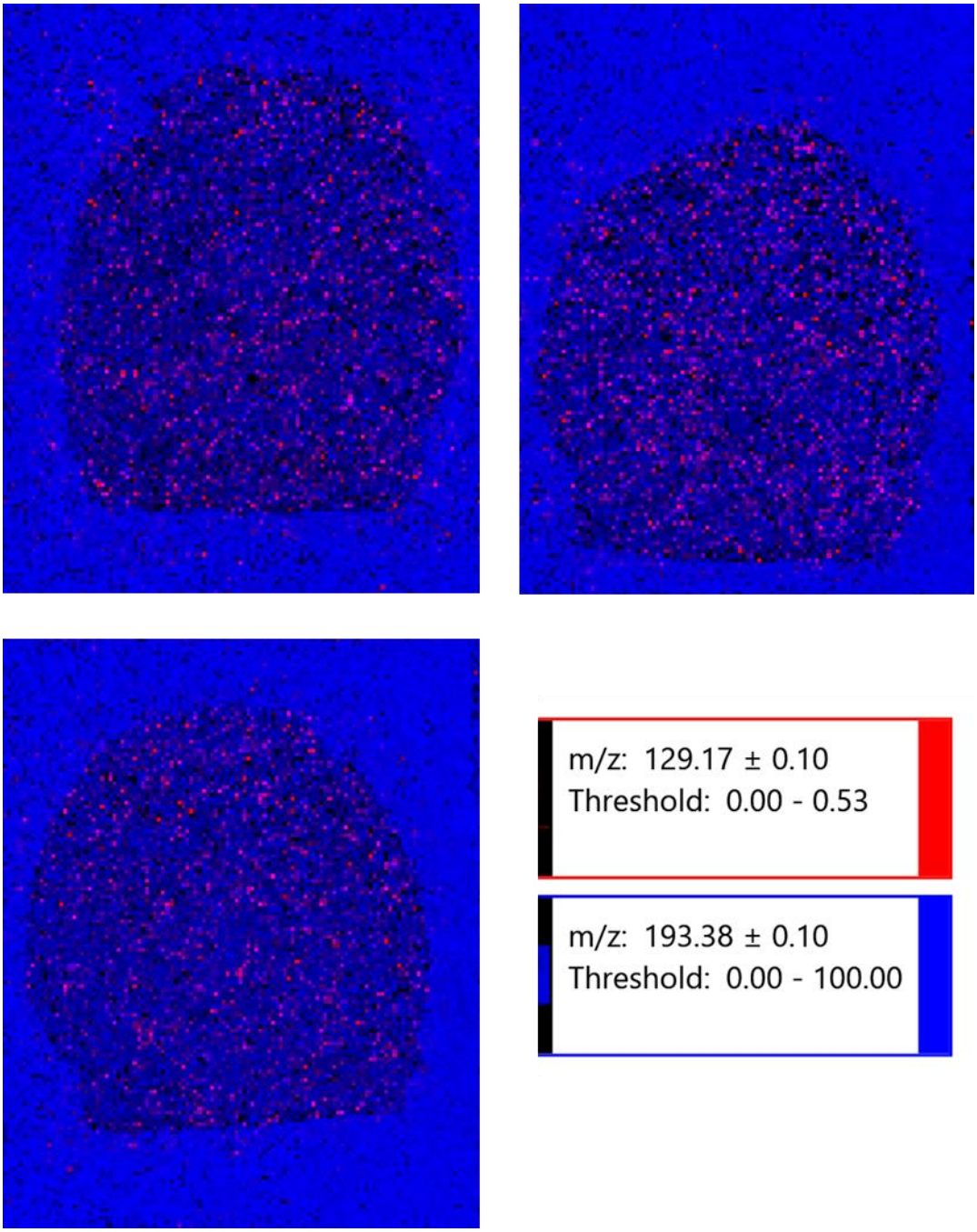

Figure 5-10. Representative sections of mouse brains imaged for m/z 129.17 (red). m/z 193.38 (blue) represents the 9-AA matrix.

Agreement between the LC-MS/MS and MALDI-TOF-MS data confirms and validates the previous LC-MS/MS analysis that carmofur can cross the blood-brain barrier (BBB). The ability of carmofur to cross the BBB can be very effective in therapeutic development for diseases of the central nervous system such as glioblastoma. It is also observed that m/z 129 delocalizes and distributes throughout the brain. It is significant for targeting glioblastoma since it can originate from any part of the brain such as frontal, temporal, parietal and occipital lobes as well as in the deeper structures[23].

Although, analyzing the spatial distribution of carmofur based on m/z 129 cannot differentiate whether the analyte is carmofur or it's active metabolite, 5-FU, it is a valuable indication that carmofur or 5-FU is reaching and distributing throughout the brain. Both carmofur and 5-FU have independent anticancer properties which can now be established in the future in glioblastoma tumor xenograft.

5.4. Conclusion

To the best of our knowledge, this is the first report of MALDI-TOF-MS method for bioanalysis of carmofur or 5-FU. Herein, we have developed the MALDI-TOF-MS method and showed the applicability by analyzing mouse brain tissues. This report reinforces and validates the LC-MS/MS analysis described in the previous chapter that carmofur can cross the blood-brain-barrier. Moreover, this method can be used for analyzing the spatial distribution of 5-FU after administration of 5-FU based any other pro-drugs as well such as capecitabine, tegafur etc.

References

1. Leopold, J.; Popkova, Y.; Engel, K. M.; Schiller, J., Recent Developments of Useful MALDI Matrices for the Mass Spectrometric Characterization of Lipids. *Biomolecules* **2018,** *8* (4).
2. Schulz, S.; Becker, M.; Groseclose, M. R.; Schadt, S.; Hopf, C., Advanced MALDI mass spectrometry imaging in pharmaceutical research and drug development. *Curr Opin Biotech* **2019,** *55*, 51-59.
3. Caprioli, R. M.; Farmer, T. B.; Gile, J., Molecular imaging of biological samples: Localization of peptides and proteins using MALDI-TOF MS. *Anal Chem* **1997,** *69* (23), 4751-4760.
4. Bonnel, D.; Legouffe, R.; Willand, N.; Baulard, A.; Hamm, G.; Deprez, B.; Stauber, J., MALDI imaging techniques dedicated to drug-distribution studies. *Bioanalysis* **2011,** *3* (12), 1399-1406.
5. Nishidate, M.; Hayashi, M.; Aikawa, H.; Tanaka, K.; Nakada, N.; Miura, S.; Ryu, S.; Higashi, T.; Ikarashi, Y.; Fujiwara, Y.; Hamada, A., Applications of MALDI mass spectrometry imaging for pharmacokinetic studies during drug development. *Drug Metabolism and Pharmacokinetics* **2019,** *34* (4), 209-216.
6. Nelson, K. A.; Daniels, G. J.; Fournie, J. W.; Hemmer, M. J., Optimization of whole-body zebrafish sectioning methods for mass spectrometry imaging. *J Biomol Tech* **2013,** *24* (3), 119-27.
7. Villacrez, M.; Hellman, K.; Ono, T.; Sugihara, Y.; Rezeli, M.; Ek, F.; Marko-Varga, G.; Olsson, R., Evaluation of Drug Exposure and Metabolism in Locust and Zebrafish Brains Using Mass Spectrometry Imaging. *ACS Chem Neurosci* **2018,** *9* (8), 1994-2000.
8. Rohner, T. C.; Staab, D.; Stoeckli, M., MALDI mass spectrometric imaging of biological tissue sections. *Mech Ageing Dev* **2005,** *126* (1), 177-85.
9. Khatib-Shahidi, S.; Andersson, M.; Herman, J. L.; Gillespie, T. A.; Caprioli, R. M., Direct molecular analysis of whole-body animal tissue sections by imaging MALDI mass spectrometry. *Anal Chem* **2006,** *78* (18), 6448-56.
10. Prideaux, B.; Stoeckli, M., Mass spectrometry imaging for drug distribution studies. *J Proteomics* **2012,** *75* (16), 4999-5013.
11. Riemann, B.; Schafers, K. P.; Schober, O.; Schafers, M., Small animal PET in preclinical studies: opportunities and challenges. *Q J Nucl Med Mol Imaging* **2008,** *52* (3), 215-21.
12. Boxer, S. G.; Kraft, M. L.; Weber, P. K., Advances in imaging secondary ion mass spectrometry for biological samples. *Annu Rev Biophys* **2009,** *38*, 53-74.
13. Wiseman, J. M.; Ifa, D. R.; Song, Q. Y.; Cooks, R. G., Tissue imaging at atmospheric pressure using desorption electrospray ionization (DESI) mass spectrometry. *Angew Chem Int Edit* **2006,** *45* (43), 7188-7192.
14. Nemes, P.; Woods, A. S.; Vertes, A., Simultaneous Imaging of Small Metabolites and Lipids in Rat Brain Tissues at Atmospheric Pressure by Laser Ablation Electrospray Ionization Mass Spectrometry. *Anal Chem* **2010,** *82* (3), 982-988.
15. Goodwin, R. J. A.; Pitt, A. R.; Harrison, D.; Weidt, S. K.; Langridge-Smith, P. R. R.; Barrett, M. P.; Mackay, C. L., Matrix-free mass spectrometric imaging using laser desorption ionisation Fourier transform ion cyclotron resonance mass spectrometry. *Rapid Communications in Mass Spectrometry* **2011,** *25* (7), 969-972.

16. Yanes, O.; Woo, H. K.; Northen, T. R.; Oppenheimer, S. R.; Shriver, L.; Apon, J.; Estrada, M. N.; Potchoiba, M. J.; Steenwyk, R.; Manchester, M.; Siuzdak, G., Nanostructure Initiator Mass Spectrometry: Tissue Imaging and Direct Biofluid Analysis. *Anal Chem* **2009,** *81* (8), 2969-2975.
17. Calvano, C. D.; Monopoli, A.; Cataldi, T. R. I.; Palmisano, F., MALDI matrices for low molecular weight compounds: an endless story? *Anal Bioanal Chem* **2018,** *410* (17), 4015-4038.
18. Vermillion-Salsbury, R. L.; Hercules, D. M., 9-aminoacridine as a matrix for negative mode matrix-assisted laser desorption/ionization. *Rapid Communications in Mass Spectrometry* **2002,** *16* (16), 1575-1581.
19. Cerruti, C. D.; Benabdellah, F.; Laprevote, O.; Touboul, D.; Brunelle, A., MALDI Imaging and Structural Analysis of Rat Brain Lipid Negative Ions with 9-Aminoacridine Matrix. *Anal Chem* **2012,** *84* (5), 2164-2171.
20. He, H. X.; Qin, L.; Zhang, Y. W.; Han, M. M.; Li, J. M. M.; Liu, Y. Q.; Qiu, K. D.; Dai, X. Y.; Li, Y. Y.; Zeng, M. M.; Guo, H. H.; Zhou, Y. J.; Wang, X. D., 3,4-Dimethoxycinnamic Acid as a Novel Matrix for Enhanced In Situ Detection and Imaging of Low-Molecular-Weight Compounds in Biological Tissues by MALDI-MSI. *Anal Chem* **2019,** *91* (4), 2634-2643.
21. Gemperline, E.; Rawson, S.; Li, L. J., Optimization and Comparison of Multiple MALDI Matrix Application Methods for Small Molecule Mass Spectrometric Imaging. *Anal Chem* **2014,** *86* (20), 10030-10035.
22. Zhang, Q.; Lee, S. B.; Chen, X.; Stevenson, M. E.; Pan, J.; Xiong, D. H.; Zhou, Y.; Miller, M. S.; Lubet, R. A.; Wang, Y.; Mirza, S. P.; You, M., Optimized Bexarotene Aerosol Formulation Inhibits Major Subtypes of Lung Cancer in Mice. *Nano Lett* **2019,** *19* (4), 2231-2242.
23. Larjavaara, S.; Mantyla, R.; Salminen, T.; Haapasalo, H.; Raitanen, J.; Jaaskelainen, J.; Auvinen, A., Incidence of gliomas by anatomic location. *Neuro-Oncology* **2007,** *9* (3), 319-325.

6. Appendices

6.1. Appendix A: The Development and validation of an LC-MS/MS method for quantitative bioanalysis of carmofur in mouse plasma and its application to pharmacokinetic study

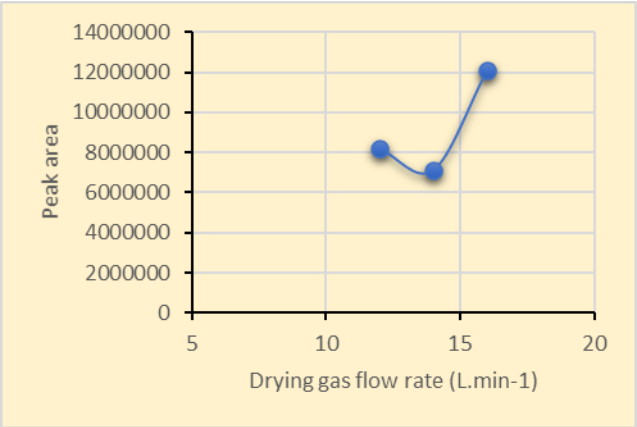

Figure A1. Optimization of drying gas flow rate.

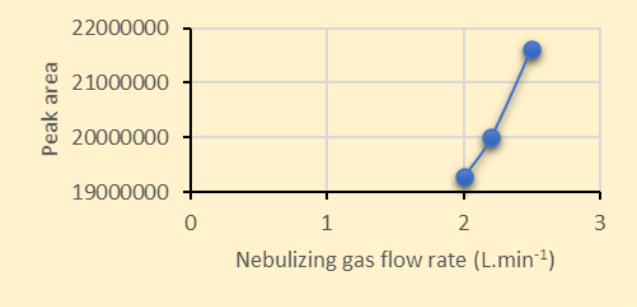

Figure A2. Optimization of nebulizing gas flow rate.

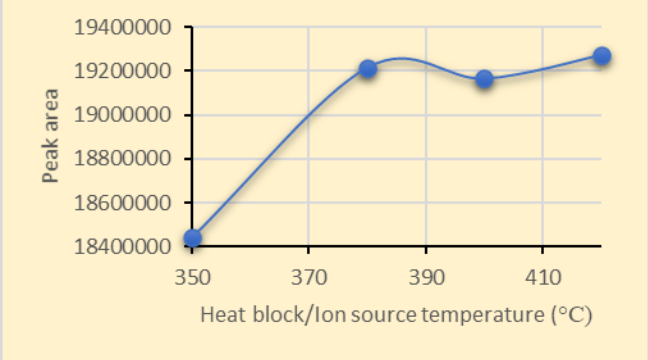

Figure A3. Optimization of Ion source temperature.

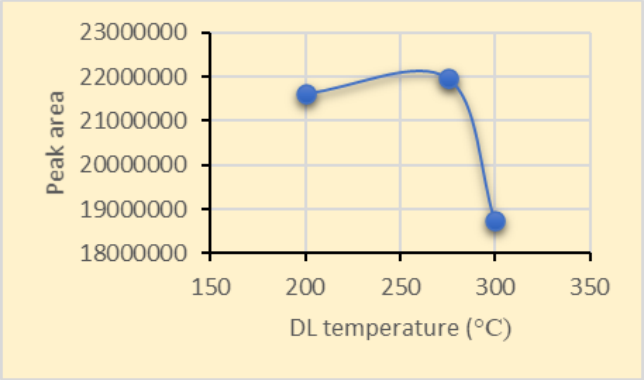

Figure A4. Optimization of DL temperature.

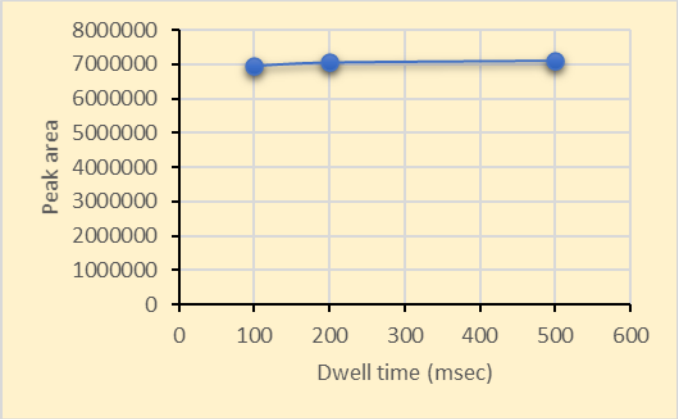

Figure A5. Optimization of Dwell time.

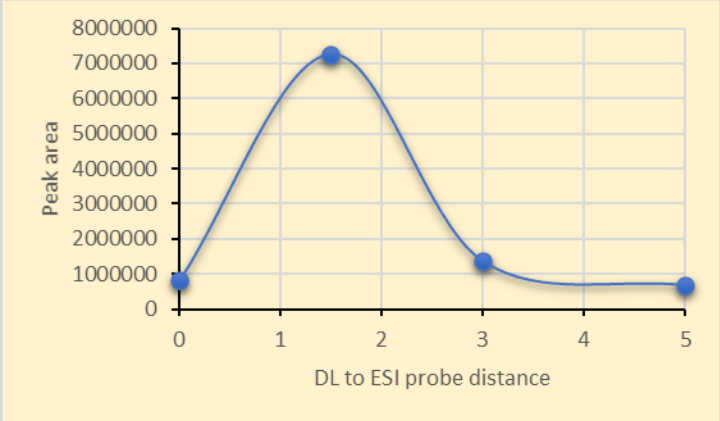

Figure A6. Optimization of DL to ESI probe distance.

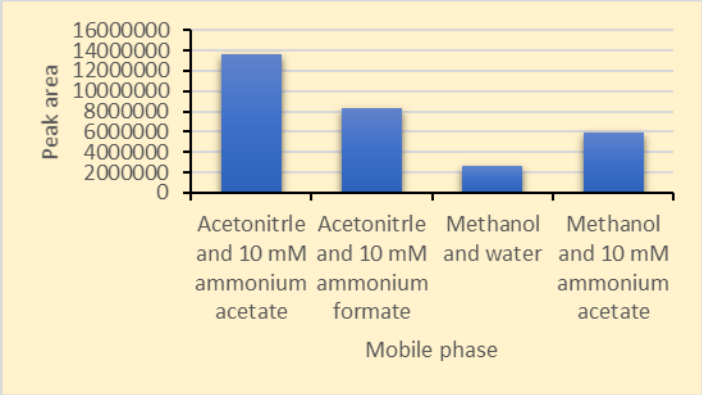

Figure A7. Optimization of mobile phases.

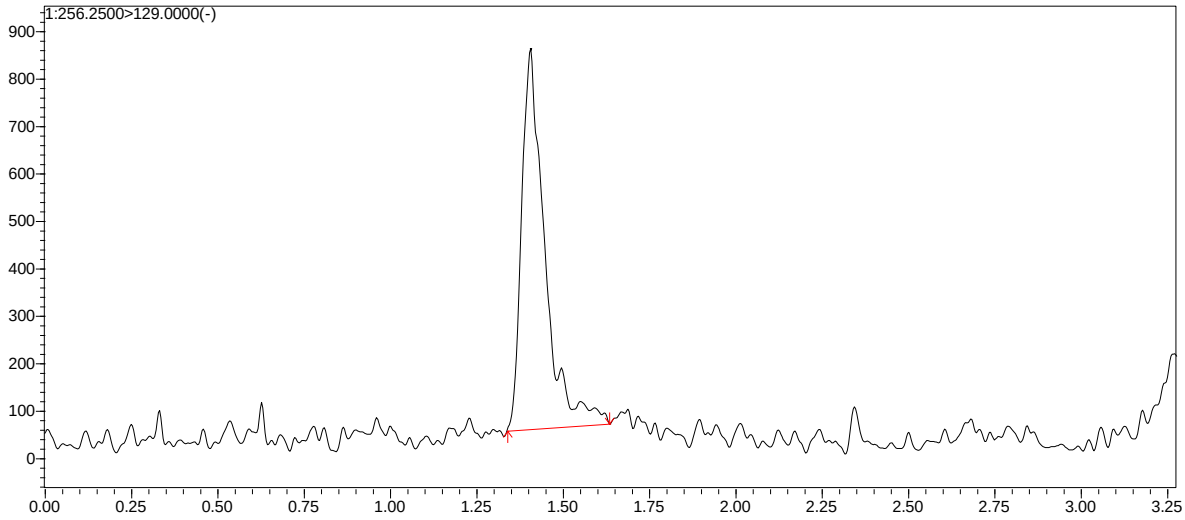

Figure A8. Carmofur peak (m/z 256.25 to m/z 129.00) at the lower limit of detection (LOD).

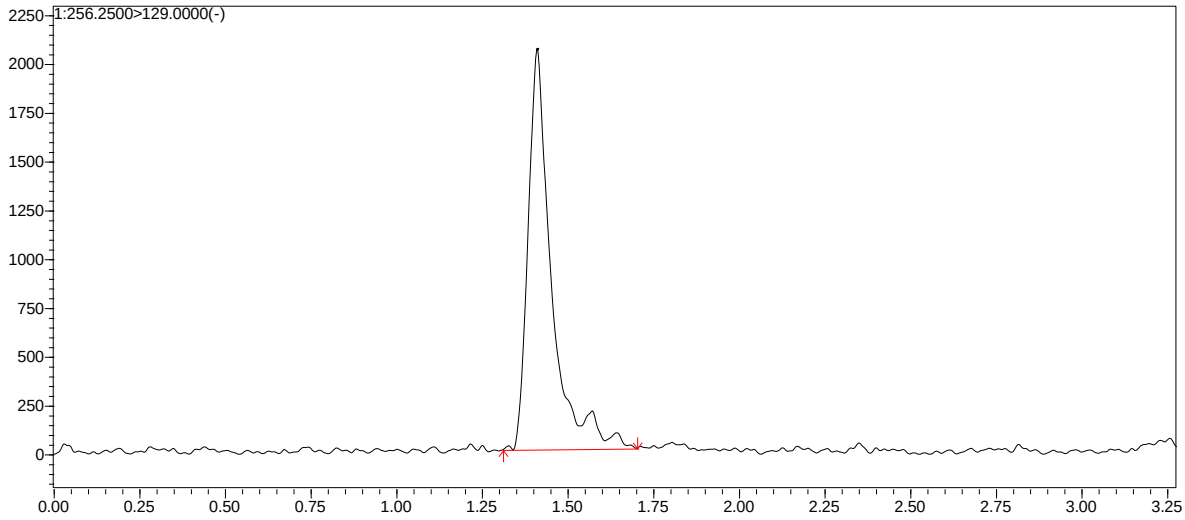

Figure A9. Carmofur peak (m/z 256.25 to m/z 129.00) at the lower limit of quantification (LOQ).

6.2. Appendix B: Development and Validation of LC-MS/MS method with application to parallel artificial membrane permeability assay (PAMPA) and permeability assessment of acid ceramidase inhibitors

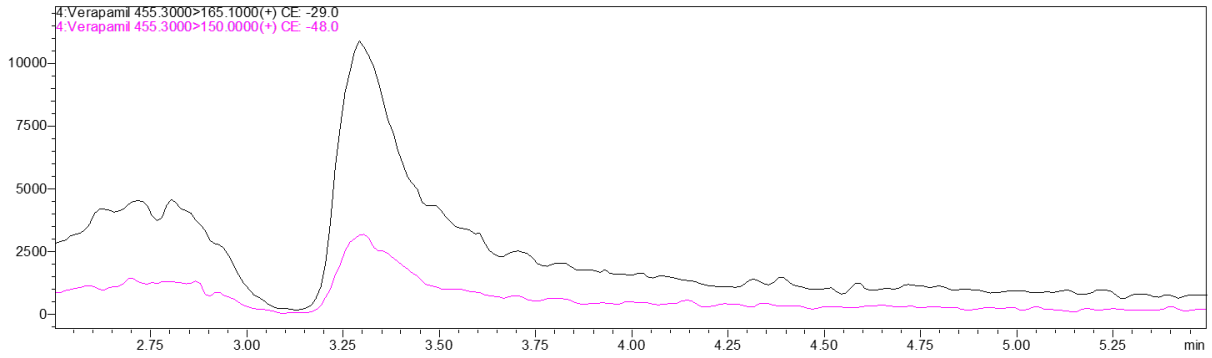

Figure B1. Mass chromatogram shows significant carryover upon verapamil analysis.

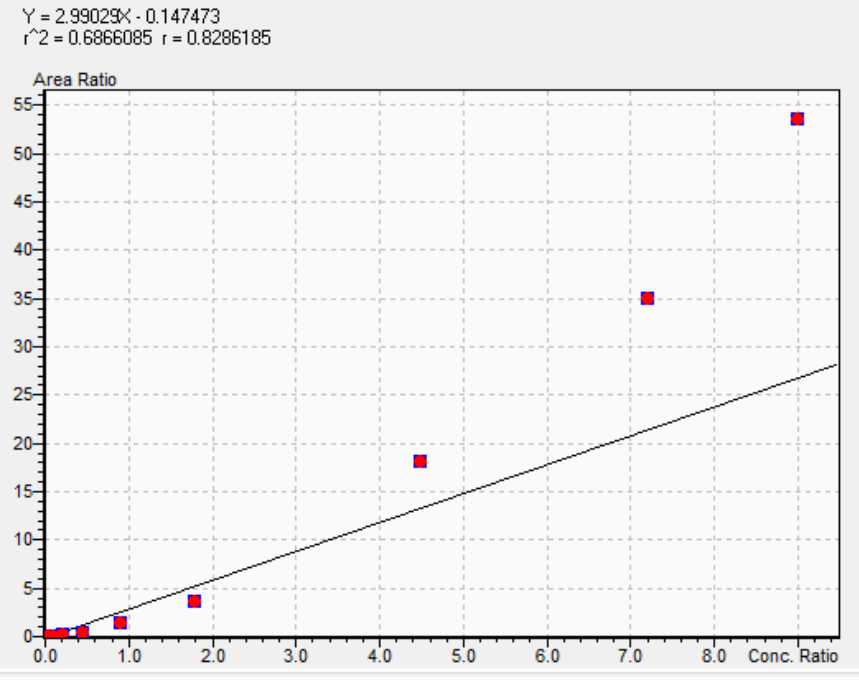

Figure B2. A representative calibration for verapamil in 5% DMSO in PBS solution.

6.3. Appendix C: Simultaneous quantitative bioanalysis of carmofur and 5-fluorouracil by LC-MS/MS with an application to drug distribution study in mouse

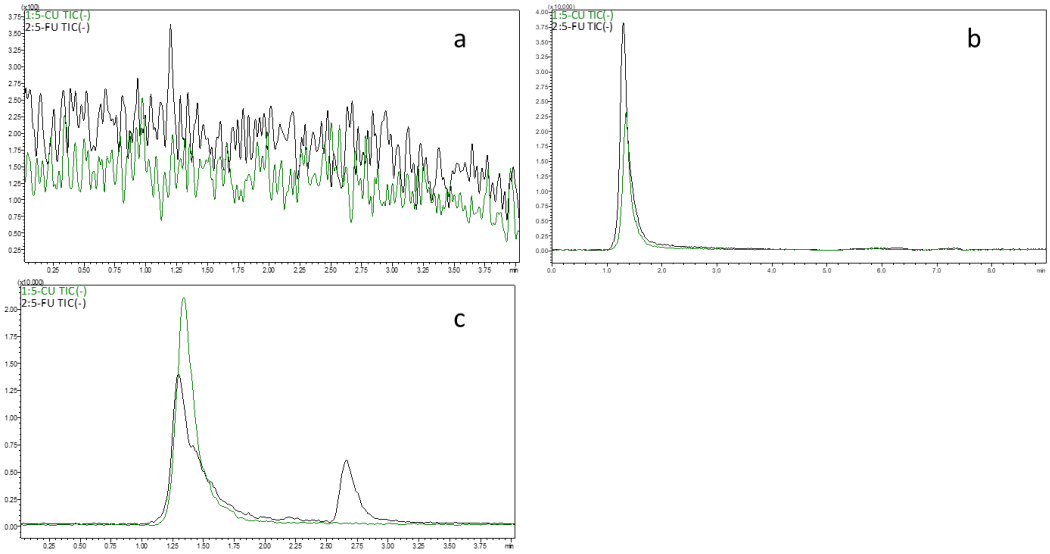

Figure C1. Representative chromatograms of a) extracted blank plasma b) blank plasma spiked with 5-FU and IS c) plasma collected after i.p. administration of carmofur.

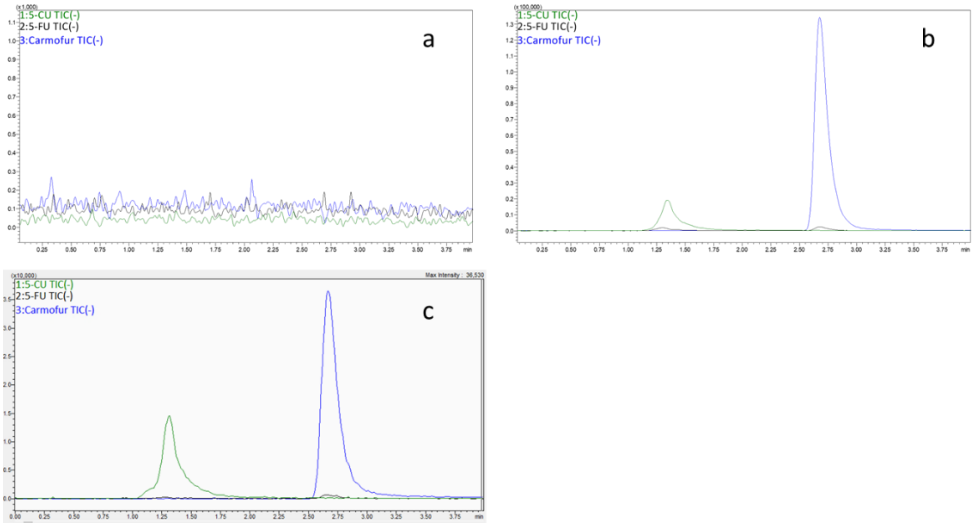

Figure C2. Representative chromatograms of a) extracted brain homogenate b) blank brain homogenate spiked with carmofur, 5-FU and IS c) brain homogenate collected after i.p. administration of carmofur.

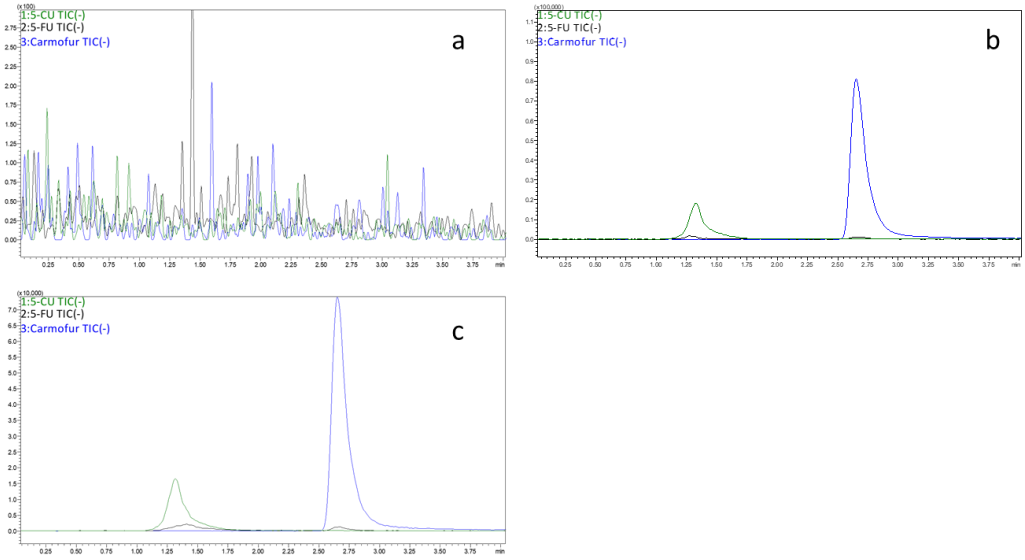

Figure C3. Representative chromatograms of a) extracted liver homogenate b) blank liver homogenate spiked with carmofur, 5-FU and IS c) liver homogenate collected after i.p. administration of carmofur.

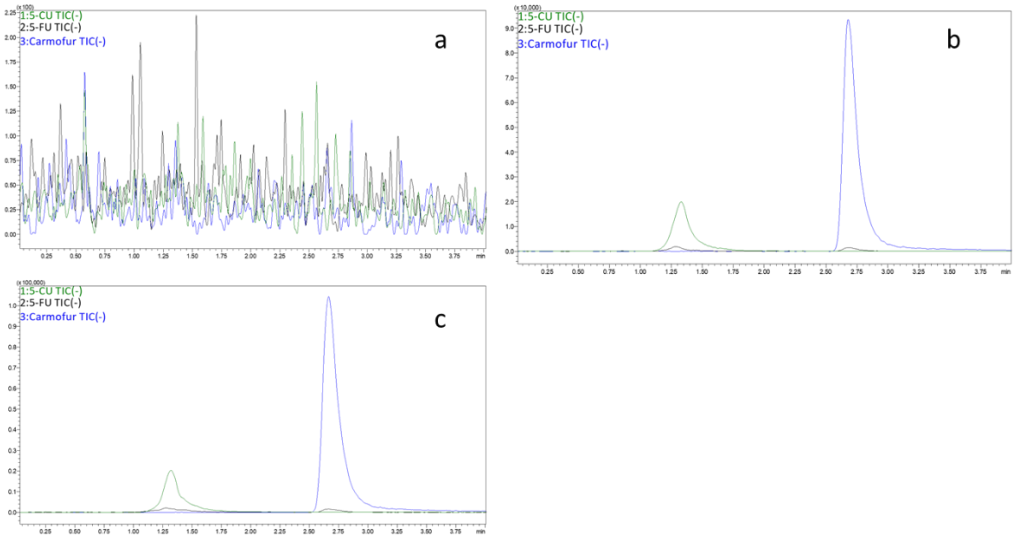

Figure C4. Representative chromatograms of a) extracted kidney homogenate b) blank kidney homogenate spiked with carmofur, 5-FU and IS c) kidney homogenate collected after i.p. administration of carmofur.

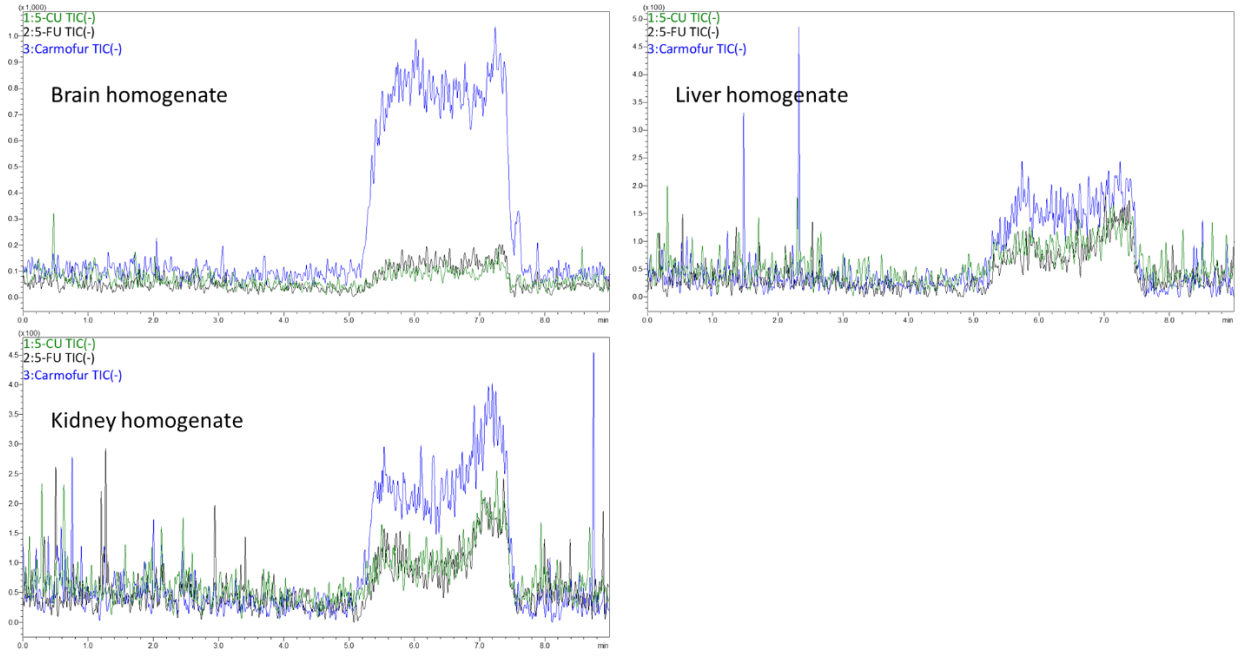

Figure C5. Representative mass chromatograms of a blank sample after running Carmofur HQC samples in brain, liver, and kidney tissue homogenate.

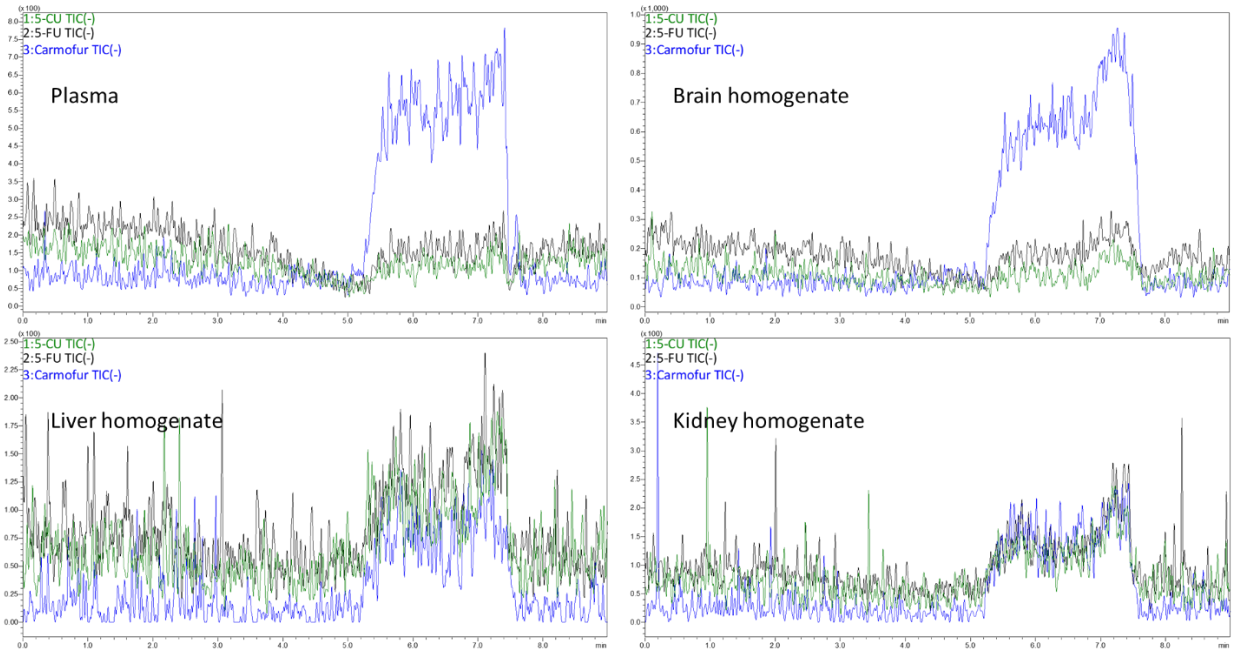

Figure C6. Representative mass chromatograms of blanks after running a 5-FU HQC sample in plasma, brain, liver, and kidney tissue homogenate

6.4. Appendix D: Development of an imaging mass spectrometry (IMS) method for the bioanalysis of carmofur/5-fluorouracil in mouse brain

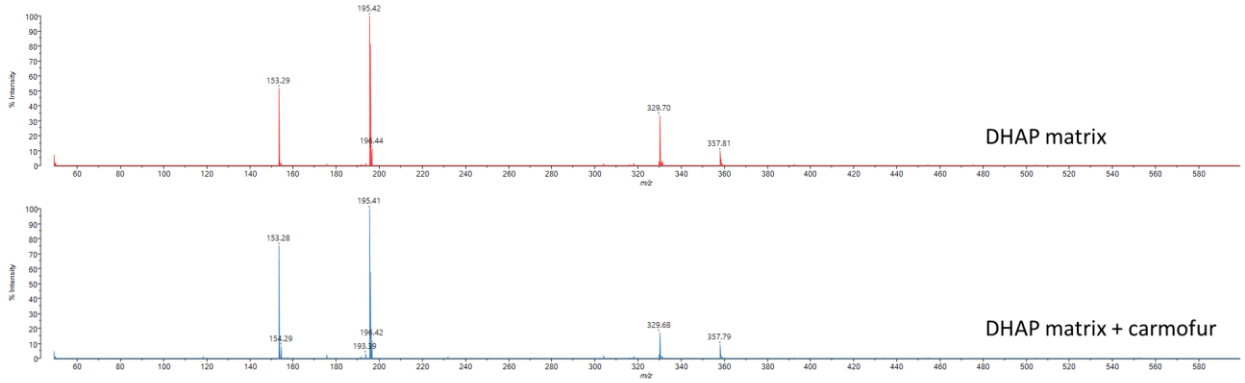

Figure D1. Mass spectra of carmofur in DHAP in reflectron positive mode.

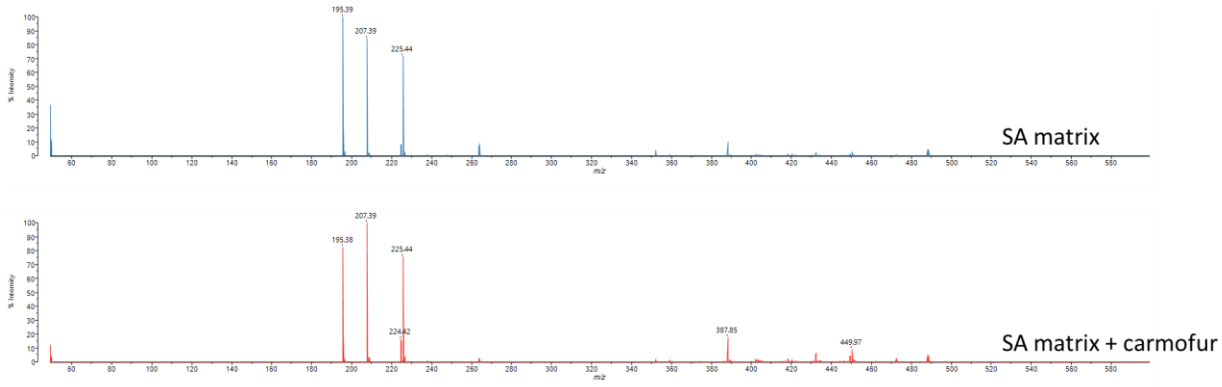

Figure D2. Mass spectra of carmofur in SA in reflectron positive mode.

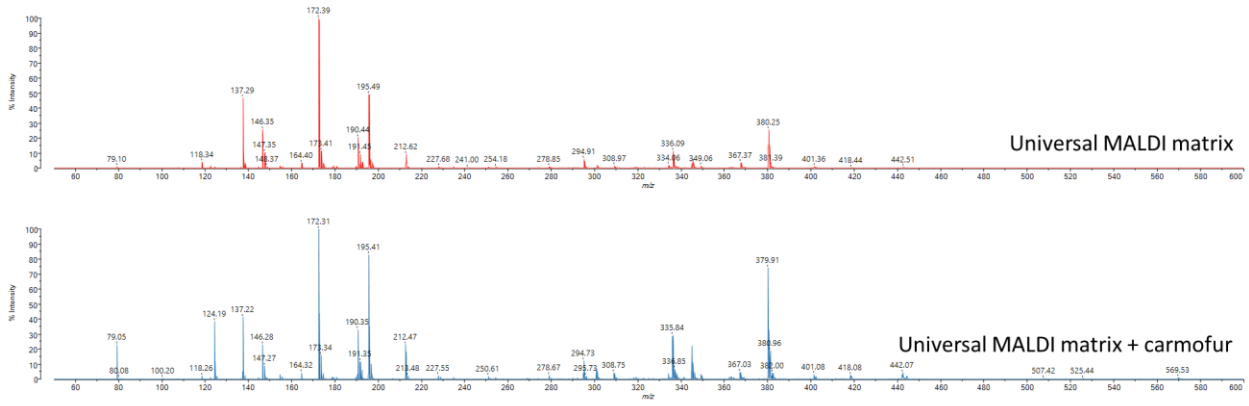

Figure D3. Mass spectra of carmofur in universal MALDI matrix in reflectron positive mode.

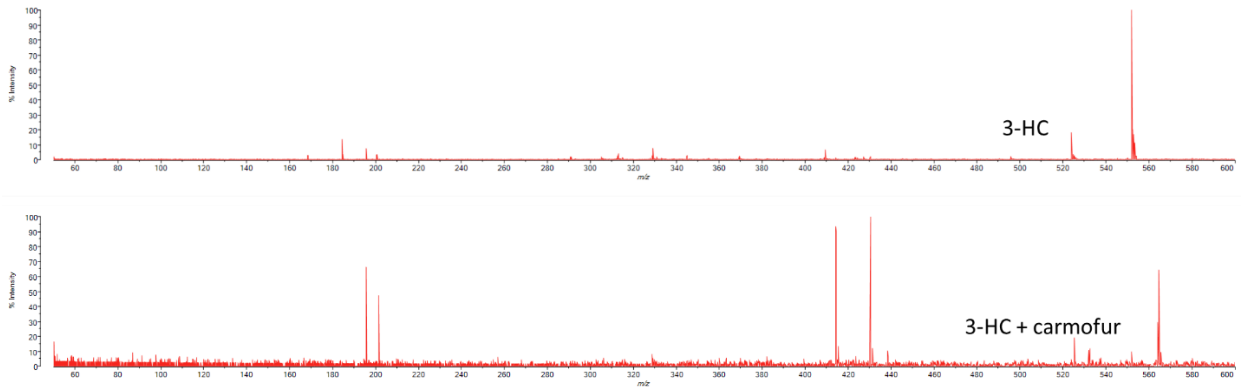

Figure D4. Mass spectra of carmofur in 3-HC in reflectron positive mode.

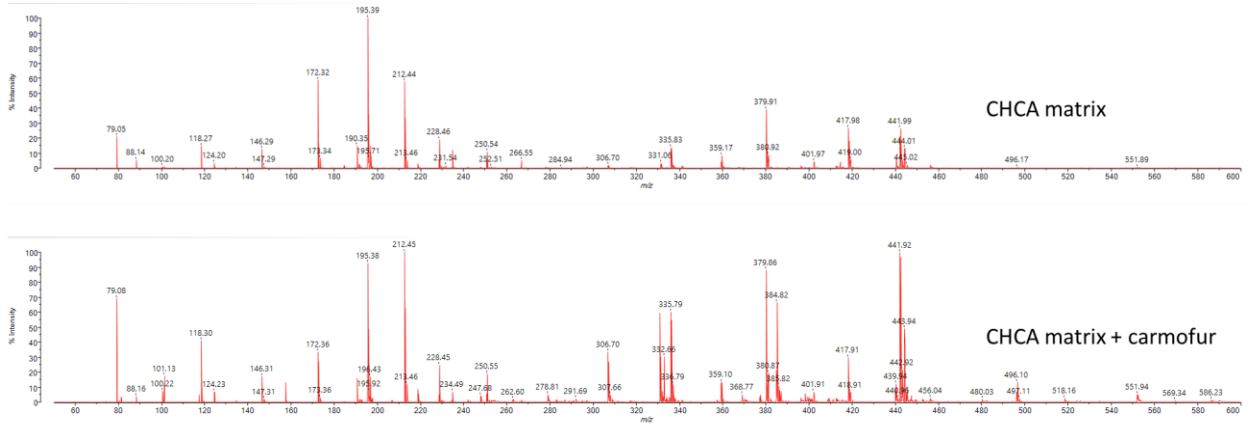

Figure D5. Mass spectra of carmofur in CHCA in reflectron positive mode.

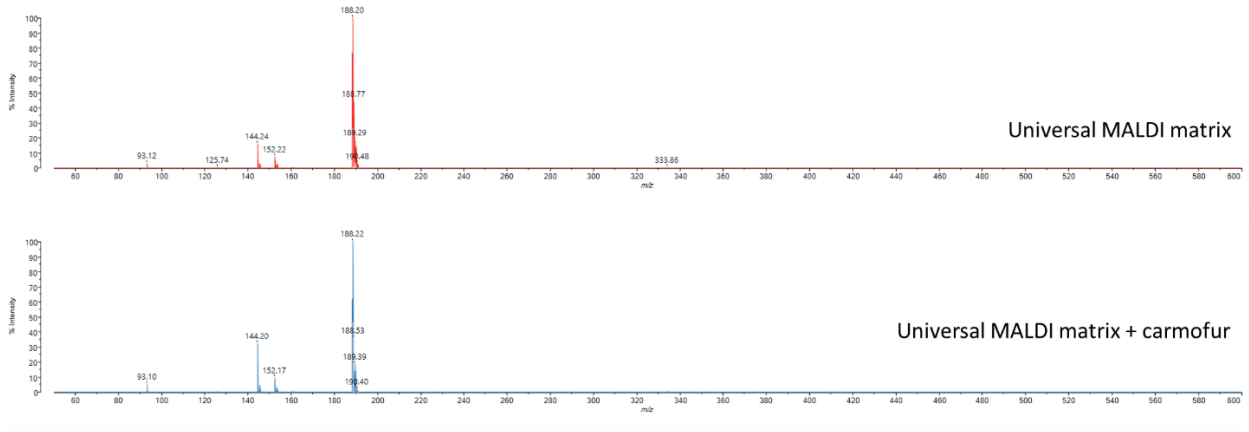

Figure D6. Mass spectra of carmofur in universal MALDI matrix in reflectron negative mode.

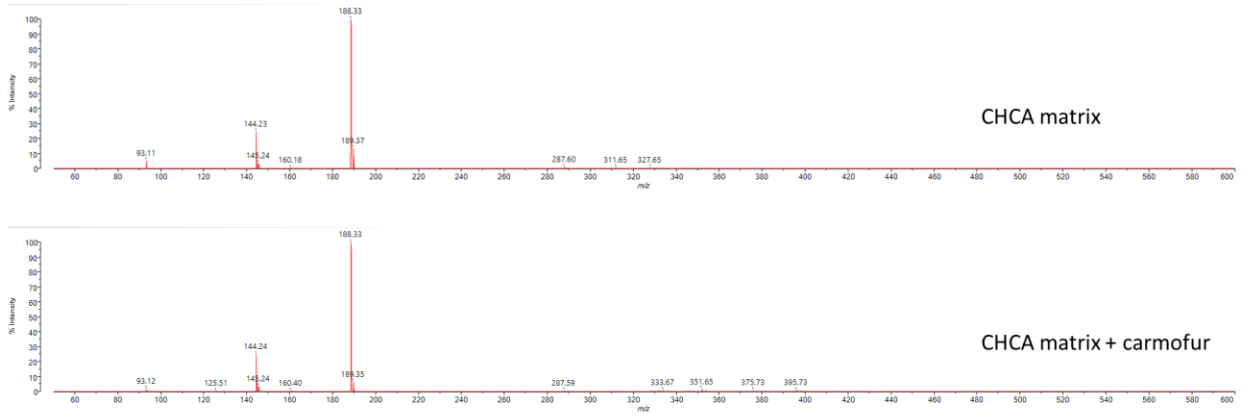

Figure D7. Mass spectra of carmofur in CHCA matrix in reflectron negative mode.

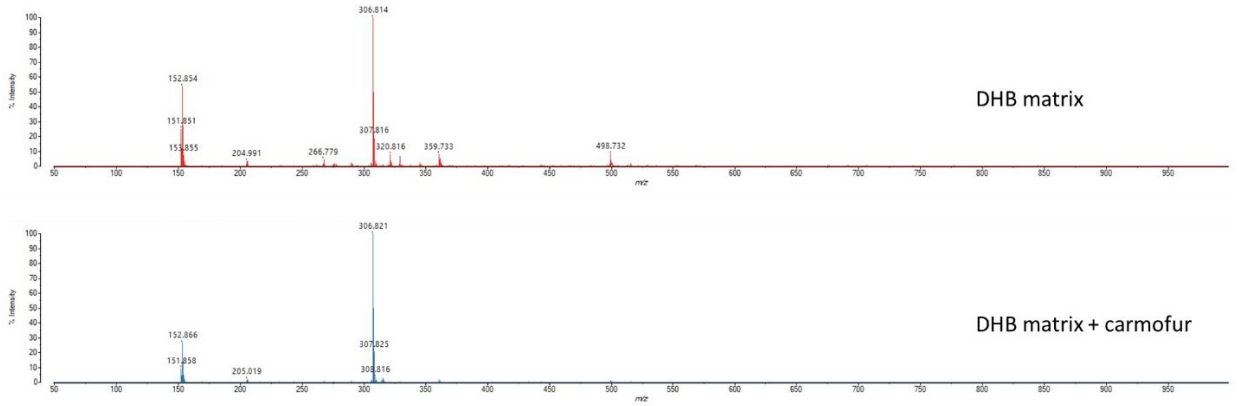

Figure D8. Mass spectra of carmofur in DHB matrix in reflectron negative mode.

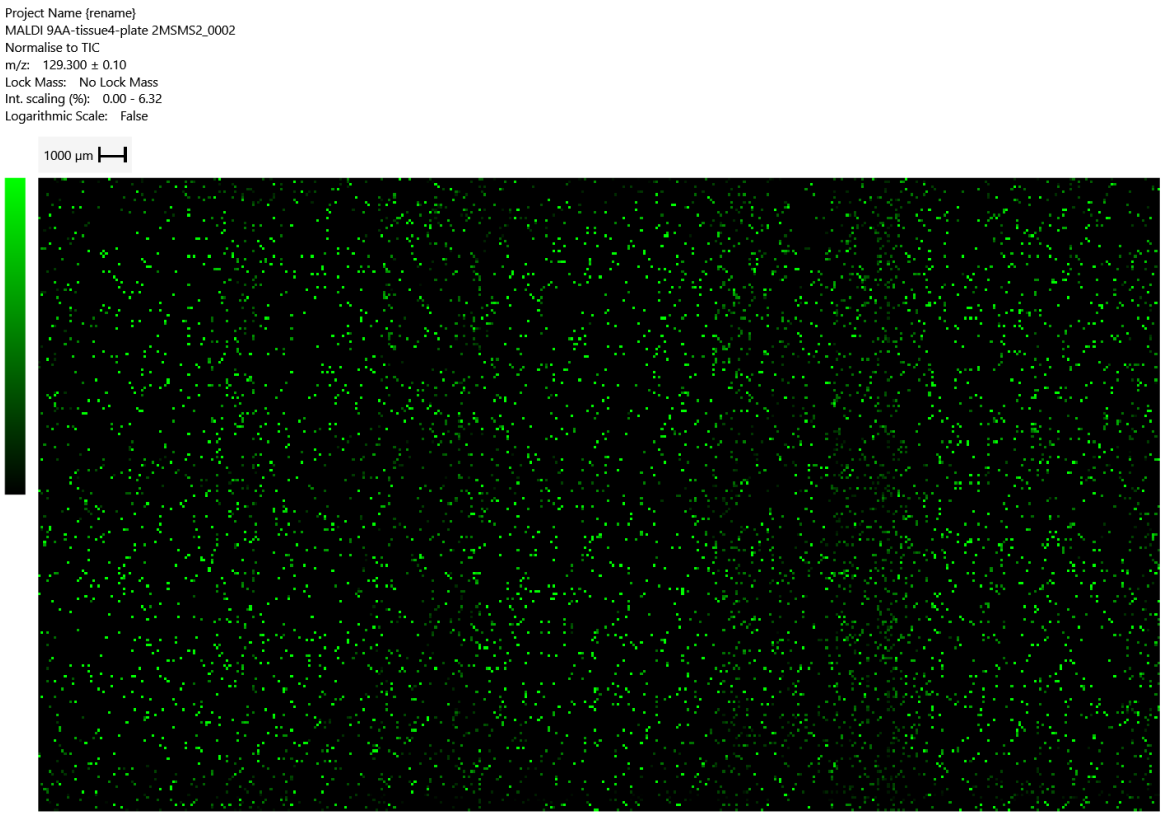

Figure D9. MSMS scan image for m/z 256 to m/z 129.0 transition in MALDI-TOF-TOF-MS with elevated level of noise.

7. CURRICULUM VITAE

Work:
Dept. of Chemistry & Biochemistry
University of Wisconsin-Milwaukee
3210 N Cramer St., Milwaukee
WI-53201, USA
islam7@uwm.edu

Summary of Qualifications:

- Mass spectrometry, chromatography, and biochemical techniques with small and large molecules (active ingredients, environmental contaminants, lipids, peptides, proteins)
- Analytical method development and verification
- Routine and non-routine analysis
- Laboratory management
- Experienced in working in industry and academic setting
- Sample preparation for complex matrixes including biological (tissue, blood, urine etc.) and non-biological (environmental, food etc.) samples
- Adequate understanding of regulatory guidelines, and good manufacturing/laboratory practice (GMP/GLP)

Education:

Ph.D. in Chemistry (Major: Analytical Chemistry) **May 2022**
University of Wisconsin-Milwaukee, USA
Supervisor: Prof. Shama P Mirza
Thesis Title: In vitro and in vivo identification and quantification of carmofur and 5-fluorouracil using tandem mass spectrometry

Master of Pharmacy in Pharmaceutical Technology **2016**
University of Dhaka, Bangladesh

Bachelor of Pharmacy **2014**
University of Dhaka, Bangladesh

Skills:

Chromatography: RP-HPLC-UV/DAD, NP-HPLC-UV, Preparative HPLC, GC-FID, Ion Chromatography (IC)

Mass spectrometry: LC-MS (Q, QqQ, IT-TOF, Q-TOF), ICP-MS, GC-MS, MALDI-TOF-TOF-MS, Multiple Reaction Monitoring (MRM) Method Development

Other Analytical Instruments: FTIR, UV-Vis Spectrophotometry, Fluorescence Microscope

Sample Preparation: Protein Precipitation, Liquid-Liquid Extraction, Solid-Phase Extraction, Trypsin Digestion, ZipTip cleanup etc.

Biochemical Techniques: Cell Culture, Western Blotting, In vitro Drug Discovery Assay (Microsomal Stability Assay, Permeability Assay etc.), Drug Metabolism and Pharmacokinetic (DMPK) Study

Animal Handling: Zebrafish (Raising, Maintenance, Dye Injection, Harvesting Brain Tissue), Mouse (Intraperitoneal Injection, Cardiac Puncture, Retro-Orbital Bleeding, Brain/Liver/Kidney Tissue Harvesting)

Software: LabSolutions, MALDISolutions, IonView, ImageJ, Pymol, AutoDock Vina, EndNote, Microsoft Excel, Microsoft word

Industrial and Research Experiences:

At the University of Wisconsin-Milwaukee (UWM):

Volunteer to Shimadzu Laboratory of Advanced and Applied Analytical Chemistry **Summer 2017, Summer 2021-Spring, 2022**
University of Wisconsin-Milwaukee, United States

- Assisted in the day-to-day operation of the mass spectrometry facility (8 mass spectrometers, 3 LC, 1 FTIR, 1 UV-Vis) including instrument maintenance and basic method and instrument troubleshooting
- Trained 15+ researchers on a variety of instruments such as FTIR, IC, HPLC, LC-MS/MS etc.
- Analyzed samples and prepared reports for external clients

Graduate Research Assistant **Fall 2019**
Collaboration between the University of Wisconsin-Milwaukee and Eurofins S-F Analytical Laboratories, New Berlin, WI

- Provided mass spectrometry support for the identification and structural elucidation of small molecules in natural extracts and food products
- Developed solid phase extraction-based sample preparation techniques for complex matrices
- Developed quantitative LCMS methods
- Prepared reports and updated clients on due timeline

Graduate Research and Project Assistant **Summer 2019, Fall 2020, Spring 2021**
Mirza lab, University of Wisconsin-Milwaukee, United States

- Continued graduate dissertation research on bioanalytical method development and validation for identifying and quantifying small molecules to understand their in vitro and in vivo permeability and distribution in different biological tissues
- Trained the new graduate students and post-doctoral researchers of the lab on operation of analytical instruments such as LC-MS/MS, MALDI-TOF-TOF-MS etc.
- Established the functional laboratory space and the standard operating procedures (SOPs)
- Acted as the safety officer of the lab. Provided training to the lab members on chemical hygiene plan, inventory management, hazardous waste management and represented the lab during the annual lab safety inspection

Before UWM:

Officer, R&D Formulation **March 2016 - December 2016**
Incepta Pharmaceutical Limited, Bangladesh

- Developed formulations in lab scale for sixteen drug products such as immediate release tablets, immediate release capsules and dry-powder inhalers
- Overseen the commercial scale up, process optimization and validation

Management Trainee **August 2014-December 2014**
Radiant Pharmaceuticals Limited, Bangladesh (Licensee of F. Hoffmann La Roche Limited, Switzerland)

- Supervising day-to-day manufacturing operations
- Representing the company during quality audits from regulatory authorities

Intern **March 2014-April 2014**
Sanofi Bangladesh Limited, Bangladesh

- Trained up on large scale manufacturing and quality assurance
- Industrial management ensuring environment, health and safety

Teaching Experiences:

Graduate Teaching Assistant for General and Analytical Chemistry **2017-May 22, 2022**
Department of Chemistry & Biochemistry, University of Wisconsin-Milwaukee
Courses Taught:

- CHEM 102 (General Chemistry I) lab and discussion: Five semesters
- CHEM 221 (Elementary Quantitative Analysis) lab: Four semesters
- CHEM 782 (Liquid Chromatography-Mass Spectrometry Fundamental and Applications): Three semesters. Assisted the instructor in sample preparation and teaching for the laboratory class

Mentor to the New Graduate Teaching Assistants **2018, 2019, 2021**
Department of Chemistry & Biochemistry, University of Wisconsin-Milwaukee, USA
Role: Guiding the new graduate students to be efficient TAs

Research Mentor to Undergraduate Students and Volunteers **2017-Present**
Mirza Lab, University of Wisconsin-Milwaukee, USA
Role: Mentored 10 undergraduate students and volunteers to instruct them on bench work, instrumentation, poster presentation and writing reports and manuscript. One of them co-authored in a publication

Publications:

Profiles: Google Scholar, ORCID
Published:

01. Rajaratnam, V. †; **Islam, M. M.** †; Yang, M.; Slaby, R.; Ramirez, H. M.; Mirza, S. P. Glioblastoma: Pathogenesis and Current Status of Chemotherapy and Other Novel Treatments. ***Cancers (Basel)*** 2020, 12 (4), 937. (shared † Co-first author)
02. Stetson, L. C.; Ostrom, Q. T.; Schlatzer, D.; Liao, P.; Devine, K.; Waite, K.; Couce, M. E.; Harris, P. L. R.; Kerstetter-Fogle, A.; Berens, M. E.; Sloan, A. E.; **Islam, M. M.**; Rajaratnam, V.; Mirza, S. P.; Chance, M. R.; Barnholtz-Sloan, J. S. Proteins inform survival-based differences in patients with glioblastoma. ***Neuro-Oncology Advances*** 2020, 2 (1), vdaa039

Submitted:

03. **Islam, M. M.;** Mirza S.P. Versatile use of Carmofur: A comprehensive review from discovery to the clinic.

Others (non-peer-reviewed):

01. Boshra SN, **Islam M. M.,** Griffiths MD. The demography and apparent risk factors of COVID-19-related suicides in Bangladesh in a seven-month period of the pandemic. medRxiv. 2020; doi:10.1101/2020.08.11.20171272 (pre-print; cited 6 times)

02. **Islam M. M.,** Boshra SN. Writing the GRE General Test at Home: Perspective of Bangladesh. Science. 2020; https://science.sciencemag.org/content/368/6498/1414/tab-e-letters (e-letter)

Conference Presentations:

Poster Presentations:

01. **Islam M. M.**, Mirza, S. P. Development and validation of LC-MS/MS method for quantitative bioanalysis of carmofur in rat plasma. **ACS Meeting Spring 2021**. DOI: https://doi.org/10.1021/scimeetings.1c00668
02. **Islam M. M.**, Rajaratnam V., Mirza, S. P. PAMPA-BBB permeability of acid ceramidase inhibitors using LC-MS/MS and UV-Vis spectrophotometry. **ACS Meeting Spring 2021**. DOI: https://doi.org/10.1021/scimeetings.1c00669
03. **Islam M. M.**, Mirza, S. P. Simultaneous quantitative bioanalysis of carmofur and 5-fluorouracil by LC-MS/MS with an application to drug distribution study in mice. **ASMS Conference 2021** (Philadelphia, USA)
04. **Islam M. M.**, Mirza, S. P. Qualitative and quantitative bioanalysis of carmofur and 5-fluorouracil using tandem mass spectrometry. **ACS Meeting Spring 2022** (San Diego, USA)
05. **Islam M. M.**, Mirza, S. P. In Vivo Identification and Quantification of Carmofur and 5-Fluorouracil using LC-MS/MS and MALDI-TOF-MS. **Pittcon Conference 2022** (Atlanta, USA) (Oral conferred into poster due to conference cancellation)
06. Kub E.F., **Islam M. M.** et al. Comprehensive Characterization of Ceramides in Glioblastoma using Mass Spectrometry. **ASMS Conference 2022** (Minneapolis, MN) (Abstract Accepted)

Reviewer Experiences:

Peer-reviews performed: 14 (Publons) **Journals reviewed for:** Analytical Letters (Taylor & Francis), Molecules (MDPI), Amino Acids (Springer-Nature), Journal of Public Health (Oxford University Press), Breast Disease (IOS press), Evidence-based Complementary and Alternative Medicine (Hindawi)

Awards & Recognition:

01. Graduate student spotlight-Spring 2022 Newsletter, UWM Chemistry & Biochemistry
02. Chancellor's Graduate Student Award in Chemistry (seven times) (2017-2021)
03. Eurofins Award in Analytical Chemistry (2019)
04. Graduate School Travel Assistance Award (Twice) (2021)
05. TA mentorship travel award (2018, 2019, 2021, 2022)
06. UWM student association travel award (2020)
07. Chemistry & Biochemistry Graduate Student Council travel award (2017, 2018, 2019)
08. Nomination to distinguished graduate student fellowship (2019)
09. 2021-2022 Chemistry Alumni Graduate Research Award (2022)

Society Membership:

01. American Chemical Society (2018-Present)
02. American Society for Mass Spectrometry (2018-Present)
03. American Association of Pharmaceutical Scientists (2022-Present)
04. American Association for Cancer Research (2022-Present)

Volunteer Works:

01. Judge, Chemistry Undergraduate Poster Session (2017, 2018)
02. Organizer: Chemistry Annual Research Symposium & Awards Day, Holiday Gathering, Departmental Picnic (2018-2020)
03. Volunteer: Milwaukee Analytical Chemistry Conference, Graduate School Open House, Majors' Day (2018, 2019)
04. Committees served: Chemistry & Biochemistry Graduate Student Council, Student Association (Senator), Graduate Faculty Committee, Senate Finance Committee, Graduate Student Representation Committee (2017-2020)
05. Judge, UWM Undergraduate Research Symposium (2022)

Professional Licenses:

01. Registered Pharmacist* with Pharmacy Council of Bangladesh (2015-2020)
*Renewal would need physical presence in the country